

TKK Dissertations 238
Espoo 2010

MICROFABRICATION OF HEATED NEBULIZER CHIPS FOR MASS SPECTROMETRY

Doctoral Dissertation

Ville Saarela



**Aalto University
School of Science and Technology
Faculty of Electronics, Communications and Automation
Department of Micro and Nanosciences**

TKK Dissertations 238
Espoo 2010

MICROFABRICATION OF HEATED NEBULIZER CHIPS FOR MASS SPECTROMETRY

Doctoral Dissertation

Ville Saarela

Doctoral dissertation for the degree of Doctor of Science in Technology to be presented with due permission of the Faculty of Electronics, Communications and Automation for public examination and debate in Large Seminar Hall of Micronova at the Aalto University School of Science and Technology (Espoo, Finland) on the 15th of October 2010 at 12 noon.

**Aalto University
School of Science and Technology
Faculty of Electronics, Communications and Automation
Department of Micro and Nanosciences**

**Aalto-yliopisto
Teknillinen korkeakoulu
Elektroniikan, tietoliikenteen ja automaation tiedekunta
Mikro- ja nanotekniikan laitos**

Distribution:
Aalto University
School of Science and Technology
Faculty of Electronics, Communications and Automation
Department of Micro and Nanosciences
P.O. Box 13500 (Tietotie 3)
FI - 00076 Aalto
FINLAND
URL: <http://nano.tkk.fi/>
Tel. +358-50-304 9085
Fax +358-9-470 26080
E-mail: ville.saarela@tkk.fi

© 2010 Ville Saarela

ISBN 978-952-60-3339-6
ISBN 978-952-60-3340-2 (PDF)
ISSN 1795-2239
ISSN 1795-4584 (PDF)
URL: <http://lib.tkk.fi/Diss/2010/isbn9789526033402/>

TKK-DISS-2802

Aalto-Print
Helsinki 2010



ABSTRACT OF DOCTORAL DISSERTATION	AALTO UNIVERSITY SCHOOL OF SCIENCE AND TECHNOLOGY P.O. BOX 11000, FI-00076 AALTO http://www.aalto.fi		
Author	Ville Saarela		
Name of the dissertation	Microfabrication of heated nebulizer chips for mass spectrometry		
Manuscript submitted	18.6.2010		
Date of the defence	15.10.2010		
<input type="checkbox"/> Monograph	<input checked="" type="checkbox"/> Article dissertation (summary + original articles)		
Faculty	Faculty of Electronics, Communication and Automation		
Department	Department of Micro and Nanosciences		
Field of research	Semiconductor Technology		
Opponent	Prof. Klaus Bo Mogensen		
Supervisor	Prof. Pekka Kuivalainen		
Instructor	Prof. Sami Franssila		
Abstract	<p>Microfabrication technologies originating from the semiconductor industry were applied to the instrumentation of analytical chemistry. Heated nebulizer (HN) chips made of silicon and glass were developed. The HN chips are used to vaporize a sample prior to detection by a mass spectrometer. The chips can be used with both liquid and gaseous samples and they are compatible with multiple atmospheric pressure ionization techniques, which enables wide applicability with different separation methods and various types of analytes. Better sensitivity, flexibility and operation with a lower sample and nebulizer gas flow rates was achieved by the miniaturization of the heated nebulizer. The chips can operate with 50 nL min⁻¹ to 5 µL min⁻¹ sample flow rates typical of microfluidic separation systems.</p> <p>Silicon and glass microfabrication methods — etching, wafer bonding and thin film technology — were developed and applied to the fabrication of the HN chips in 40 different layout and process variations. The thermal behaviour of the chips and the shape of the gaseous jet produced by the chips was studied. A method was developed for measuring the temperature distribution of a gaseous jet using a miniature thermocouple attached to a computer controlled xyz stage.</p> <p>Different methods for making capillary tube and electrical interconnections to the chips were also studied.</p> <p>Liquid chromatography (LC) column chips were developed resulting in an integrated chip having both an LC column and a heated nebulizer on a single chip. At the end of the LC column there is a high aspect ratio micropillar frit which enables packing the column with particles.</p> <p>The novel chips developed in this work extend the available ionization methods and the range of suitable analytes compared to the previously presented chips for mass spectrometry.</p>		
Keywords	chip; heater; liquid chromatography; mass spectrometry; microfabrication; nebulizer		
ISBN (printed)	978-952-60-3339-6	ISSN (printed)	1795-2239
ISBN (pdf)	978-952-60-3340-2	ISSN (pdf)	1795-4584
Language	English	Number of pages	88 + 49
Publisher	Department of Micro and Nanosciences		
Print distribution	Department of Micro and Nanosciences		
<input checked="" type="checkbox"/> The dissertation can be read at http://lib.tkk.fi/Diss/2010/isbn9789526033402/			

VÄITÖSKIRJAN TIIVISTELMÄ		AALTO-YLIOPISTO TEKNILLINEN KORKEAKOULU PL 11000, 00076 AALTO http://www.aalto.fi	
Tekijä		Ville Saarela	
Väitöskirjan nimi Mikrovalmistettuja kuumasumutussiruja massaspektrometriaan			
Käsikirjoituksen päivämäärä		18.6.2010	
Väitöstilaisuuden ajankohta		15.10.2010	
<input type="checkbox"/> Monografia		<input checked="" type="checkbox"/> Yhdistelmäväitöskirja (yhteenveto + erillisartikkelit)	
Tiedekunta	Elektroniikan, tietoliikenteen ja automaation tiedekunta		
Laitos	Mikro- ja nanotekniikan laitos		
Tutkimusala	Puolijohdeteknologia		
Vastaväittäjä	Prof. Klaus Bo Mogensen		
Työn valvoja	Prof. Pekka Kuivalainen		
Työn ohjaaja	Prof. Sami Franssila		
<p>Tiivistelmä</p> <p>Puolijohdeteollisuudesta lähtöisin olevia mikrovalmistustekniikoita sovellettiin analyyttisen kemian laitetekniikkaan. Väitöskirja käsittelee lasista ja piistä valmistettuja kuumasumutussiruja, joita käytetään näytteen höyrystämiseen ennen massaspektrometrista analyysiä. Kuumasumutussiruja voidaan käyttää sekä neste- että kaasumaisten näytteiden kanssa ja ne soveltuvat useille eri normaalissa ilmanpaineessa tehtäville ionisaatiotekniikoille, mikä mahdollistaa sirujen laajan sovellettavuuden erilaisten erotusmenetelmien ja analyyttien kanssa. Kuumasumutuksen miniatyrisoinnilla saavutetaan aiempaa parempi herkkyys, monikäyttöisyys ja tarvittavat näytteen ja sumutuskaasun virtausnopeudet ovat pienemmät. Sirut soveltuvat mikrofluidistiikassa tyyppiselle näytevirtauksille välillä 50 nL/min ... 5 µL/min.</p> <p>Työssä kehitettiin ja sovellettiin piin ja lasin etsausmenetelmiä, kiekkosubstraattien liitosmenetelmiä ja ohutkalvotekniikkaa 40 erilaisen kuumasumutussirun valmistamiseen. Lisäksi tutkittiin valmistettujen sirujen lämpöilmiöitä ja siruista lähtevän kaasusuihkun muotoa. Kaasusuihkun lämpöjakauman mittaamiseen kehitettiin menetelmä, joka perustuu tietokoneohjattuun xyz-pöytään kiinnitettyyn pienoistermoparianturiin.</p> <p>Lisäksi tutkittiin erilaisia tapoja tehdä siruille tarvittavat kapillaariputkiliitännät ja integroidun lämmittimen sähköiset kontaktit.</p> <p>Työssä kehitettiin nestekromatografiakolonnisiruja ja yhdistettiin ensimmäistä kertaa nestekromatografiakolonne ja kuumasumutus samalle sirulle. Nestekromatografiasiruiissa on kolonnikanavan loppupäässä suodattimena toimiva mikropilaririvistö, mikä mahdollistaa kolonnin pakkaamisen kiinteäfaasimateriaalipartikkeleilla.</p> <p>Työssä kehitetyt uudet sirut lisäävät käytettävissä olevia ionisaatiotekniikoita ja tutkittavissa olevia analyyttejä verrattuna aiemmin julkaistuihin massaspektrometriasiruihin.</p>			
Asiasanat	lämmitin; massaspektrometria; siru; mikrovalmistus; nestekromatografia; sumutin		
ISBN (painettu)	978-952-60-3339-6	ISSN (painettu)	1795-2239
ISBN (pdf)	978-952-60-3340-2	ISSN (pdf)	1795-4584
Kieli	Englanti	Sivumäärä	88 + 49
Julkaisija	Mikro ja nanotekniikan laitos		
Painetun väitöskirjan jakelu	Mikro- ja nanotekniikan laitos		
<input checked="" type="checkbox"/> Luettavissa verkossa osoitteessa http://lib.tkk.fi/Diss/2010/isbn9789526033402/			

Preface

In May 2003 after two years of studies in the Degree Programme in Electronics and Electrical Engineering at Helsinki University of Technology I was hired as a summer trainee at the Microelectronics Centre that was in charge of the university's newly built cleanroom facilities at Micronova. During that summer I got fascinated by the world of microfabrication and focused my subsequent studies towards the field. I also continued as an employee in the research group lead by Prof. Sami Franssila where I still reside after several organizational changes and the university's transformation into Aalto University. I have enjoyed becoming familiar with the multidisciplinary world of microfluidics and putting the theory into practice. I have learned a lot, but at the same time I have realized that there is so much more to explore. Well, I suppose that is the very nature of science – the work is never truly completed!

I wish to express my warmest thanks to all my co-workers here at Micronova – especially to Prof. Sami Franssila and Prof. Pekka Kuivalainen for instructing and supervising my dissertation, respectively. Thanks to the pre-examiners: Dr. Ciprian Iliescu and Prof. Levent Yobas.

This work would not have been possible without the collaboration with the groups of Prof. Risto Kostianen and Prof. Tapio Kotiaho at the University of Helsinki where the chips I fabricated were put into use with mass spectrometers. Big thanks to all the co-authors of my publications – two of which are shared in the thesis of Dr. Markus Haapala who provided me with plenty of valuable feedback and discussion about improving the chips. Thanks to Dr. Kai Kolari at VTT for the DRIE of silicon and glass. Thanks to William Martin for proofreading the final version of the manuscript.

In summer 2007 I had the opportunity to get two months of hands on experience with micro powder blasting at EPFL, Switzerland. Thanks to Dr. Abdeljalil Sayah for supervising my work during my stay and all the others in Prof. Martin Gijs's group for the hospitality.

I am grateful for the funding and grants provided by CHEMSEM graduate school, TEKES – the Finnish Funding Agency for Technology and Innovation, the Academy of Finland, TES – the Finnish Foundation for Technology Promotion, the Walter Alhström Foundation and the Emil Aaltonen Foundation.

Last, but certainly not least, I am deeply indebted to my family and friends for the love, support and joy you have given me. I love you!

In Espoo, September 2010,

Ville Saarela

Contents

Abstract of doctoral dissertation	iii
Väitöskirjan tiivistelmä	v
Preface	vii
List of publications	xii
Author's contribution	xiii
Abbreviations and symbols	xiv
1 Introduction	1
1.1 Background.....	1
1.1.1 Microtechnology.....	1
1.1.2 Analytical chemistry and mass spectrometry.....	2
1.1.3 Microfluidics, μ TAS, BioMEMS and Lab-on-a-Chip.....	3
1.2 Microchips for mass spectrometry.....	5
1.3 Aim of research.....	6
1.4 Summary of publications.....	6
1.4.1 Publication I: Re-usable multi-inlet PDMS fluidic connector.....	6
1.4.2 Publication II: Glass microfabricated nebulizer chip for mass spectrometry	7
1.4.3 Publication III: Deep plasma etching of glass for fluidic devices with different mask materials.....	8
1.4.4 Publication IV: Microfluidic heated gas jet shape analysis by temperature scanning.....	8
1.4.5 Publication V: On-chip liquid chromatography – atmospheric pressure ionization – mass spectrometry.....	9
1.4.6 Publication VI: Integrated liquid chromatography – heated nebulizer microchip for mass spectrometry.....	9
2 Microfabrication for fluidics	13
2.1 Materials.....	13
2.1.1 Substrate materials.....	13

2.1.2	Thin-film materials and deposition.....	15
2.1.3	Diffusion and high temperature processing.....	16
2.2	Patterning and micromachining.....	17
2.2.1	Lithography.....	17
2.2.2	Etching.....	18
2.2.3	Lift-off patterning and shadow masks.....	19
2.2.4	Polymer micromachining.....	20
2.2.5	Other micromachining methods.....	21
2.3	Silicon micromachining.....	21
2.3.1	Wet etching of silicon.....	21
2.3.2	Dry etching of silicon.....	22
2.4	Glass micromachining.....	24
2.4.1	Wet etching of glass.....	24
2.4.2	Dry etching of glass.....	25
2.4.3	Powder blasting.....	26
2.4.4	Discussion about glass machining.....	27
2.5	Wafer bonding.....	28
2.5.1	Direct bonding.....	29
2.5.2	Anodic bonding.....	30
2.6	Packaging and chip-to-world interfacing.....	30
2.6.1	Fluidic interconnections.....	31
3	Heated nebulizer chips	35
3.1	Different chip designs and fabrication processes.....	35
3.1.1	Substrate materials.....	36
3.1.2	Channel fabrication processes.....	37
3.1.3	Cover wafer bonding.....	40
3.1.4	On-chip heater.....	41
3.2	Lifetime and failure mechanism of the platinum heater	43
3.3	Fluidic and electrical interconnections.....	45
3.4	Jet shape and temperature.....	46
3.5	Applications of the heated nebulizer chips.....	50
4	On-chip liquid chromatography	53
4.1	Review of LC chips.....	53
4.1.1	Materials.....	53

4.1.2	Columns.....	53
4.1.3	Interconnections, sample injection and pumping.....	55
4.1.4	Detection.....	56
4.2	All-glass LC-nebulizer chip.....	56
5	Conclusions and outlook	59
	References	61
	Appendices: Publications I – VI	

List of publications

This thesis consists of an overview and of the following publications which are referred to in the text by their Roman numerals.

- I** Ville Saarela, Sami Franssila, Santeri Tuomikoski, Seppo Marttila, Pekka Östman, Tiina Sikanen, Tapio Kotiaho, and Risto Kostiainen, Re-usable multi-inlet PDMS fluidic connector, *Sensors and Actuators B: Chemical* **114** (2006) 552-557 doi:10.1016/j.snb.2005.06.009
- II** Ville Saarela, Markus Haapala, Risto Kostiainen, Tapio Kotiaho, and Sami Franssila, Glass microfabricated nebulizer chip for mass spectrometry, *Lab on a Chip* **7** (2007) 644-646 doi:10.1039/b700101k
- III** Kai Kolari, Ville Saarela, and Sami Franssila, Deep plasma etching of glass for fluidic devices with different mask materials, *Journal of Micromechanics and Microengineering* **18** (2008) 064010 (6pp) doi:10.1088/0960-1317/18/6/064010
- IV** Ville Saarela, Markus Haapala, Risto Kostiainen, Tapio Kotiaho, and Sami Franssila, Microfluidic heated gas jet shape analysis by temperature scanning, *Journal of Micromechanics and Microengineering* **19** (2009) 055001 (10pp) doi:10.1088/0960-1317/19/5/055001
- V** Ville Saarela, Markus Haapala, Jaroslav Pól, Nisse Kalkkinen, Marko Hukka, Kai Kolari, Raimo A. Ketola, Risto Kostiainen, Tapio Kotiaho, and Sami Franssila, On-chip liquid chromatography - atmospheric pressure ionization - mass spectrometry, *The Proceedings of μ TAS 2007 Conference* **2** (Paris, France, 7–11 October 2007) 1435-1437
- VI** Markus Haapala, Ville Saarela, Jaroslav Pól, Kai Kolari, Tapio Kotiaho, Sami Franssila, and Risto Kostiainen, Integrated liquid chromatography–heated nebulizer microchip for mass spectrometry, *Analytica Chimica Acta* **662** (2010) 163-169 doi:10.1016/j.aca.2010.01.005

Author's contribution

- I The PDMS connector was invented by the author. Experimental work except for the microfabrication of the nebulizer chips and mass spectrometry measurements was performed by the author. The article was written by the author with contribution from the others.
- II All experimental work except for the mass spectrometry was conducted by the author. The article was written by the author with contribution from the others.
- III Design of the APCI chip and partial microfabrication of the samples were carried out by the author. The article was written by Dr. Kai Kolari with contribution from the author and Prof. Sami Franssila.
- IV Microfabrication of the chips and computer simulations were carried out by the author. Thermocouple measurements were done together with Dr. Markus Haapala. The article was written equally by the author and Dr. Markus Haapala with contribution from the others.
- V Layout and process design, microfabrication of the chips and writing of the paper were performed by the author.
- VI Microfabrication and chip layout design were carried out by the author. The publication was written equally by the author and Dr. Markus Haapala.

In addition to the publications above, the author fabricated the heated nebulizer chips and contributed to the writing of other journal articles [1-12] that show different applications of the chips.

Abbreviations and symbols

AFM	atomic force microscope
APCI	atmospheric pressure chemical ionization
API	atmospheric pressure ionization
APPI	atmospheric pressure photoionization
APTSI	atmospheric pressure thermospray ionization
ARDE	aspect ratio dependent etching
CE	capillary electrophoresis
CEC	capillary electrochromatography
CMOS	complementary metal-oxide-semiconductor
COC	cyclic polyolefin (also known as cyclo olefin polymer, COP)
DAPPI	desorption atmospheric pressure photoionization
DRIE	deep reactive ion etching
DSP	double side polished (wafer)
EBL	electron beam lithography
ECDM	electrochemical discharge machining
EDM	electric discharge machining
EDP	ethylenediamine pyrocatechol
EDS	energy dispersive spectroscopy
ESI	electrospray ionization
FIB	focused ion beam
FT-ICR MS	Fourier transform ion cyclotron resonance mass spectrometry
GC	gas chromatography
HN	heated nebulizer
IC	integrated circuit
IPA	isopropyl alcohol, 2-propanol
IS	ionspray
KOH	potassium hydroxide
LC	liquid chromatography
LIF	laser-induced fluorescence
<i>M</i>	molecular weight in unified atomic mass units or daltons (Da)
<i>m/z</i>	mass to charge ratio in mass spectrometry
MEMS	micro electro mechanical systems
MS	mass spectrometry
MS/MS	tandem mass spectrometry
MST	micro system technology
μ TAS	micro total analysis system
NIL	nanoimprint lithography

PDMS	polydimethylsiloxane
PLIF	planar laser-induced fluorescence
RIE	reactive ion etching
SEM	scanning electron microscope
SOI	silicon-on-insulator
SSI	sonic spray ionization
SSP	single side polished (wafer)
T	temperature
TMAH	tetramethylammonium hydroxide
UV	ultraviolet
xyz	three dimensional coordinate system with orthogonal axes

1 Introduction

1.1 Background

This work is about applying microfabrication technology to create instrumentation for analytical chemistry. This section introduces these two fields of science and their multidisciplinary combination.

1.1.1 Microtechnology

Applications of microtechnology have revolutionized the world since the first integrated circuits (IC) were made in the 1950's. Originally, most microfabrication processes have been developed with semiconductor ICs in mind, but the same methods can be applied in countless applications. Our everyday life is full of appliances that have microfabricated parts inside; flat-panel displays, ink-jet printers, acceleration sensors for car airbag systems and game consoles — just to name a few examples — could not exist without the development of microfabrication processes. Even mechanical wrist watches may have small gearwheels made with microfabrication techniques. The abbreviations MST (micro system technology) and MEMS (micro electro mechanical systems) are used with microfabricated non-IC devices that include various sensor and actuator devices and mechanical microstructures.

Microfabrication is based on the addition, patterning and selective removal of layers of various materials on flat substrates. Layer thicknesses range from sub-nanometre to hundreds of micrometers. Microfabrication is ideally suited for mass production because multiple copies of the same component can be made with the same amount of work that is required to make a single component on the substrate. For example, with the fabrication steps that are needed to make a single transistor on a silicon wafer there can be hundreds of individual IC chips on the wafer each consisting of billions of transistors. The famous Moore's law formulated by Gordon E. Moore, the co-founder of the Intel Corporation, in 1965 predicted an exponential growth in the number of components on a single IC chip [13] and the trend has continued already for half a century. This has been enabled by the tremendous advances in several aspects of microfabrication technology. Most importantly the patterning resolution has steadily improved. The minimum linewidth has decreased from 10 μm of the early 1970's to 45 nm used for production today with 32 nm and 22 nm processes in the development phase [14]. For comparison, the diameter of a human hair is over a thousandfold. In this respect it is not difficult to understand that dust-free cleanrooms and protective gowning on the human operators therein are needed for successful microfabrication. Cleanrooms have precise temperature and moisture control in

order to achieve repeatable results with the sensitive process equipment. The microfabrication methods will be further discussed in Chapter 2.

The infrastructure needed for microfabrication is expensive to set up and maintain. Setting up a newest generation IC factory (fab) with a cleanroom and a comprehensive equipment base costs billions of dollars [15] and only a few major companies can afford them. Therefore, the industry relies on mass production in order to keep the business profitable. However, thanks to IC foundries that sell their wafer processing capabilities, it is possible for small fab-less design companies to work in the industry as well. Of course, not all microdevices require a multi-billion dollar manufacturing infrastructure. For example, many MST devices (e.g. fluidics) require minimal processing equipment and the cleanroom requirements may be less strict. Sometimes older generation equipment is sufficient and can be bought refurbished at a fraction of the cost of the latest generation automated production tools.

1.1.2 Analytical chemistry and mass spectrometry

Analytical chemistry is the study of the composition of materials, identification of the molecular components in a sample and their concentrations. Analytical information and methods are widely applied in biomedical applications, environmental monitoring, industrial quality control and forensic science.

A plethora of analytical methods exist and, depending on the specific application, different combinations of them are used for optimal results. Typically, an analytical process can be divided in the following three sub-processes: sample pretreatment (e.g. purification and concentration), separation of the sample components (analytes) and detection. Naturally, for any meaningful results the raw signal of the detector has to be interpreted by a skilled chemist. The flowchart of an analytical method is shown in Figure 1.1. Liquid chromatography–mass spectrometry (LC–MS) is a widely used analytical technique which has also been used in this work.

In liquid chromatography (LC) a liquid sample plug is introduced to an eluent flowing through a porous column. With proper eluent composition the analytes may be adsorbed and thus concentrated at the beginning of the column. By changing the eluent composition the analytes will then start passing through the column where different components of the

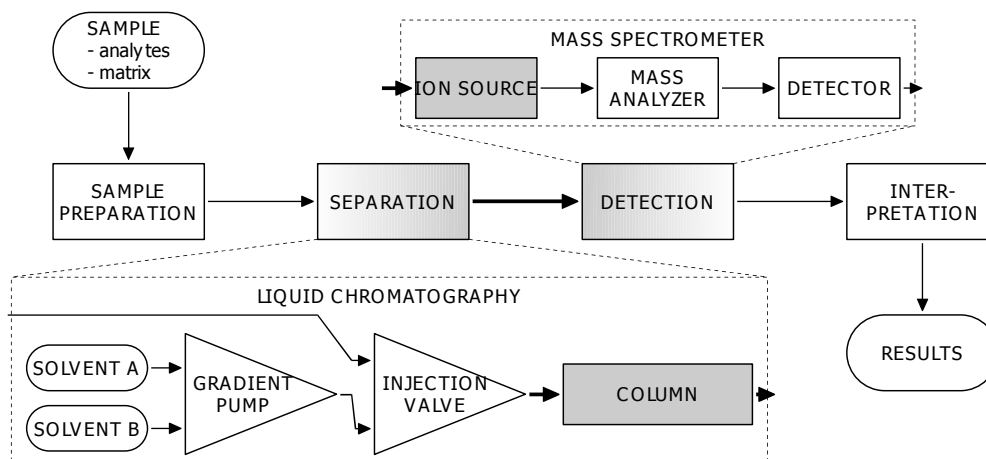


Figure 1.1: Flowchart of a generic analytical method with schematic details of liquid chromatography and mass spectrometry as possible choices as the separation and detection methods. This work deals with the highlighted parts.

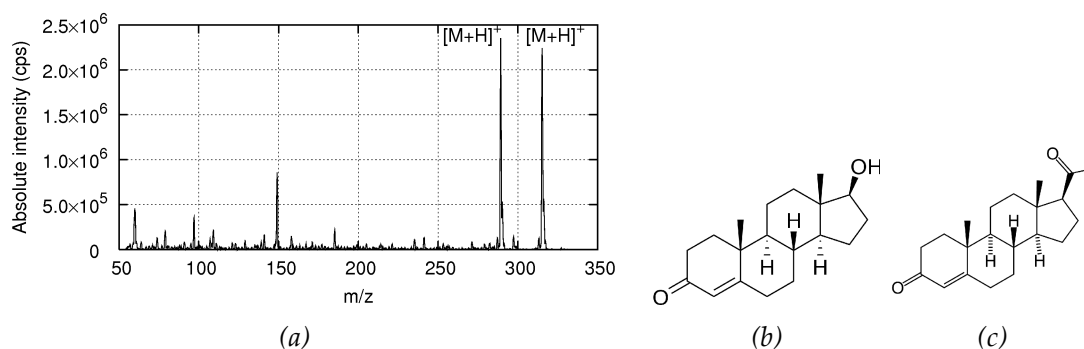


Figure 1.2: (a) Mass spectrum of testosterone ($M = 288$) and progesterone ($M = 314$) using APPI. Concentration of both analytes was $1 \mu\text{mol L}^{-1}$ and sample flow rate was $5 \mu\text{L min}^{-1}$. **[II]** Molecule structure of testosterone (b) and progesterone (c).

sample adsorb and desorb between the stationary (particles packed in the column) and the mobile (eluent) phases at different rates leading to spatial separation of the sample components. A detector placed at the end of the column provides a chromatogram containing the detector signal as a function of time. LC will be further discussed in Chapter 4.

Mass spectrometry (MS) is a very powerful analytical method offering both high sensitivity and specificity. Mass spectrometers measure the mass-to-charge (m/z) ratios of ions and from the mass spectra it is possible to identify the sample compounds by their molecular masses. Large molecules can be fragmented into several ions producing characteristic peaks in the mass spectrum. A liquid sample needs to be vaporized and ionized prior to analysis and detection in a mass spectrometer. For higher analytical performance, a sample separation step, such as LC, is typically done before the ionization and detection. In this way it is easier to identify different sample components from the mass spectra. There are several ionization methods and the optimal choice depends on the sample type. Atmospheric pressure ionization (API) methods are widely applied for introducing liquid samples into mass spectrometers [16]. A common API method is atmospheric pressure chemical ionization (APCI) where the sample is sprayed by a heated nebulizer which vaporizes and mixes the sample with nebulizer gas. The mixture is directed towards the ion inlet of a mass spectrometer. A sharp needle with high electric potential is used for ionization. A corona discharge takes place at the tip of the needle leading to ionization of the analytes via complex gas phase charge transfer processes before the inlet. Another ionization method, atmospheric pressure photoionization (APPI), is similar to APCI but a 10 eV photon energy photoionization lamp is used to initiate the ionization. Figure 1.2 shows a mass spectrum of protonated analytes with APPI-MS. Ionization methods utilizing microchip technology will be further discussed in Sections 1.2 and 3.5.

1.1.3 Microfluidics, μTAS , BioMEMS and Lab-on-a-Chip

Microfabricated separation and ionization chips are examples of microfluidic devices. The best known microfluidic devices are ink-jet printer heads that have the highest commercial value with estimated 28% share of the \$6,000 million total value of the MEMS market [17]. Ink-jet heads contain an array of tiny nozzles that shoot out picolitre-size droplets ($\sim 1 \mu\text{m}$ diameter spheres) of ink. Other applications for micronozzles can be found, for example, in micropropulsion engines for miniaturized satellites [18], liquid dispensers [19], steam

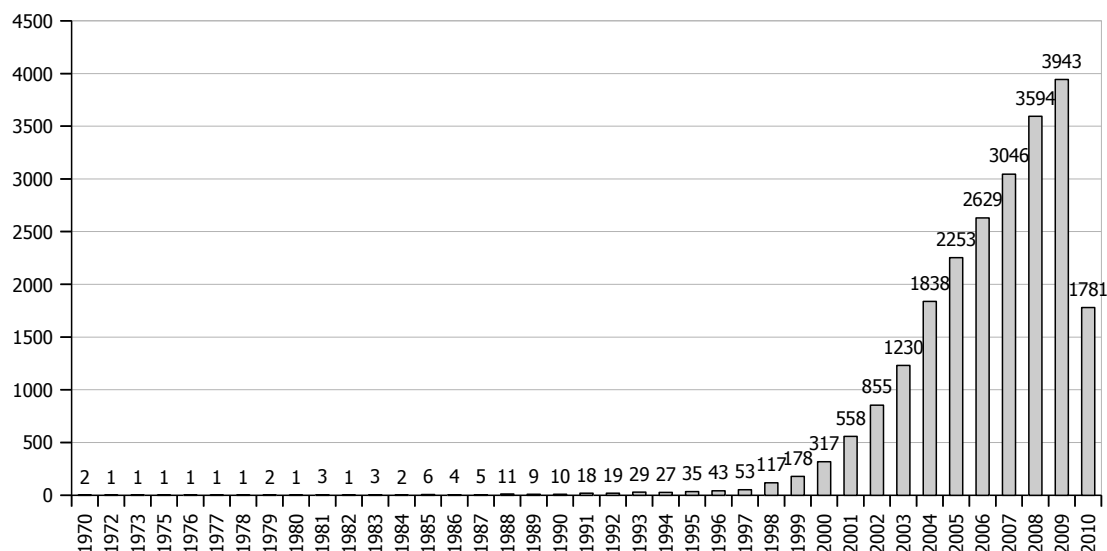


Figure 1.3: Number of references found by SciFinder Scholar containing the concept 'microfluidics' between years 1970–2010. (Status of June 17th 2010.)

locomotive power generator [20], micro flame ionization detector [21] and the heated nebulizer (HN) chips of this dissertation. A seminal example of a microfluidic chip for analytical chemistry is the gas chromatograph made on a two inch silicon wafer by Terry et al. in 1979 [22]. In 1990, Andreas Manz conceived a concept called the miniaturized total chemical analysis system [23] that has since then been established as μ TAS (micro total analysis system) [24]. The number of yearly publications containing the concept 'microfluidics' has been increasing for two decades as shown by the statistics in Figure 1.3. BioMEMS is sometimes used as an alternative term for microfluidics, but the applications are focussed for biological analytes, such as viruses, bacteria, cells and DNA. Term "lab-on-a-chip" is also frequently used in conjunction with chips for analytical chemistry.

μ TAS holds a great promise from scientific, commercial and health care point of views. For example, rapid point-of-care or even home diagnosis tools can help in treatment of diseases [25]. In micro and nano scale different phenomena can become dominant. For example, fluid flow will be laminar, instead of turbulent and mixing will only take place through diffusion. Miniaturization of analytical tools has several potential advantages:

- Suitability for smaller sample volumes because of smaller dimensions and smaller dead volumes.
- Higher sensitivity because analytes can be more precisely guided to the detector.
- Faster analysis because of faster transportation and diffusion over short distances.
- Integration of several analytical steps on a single device, for example, drop metering, mixing, thermal reactions, electrophoresis and detection [26].
- A plethora of suitable detection methods based on various electrochemical [27] and optical [28] principles or mass spectrometers [29,30].
- Improving a key part in a larger system (this work) or
- Portable instruments after complete miniaturization of the system.
- Easy mass production and lower manufacturing cost of batch fabrication compared to conventional machining.

To date the examples of lab-on-a-chip devices that do not require any additional instrumentation are few. Most publications concentrate on the miniaturization of a single or a couple of functions and rely on external equipment for sample pretreatment, pumping, power, detection or output of the results. In many cases it might be more appropriate to talk about chip-in-a-lab instead of lab-on-a-chip. Also, the benefits of miniaturization are sometimes exaggerated. For example, the fabrication cost of microfluidic devices may be very high if only a few devices are produced in a cleanroom with high capital and running costs. Also, some microfabrication processes are still experimental and unsuitable for mass production because of repeatability problems and low yield. The economics are analogous to the semiconductor industry where high utilization rate of production equipment is crucial for a profitable business. Nevertheless, μ TAS technology and applications are constantly evolving and in the near future plenty of success stories should arise from the field. The acceptance and validation of revolutionizing new technology always takes time.

1.2 Microchips for mass spectrometry

Mass spectrometers enable accurate detection of the smallest amounts of sample. In principle a single ion could be detected. Microfluidic devices operate with small sample flows and, therefore, mass spectrometric detection is well suited for use with microfluidic devices. During the past decade, microchip technology has been applied in ion sources, mass analysers and even in complete miniature mass spectrometers [29].

Electrospray ionization (ESI) has gained the widest interest from the microfabrication community [29,31,30]. In principle, the implementation of an ESI source is straightforward as it only requires a high voltage preferably applied to a sharp tip. This dissertation work has been a part of larger research project where also different ESI microchips have been developed made of SU-8 [32] and silicon [33]. On-chip capillary electrophoresis (CE) separation has also been integrated to the SU-8 ESI source [34]. Others have reported microchips that combine LC and ESI with either monolithically integrated [35-37] or hybrid integrated [38] emitters. Agilent Technologies Inc. has a commercial LC-ESI chip platform based on laser ablated polyimide films [35,39-44]. LC chips will be further discussed in Section 4.1.

Although ESI is convenient with microchips it is not capable of ionizing all kinds of sample molecules. Nonpolar molecules are not efficiently ionized by ESI [45]. In contrast, other atmospheric pressure ionization methods, such as APCI and APPI are applicable to less polar and nonpolar samples. The HN chip is an essential part of the miniaturized APCI and APPI methods. The fabrication, properties and applications of the HN chips will be covered in Chapter 3.

Desorption ionization methods are used in combination with microchips as well. Matrix-assisted laser desorption/ionization (MALDI) plates can be prepared with microfluidic dispensers [31]. Porous silicon desorption plates have been demonstrated [46]. In desorption ESI (DESI) both microfabricated nebulizers [47] and microfabricated desorption surfaces [48] can be used. Also the HN chips are suitable for desorption ionization as will be discussed in Section 3.5.

Most of the work on ionization chips has been done with ordinary mass spectrometers that are of the size of a refrigerator. Nevertheless, miniaturized mass spectrometers have also been developed [49] and a complete mass spectrometer has been enclosed in the size of

a shoebox allowing portability [50]. Mass analysers are based on ion trap, quadrupole or time-of-flight principles, or on electrostatic and magnetic filters [29,51]. So far, the analytical performance — in terms of mass range, resolution and accuracy — of miniaturized mass spectrometers has been inferior compared to ordinary mass spectrometers. For example, a typical miniature mass spectrometer offers a mass range (m/z) of a few hundred with unit resolution whereas a typical laboratory mass spectrometer has a few orders of magnitude better performance values. Therefore, the current miniature mass spectrometers can only be applied in some special applications, where small size or low price outweigh the performance, such as space exploration or process monitoring, respectively. The miniaturization of mass spectrometers is mostly limited by the size and power consumption of the required vacuum pumps.

1.3 Aim of research

This work deals with the microfabrication, materials and integration of the HN chips. The first prototypes of the chips were published in [52-54] and they have a patent pending [55]. The HN chips are used to vaporize a sample, mix it with a nebulizer gas and spray the mixture out for analysis in a mass spectrometer. Various aspects of the HN chips were further developed and studied during this work. These include:

- Layout of the fluidics and heater (**II** and Section 3.1)
- Different fabrication processes (**II**, **III** and Section 3.1)
- Lifetime of the chip (Section 3.2)
- Fluidic and electrical interconnection schemes (**I** and Section 3.3)
- Characterization of jet shape (**IV** and Section 3.4)
- Development of new applications for the chip (Section 3.5)
- Optimization of the chip for different applications (Section 3.5)
- Development on a pillar frit LC column chip (**V** and Chapter 4)
- Integration of an LC column to the HN chip (**VI** and Chapter 4)

1.4 Summary of publications

1.4.1 Publication I: Re-usable multi-inlet PDMS fluidic connector

Publication I addresses an important practical issue with microfluidic chips by presenting a method for connecting small tubes to microfluidic chips. A connector block with holes for the tubes is cast from polydimethylsiloxane (PDMS). The mould has a matching surface topography as the fluidic chip for which the connector is intended for enabling easy alignment of the connector and the chip. When the connector block is contacted with the chip a leak tight connection is formed due to the self sealing nature of PDMS. It reversibly adheres to various polished surfaces, such as glass and silicon. The pressure tolerance of the connector can be increased with an additional compressing fixture or by making the PDMS bonding permanent by oxygen plasma activation prior to contacting of the surfaces. Various leakage tests were conducted. Figure 1.4 shows a comparison of the PDMS connector with commercial NanoPort connectors. The chip size in an early HN chip design was limited by the area required by the three NanoPort connectors. Significant chip size

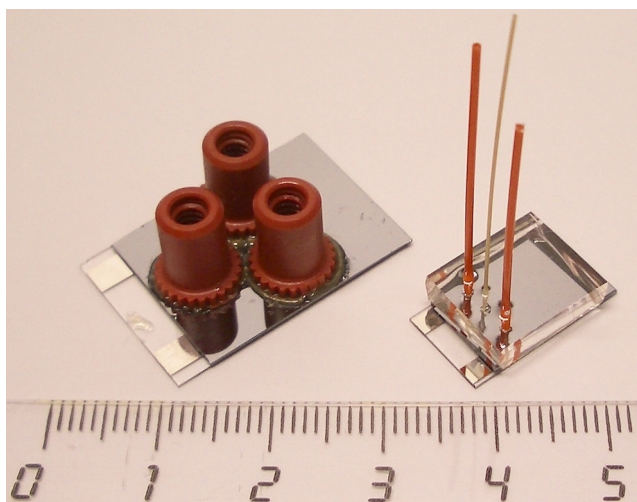


Figure 1.4: Nebulizer chips with three NanoPort connectors (left) and a PDMS connector (right). [I].

reduction was possible when using a PDMS connector. Fluidic interconnection schemes will be further discussed in Sections 2.6.1 and 3.3.

Although the PDMS connector principle is mechanically working, other connection methods have been used with the HN chips after the publication of the paper. The operating temperature of the HN chips is too high for PDMS and the outgassing from PDMS increases background noise in mass spectra. Therefore, the use of PDMS connectors is limited to room temperature applications or in use with less sensitive detection methods than mass spectrometry.

1.4.2 Publication II: Glass microfabricated nebulizer chip for mass spectrometry

The first generations of HN chips were fabricated from silicon and glass substrates [52,56]. Publication II describes how these chips can be made from two glass wafers. In addition, a fluidic connection method that uses a custom made holder and a commercial flat-bottom fitting is presented (see Figure 1.5). Through-wafer glass wet etching is done with an LPCVD silicon hard mask. Alternative approaches to glass-to-glass bonding and platinum patterning are evaluated. Compared with silicon–glass nebulizer chips the all-glass design enables higher on chip thermal gradients – thanks to the lower thermal conductivity of glass. This enables higher operating temperature at the vaporizer end of the chip as the interconnections end can remain at a lower temperature. Different chip materials and fabrication processes will be further discussed in Section 3.1.

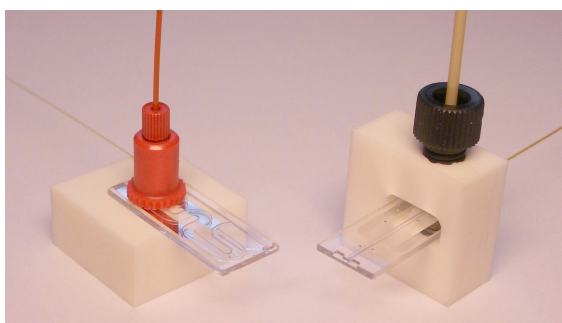


Figure 1.5: All-glass nebulizer chips with a NanoPort connector and a custom made holder. [II]

Similar all-glass HN chips are still being fabricated in the follow-up research project MISIMA but there has been modifications to the chip layout and the glass-to-glass bonding process has been fine-tuned to give better yield.

1.4.3 Publication III: Deep plasma etching of glass for fluidic devices with different mask materials

Deep reactive ion etching (DRIE) of Pyrex and silica glass substrates is demonstrated in publication III with the use of four different masking materials: silicon shadow mask, electroplated nickel, LPCVD amorphous silicon and SU-8. Over 100 μm etch depth was achieved with nearly vertical side wall profiles. The challenge in glass DRIE etching is limited selectivity between the etch rates of glass and the mask material. Fairly good selectivity (up to 35:1) is obtained with silica glass. However, Pyrex glass contains metal oxides that do not produce volatile etch products and hence requires more physical etching. Therefore, mask selectivity is reduced by one decade compared to silica glass. Figure 1.6 shows a nebulizer chip nozzle structure etched with a silicon shadow mask. Glass micromachining methods including plasma etching will be further discussed in Section 2.4.

The presented glass DRIE methods have been applied in the fabrication of both HN chips (see Section 3.1.2) and integrated LC–HN chips (Section 4.2). However, because of added process complexity and lack of a high selectivity Pyrex glass etch process these experiments are currently on hold.

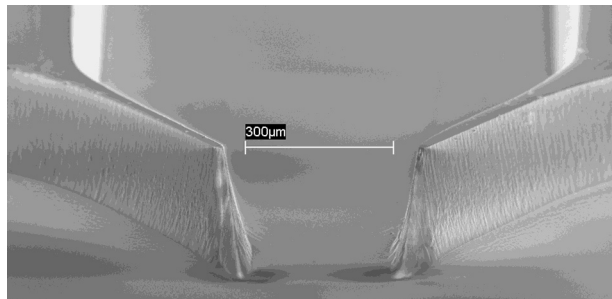


Figure 1.6: Nebulizer chip nozzle structure DRIE etched in Pyrex glass. [III]

1.4.4 Publication IV: Microfluidic heated gas jet shape analysis by temperature scanning

Publication IV presents a new measurement technique for determining the temperature distribution of a gaseous jet. A miniature thermocouple is attached to a computer controlled xyz stage which scans over the jet. Temperature data with spatial resolution below 100 μm is easily achieved. The jet shapes from two different nebulizer chip nozzles are compared. A computer simulation was done to study the relationship between temperature and velocity distributions. A previously unpublished 3D temperature measurement of a jet produced by a HN chip is shown in Figure 1.7.

The thermocouple scanning method has been used to study differences in jet shapes with different nozzles. The shape of the jet from a HN chip has an influence on both ionization and ion collection efficiencies. HN chip jet shape measurements will be further discussed in Section 3.4.

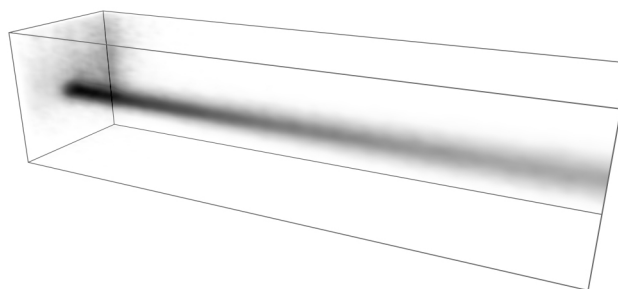


Figure 1.7: $3 \times 3 \times 12 \text{ mm}^3$ 3D temperature scan of a gas jet coming from the rear left. The darker the colour, the higher the temperature. Measured with the technique presented in publication IV.

1.4.5 Publication V: On-chip liquid chromatography – atmospheric pressure ionization – mass spectrometry

A microfabricated LC column with a micropillar frit is presented in publication V. The chip consists of bonded silicon and glass wafers with DRIE etched channels in the silicon part. The LC column is a 40 mm long, 200 μm wide and 170 μm deep meandering channel and it ends in an array of 5 μm diameter pillars with 5 μm gaps. Layout of the LC chip is shown in Figure 1.8 (a). Either optical detection, such as laser-induced fluorescence (LIF), through the glass cover can be used or the LC outlet can be connected to an external detector via tubing. The tubes are inserted from the side of the chip and sealed with glue. The LC column is packed with particles prior to use. The inlet capillary used during packaging will be filled with particles too, but it can be easily removed by snapping a 5 mm part of the chip away and inserting a fresh capillary to the column. The break up point is determined by a shallow cut made with a dicing saw during the dicing of the wafer.

Mass spectrometric detection was demonstrated by connecting the LC chip to a HN chip for APCI (Figure 1.8 (b)). This LC chip design was an intermediate step on the way towards an integrated chip with both the LC column and the heated nebulizer on the same chip. The integrated chip is presented in publication VI.

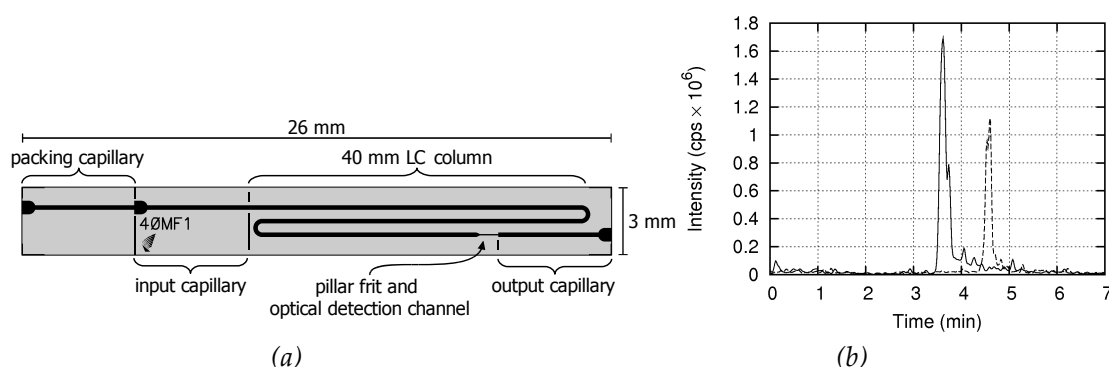


Figure 1.8: (a) Layout of the liquid chromatography chip. (b) Extracted ion chromatograms of corticosterone (solid line) and 5α -pregnan- 3β -ol-20-one (dashed line) measured with LC-APCI-MS. [V]

1.4.6 Publication VI: Integrated liquid chromatography – heated nebulizer microchip for mass spectrometry

Publication VI describes a silicon–glass HN chip with a integrated LC column (LC–HN chip). The LC column of the integrated chip has a similar micropillar frit as the LC chip in

publication V. However, the column is straight and the interconnections are done with through-holes in the silicon part. The construction of the chip is illustrated in Figure 1.9. In addition to the LC inlet, the chip has inlets for nebulizer gas which is mixed with the LC eluent flow at the end of the LC column. A vaporization channel ends to a nozzle at the edge of the chip. The glass cover has separate platinum heater elements for the LC column and HN part of the chip. However, the LC column heating was not yet used in the experiments presented in the publication. Figure 1.10 shows the LC–HN chip with its fluidic connector and water cooler blocks. Cooling was necessary to prevent excess heating of the LC column part because a lot of heat would otherwise be conducted the vaporizer part of the chip. Silicon is an excellent thermal conductor.

The chips were successfully tested using both optical and MS detection. Figure 1.11 shows the separation of two fluorescent compounds detected by LIF after the micropillar frit. Results from a LC–APPI–MS/MS experiment are shown in Figure 1.12. MS/MS denotes tandem mass spectrometry. The results show clear separation of the analytes but the peaks in the chromatograms are tailing. Ideally, the peaks should have a sharp Gaussian profile.

LC chips will be further discussed in Chapters 4 and 5.

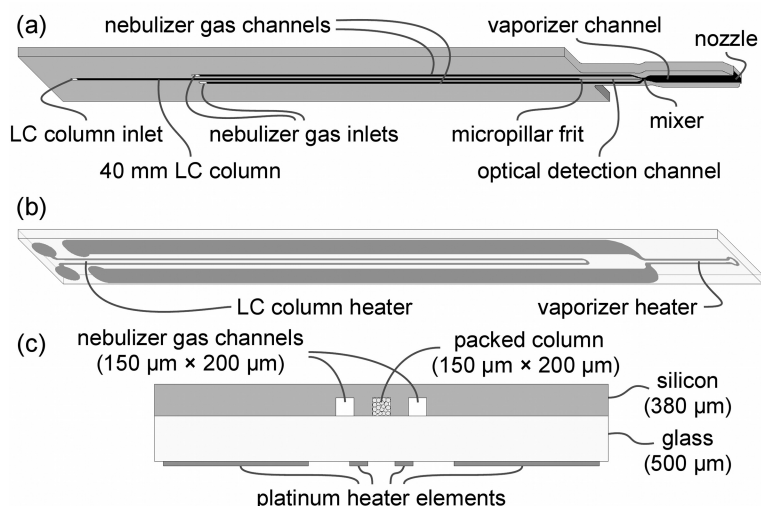


Figure 1.9: Layout of the 55 mm × 5 mm LC–HN chip. A silicon chip (a) with etched structures is anodically bonded with a glass cover (b) with heater elements. (c) Chip cross-section at the column section. [VI]

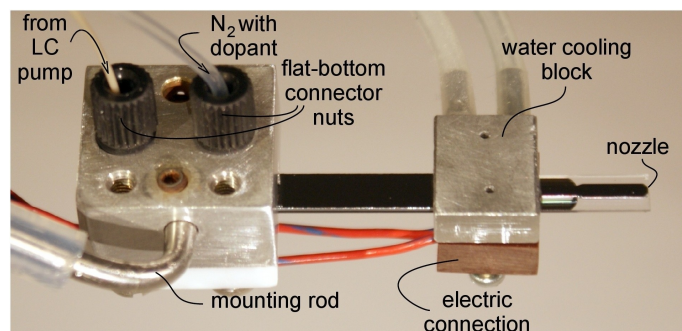


Figure 1.10: The integrated LC–HN chip with its fluidic connections, and the water cooler block with electrical connections. [VI]

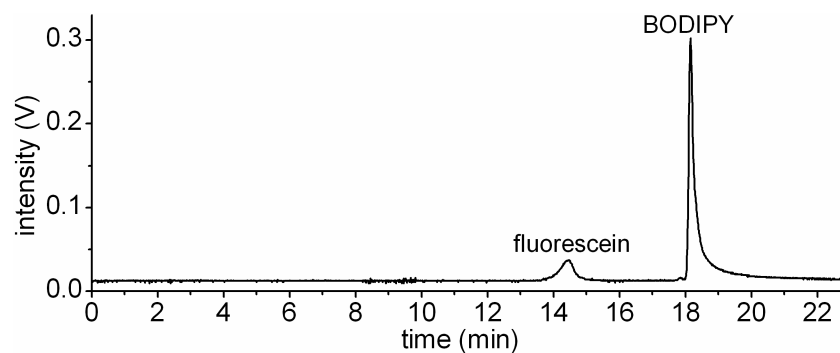


Figure 1.11: Chromatogram of fluorescein and BODIPY® 493/503 separated and detected by microchip LC-LIF. Concentrations were 1 μM and injection volume was 0.1 μL . [VI]

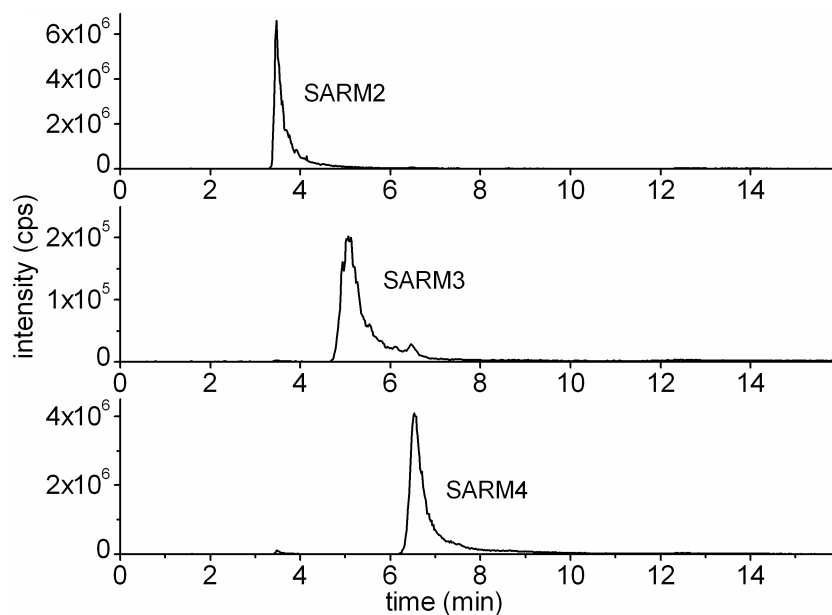


Figure 1.12: Selected reaction monitoring chromatograms of three different compounds (selective androgen receptor modulators, SARM) measured by chip LC-APPI-MS/MS. Concentrations were $10 \mu\text{g mL}^{-1}$ and injection volume 0.5 μL . [VI]

2 Microfabrication for fluidics

Microfabrication methods can be applied in countless ways to produce different components. Figure 2.1 lists the basic microfabrication processes steps that each have numerous alternative practical implementations. A fabrication process starts with choosing a suitable substrate, e.g. a silicon wafer, and then the process continues with thin-film deposition, diffusion or etching into the wafer. In principle, all processing affects the whole surface of the substrate or at least one side of the substrate. Patterns are generated through lithography. Typically, a substrate contains multiple copies of a component and at the end of the processing the substrate is diced and the chips are individually packaged. This chapter reviews the basic microfabrication process steps from the viewpoint of fluidic devices – the HN chips in particular. For additional information and other applications there are plenty of good books [57-61].

2.1 Materials

Materials for microfabrication can be divided into two categories: substrate and thin-film materials. Early CMOS ICs were composed of only five elements: Si, O, B, P and Al. Silicon substrates were doped with boron and phosphorous. Thin-films of silicon dioxide and aluminium were used as electrical insulators and conductors, respectively. In principle, all elements, compounds and alloys can be applied in microfabrication. However, most cleanrooms are made for IC processing which limits the allowed materials therein. For example, even the smallest traces of alkali, noble and transition metals have detrimental effects on the electrical properties of semiconductors. IC compatible materials and chemicals can be obtained in very pure and well controlled form with extremely low levels of contaminating agents. For microfluidic components the IC compatibility is usually not an issue and therefore the range of materials used for fluidics is wider – although sometimes limited by restrictions in shared cleanrooms.

2.1.1 Substrate materials

The most common substrates in microfabrication are single crystal silicon wafers. The diameter of the wafers has increased along with the development of manufacturing technology from 1 inch of the early days of ICs to 450 mm that are expected to come in industrial use in a few years [15]. Usually, all the process equipment in a cleanroom is dedicated to a single wafer size, for example, at TTK Micronova 100 mm wafers are used. Smaller substrates can in some cases be processed using the same equipment with additional fixtures or by temporary gluing to normal size carrier wafer. However, when moving into larger substrates the equipment base needs to be renewed which is very expensive.

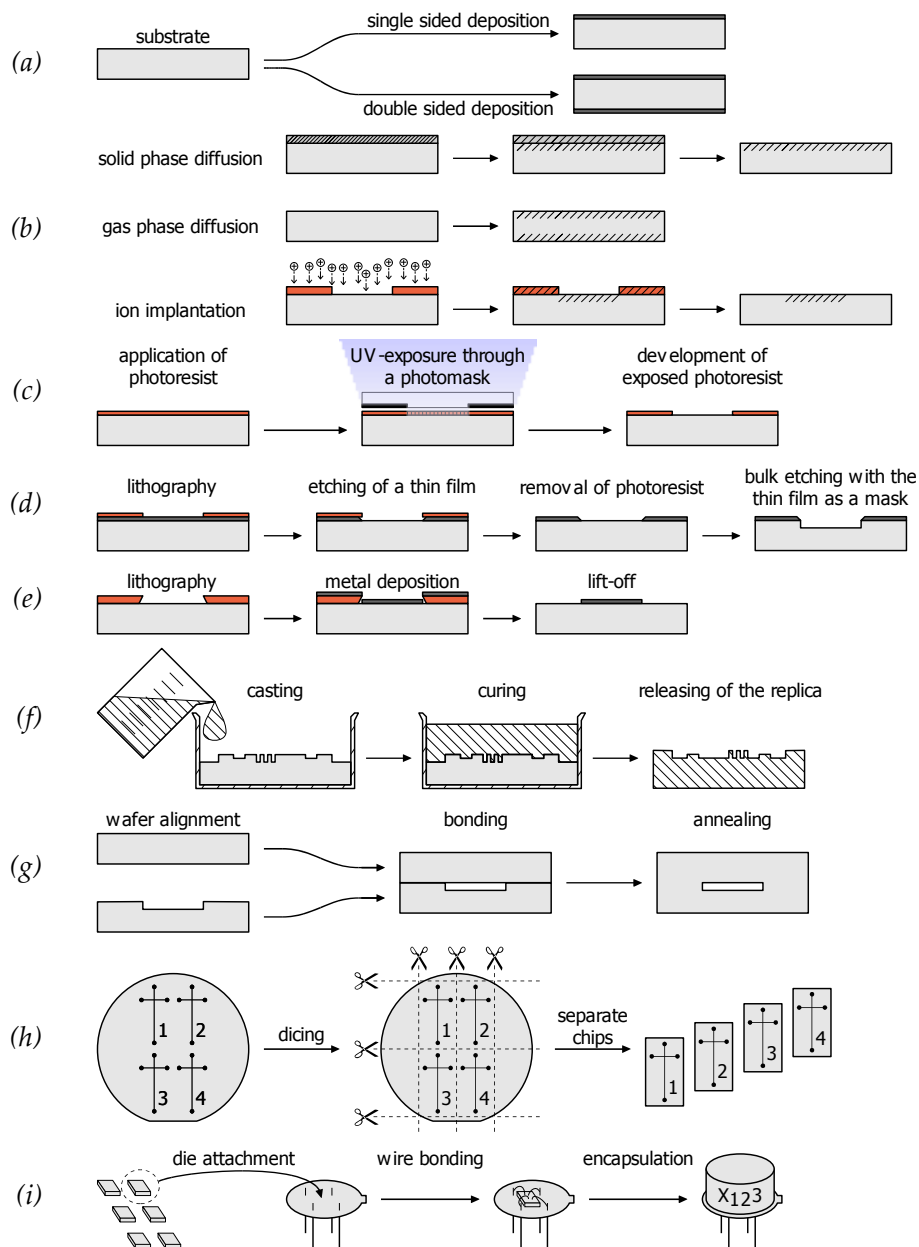


Figure 2.1: Basic microfabrication processes steps: (a) thin-film deposition, (b) diffusion, (c) lithography, (d) etching, (e) lift-off, (f) master replication, (g) wafer bonding, (h) wafer dicing and (i) packaging.

In fluidic applications, glass wafers are often used as substrates in addition to silicon wafers. The advantages of glass are optical transparency, electrical insulation and good chemical resistance. In addition, it is possible to tailor a lot of the material properties by adjusting the composition of the glass. A good book about microstructuring of glasses was recently published [57]. Two most common glass types that are available in wafer format are fused silica and borosilicate glasses. Fused silica is pure SiO_2 in amorphous form. Borosilicate glass brand names include Corning Pyrex 7740 and Schott Borofloat 33. They contain approximately 81% SiO_2 , 13% B_2O_3 , 4% Na_2O , 2% Al_2O_3 and traces of other compounds. The coefficient of thermal expansion of borosilicate glasses is close to that of silicon, which is important if they are bonded with silicon wafers. Different bonding methods will be discussed in Section 2.5.

The typical thickness range of 100 mm diameter wafer is 300...1,000 μm and the wafer has a 32.5 mm flat for aiding both physical and crystal orientation alignment. Single crystal silicon wafers can be polished to atomically smooth surface with RMS roughness below 0.5 nm. Glass polishing is more challenging but typical surface roughness is below 2 nm. There are both single side polished (SSP) and double side polished (DSP) wafers. SSP wafers are used in IC processing, but MEMS often requires DSP wafers.

Several fluidic devices are made on polymer substrates [62]. They have potential for cheap and disposable mass production. Polymers are composed of long organic molecules which offer wide selection of different physical and chemical properties. Polymers have limited temperature tolerance and they are usually intended for room temperature operation. Nevertheless, some polymers can tolerate temperatures slightly above 300 $^\circ\text{C}$ and in the case of polyimide thin-films even up to 450 $^\circ\text{C}$ [63].

Table 2.1 lists some key properties of substrate materials. Depending on the composition of glasses and polymers they offer a wide range of different material properties. Naturally, most material properties are temperature dependent.

Table 2.1: Selected properties of different materials at room temperature.

	Density (g cm^{-3})	Resistivity ($\Omega \text{ cm}$)	Thermal conductivity ($\text{W m}^{-1} \text{ }^\circ\text{C}^{-1}$)	Coefficient of thermal expansion ($10^{-6} \text{ }^\circ\text{C}^{-1}$)	Melting /softening point ($^\circ\text{C}$)	Young's modulus (GPa)
Silicon	2.33	$10^{-5} \dots 10^4$ ^(a)	150 ^(a)	2.6	1,400	180 ^(b)
Fused silica	2	10^{16}	1.3	0.55	1,650	70
Pyrex 7740	2.24	10^6	1.13	3.25	821	63
Platinum	21.45	10.6×10^{-6}	71.6	8.9	1770	160
Polymers ^(c)	0.9 ... 2	$10 \dots 10^{18}$	0.1 ... 0.4	10 ... 100	90 ... 410	0.01 ... 4

^(a) Doping dependent

^(b) Crystal orientation dependent

^(c) Typical property ranges for the material category

2.1.2 Thin-film materials and deposition

In microfabrication, thin layers of different materials are deposited on the substrate (Figure 2.1 (a)). Thin-films with thickness ranging from atomic layers to several micrometers can be deposited on a substrate with various methods. Physical vapour deposition (PVD) methods such as vacuum evaporation and sputtering are mostly used to deposit metal films. Dielectric and semiconductor thin-films are usually deposited using chemical vapour deposition (CVD) methods. PVD films are deposited only on one side of the substrate at a

time, but some CVD processes can deposit on both sides simultaneously. Low pressure CVD (LPCVD) and plasma enhanced CVD (PECVD) are the two dominant CVD methods. Thin-films can also be deposited in liquid form by applying a drop on the wafer and then spinning the wafer for the drop to spread out throughout the wafer surface. This is called spin-on coating. Electroplating is another method where the deposited material comes from liquid solution.

The properties of thin-films are very diverse and they usually differ from the properties of the corresponding bulk material. For example, the resistivity of metal thin-films are frequently two times higher than the table value for the bulk metal. Relevant film properties include elemental composition (stoichiometry), microstructure (amorphous vs. polycrystalline vs. single crystal), film stress (tensile vs. compressive), thickness uniformity (across wafer), step coverage (over topography) and surface roughness. The exact properties depend from the deposition method, equipment and process variables such as deposition chamber pressure, gas composition, temperature, applied electric field, plasma power and frequency. Sometimes repeatable results are not easy to obtain, especially in a research environment where the same equipment is used for multiple processes.

Some materials and deposition methods are incompatible. Thermal budget and contamination issues have to be considered beforehand, because they can limit the applicable deposition methods. In general, no high temperature processes above 450 °C are allowed after deposition of metals to ensure contact stability between silicon and metal or to avoid softening and deformation of glass.

2.1.3 Diffusion and high temperature processing

Diffusion is concentration gradient driven movement of material. Concentration differences will gradually smooth out with a rate exponentially proportional to temperature. In microfabrication, various high temperature process are used to modify the surface layer of the substrate or a thin-film or to promote reactions that would not occur at room temperature where diffusion is usually negligible. Different diffusion methods are presented in Figure 2.1 (b). Group III or V elements are diffused into silicon to change the conductivity at the subsurface region of the substrate. For example, boron doping can be made either by applying a boron-rich spin-on-glass film on the substrate and then annealing at high temperature (solid phase diffusion) or by adding BCl₃ gas to the annealing atmosphere (gas phase diffusion) or by exposing the wafer with accelerated B⁺ ions (ion implantation) followed by activation annealing.

Thermal oxide is frequently used in the fabrication of microfluidic components. Thermal oxidation of silicon is a thin-film deposition process where oxygen diffuses through the surface oxide layer to react with underlying silicon. Oxidation furnace temperatures are from 900 °C to 1,200 °C with either oxygen (dry oxidation) or water vapour (wet oxidation) in the furnace atmosphere. Compared to CVD deposited oxides, thermal oxidation provides superior quality SiO₂ layers. Oxide layers are used for several purposes, for example, as etch masks, electrical insulators, adhesion or etch-stop layers.

Semiconductor pn-junctions can be used as detectors but, in general, microfluidic components rarely utilize the electronic semiconductivity of silicon. However, the doping dependent material properties have other applications, too. For example, diffused silicon resistors can be used as heaters and optical waveguides can be made by doping oxide films. Doping and crystal orientation determines silicon piezoelectricity which can be utilized for

measuring strain of cantilever structures. Membranes with precise thickness control can be achieved with the help of doped etch-stop layers (further discussed in Section 2.3.1).

2.2 Patterning and micromachining

For most practical applications, it is not enough to have layers of thin-films covering the whole substrate. Instead, the thin-films are patterned and recesses are made to the bulk of the substrate. The pattern making mostly relies on lithography and etching. These processes are discussed in this section along with some less conventional ways for micromachining.

2.2.1 Lithography

Lithography is the basis of making patterns on the substrate. Historically, different kind of lithography and etching have been used by artists and printers for centuries before they were adapted by the microfabrication industry. Also in microfabrication there are various lithography processes (optical lithography, electron beam lithography, X-ray lithography etc.) but they all follow the same basic procedure. The basic steps of photolithography are illustrated in Figure 2.1 (c). First, a thin layer of photoresist is applied on a substrate. Then, the photoresist is exposed with a mask pattern followed by development of the photoresist leaving a patterned photoresist layer on the substrate. This layer can then be used as a mask in subsequent processing, for example, in etching.

Optical lithography is the dominant technique for microfluidics. The photoresist is sensitive to ultraviolet (UV) light and the exposure is done through a transparent photomask with opaque patterns. Typically, a glass plate with patterned chromium thin-film is used as the photomask. A five inch square photomask with 1 μm minimum feature size costs about €500. For rapid prototyping of many microfluidic devices lower resolution photomasks are sufficient. Around 100 μm patterns can be printed on transparency films with ordinary office laser printers. Laser photoplotter films that are used in the manufacture of printed circuit boards have a minimum feature size of about 20 μm and they cost only a few Euros. However, the pattern edges are not sharp but have several micrometres of ripple. In addition to the resolution of the photomask, diffraction limits the maximum resolution of optical lithography. Diffraction depends on the wavelength of the light source, the photoresist thickness and distance between the photomask and the substrate. In contact lithography, the photomask and wafer are contacted during exposure and the whole wafer is exposed simultaneously. Step-and-repeat aligners can have reducing optics between the photomask and substrate. Step-and-repeat aligners are more expensive than simple contact aligners but on the other hand they can reduce photomask costs as smaller mask area or pattern resolution is sufficient for reproducing similar patterns in photoresist.

Photoresists are divided into two categories: positive and negative tone photoresists. A positive tone photoresist is rendered soluble upon exposure whereas an exposed negative tone photoresist will cross-link further preventing it from dissolving in the developer. AZ5214E photoresist from Clariant is a special photoresist that can be used both as positive and negative tone photoresist. With normal process sequence (spinning, pre-bake, exposure, development, post-bake) it is a positive tone photoresist. However, two additional process steps after the exposure (baking followed with a flood exposure without

a photomask) will result in a photoresist layer with the negative image of the mask pattern. Various photoresist chemistries exist with wide range of properties such as thickness, resolution, exposure sensitivity, sidewall profile, temperature and chemical tolerances.

There are also other means to pattern a photoresist in addition to optical lithography. These methods are also used for fabricating photomasks. Down to 0.6 μm feature size can be patterned using laser lithography systems [64]. Ultimate resolution is achieved with electron beam lithography (EBL) which uses a focused electron beam to expose the photoresist. The beam itself can be only a few nanometres in diameter but the exposed resist area will be larger due to electron scattering. There is plenty of activity in the development of EBL resists [65]. Sub-100 nm features are patterned on a routine basis but sub-20 nm resolution is still in the development phase. The major problem of EBL is limited throughput. Scanning over a large area takes long time, even several days, which renders EBL unsuited for mass production. Another type of lithography is nanoimprint lithography (NIL) where a master with the desired pattern as 3D surface topography is pressed against the resist. Either UV curable or thermosetting resist types can be used. NIL has the potential for high throughput nanometre scale lithography [66].

In microfluidics, a negative photoresist SU-8 is frequently used as a structural material [62]. Different variations of SU-8 allow spin coating in wide thickness range from a few hundred nanometres up to a few millimetres [67]. Polymer micromachining is further discussed in Section 2.2.4.

2.2.2 Etching

In an etch process material is being removed starting from the surface of the sample. Etching is done either with a corrosive solution (wet etching) or with aggressive gasses (dry etching). Typically, the etch process follows lithography and the patterned photoresist is used to protect some areas from being etched (Figure 2.1 (d)). This requires that the photoresist tolerates the etchant. However, most etchants will attack the polymer photoresist as well – either gradually during a long etch process or sometimes very fast. In such a case, the photoresist mask is first used to pattern a thin-film which is then used as an etch mask in a subsequent etch process that would be too harsh for the photoresist. The etch mask films – typically silicon dioxide, silicon nitride or silicon – are called hard masks.

Different materials are etched at different rates. Usually it is important to have etch selectivity between materials so that some materials are etched while some are affected as little as possible. Etching can be based on chemical reactions or physical erosion and it can take place in either wet or dry phase. Categorization of a few etch methods are shown in Table 2.2. In wet chemical etching the samples are immersed in liquid solutions and the

Table 2.2: Categorization of a few different etch methods.

	Physical etching	Both physical and chemical etching	Chemical etching
Dry etching	Ion milling Powder blasting FIB	RIE DRIE	HF vapour
Wet etching	Water jet machining	ECDM	HF KOH TMAH

etch chemicals in the solution will react at the sample surface to produce soluble reaction products. Etching can also be done in the dry phase either with chemically reactive etch gasses producing volatile etch products with the substrate or by physical etching with mechanical bombardment of the surface breaking off small pieces out of the substrate. Some etch methods, such as reactive ion etching (RIE), combine both physical and chemical etching.

Different etchants produce different etch profiles. Four typical etch profiles are presented in Figure 2.2. An isotropic etch has no preferential directionality and the etch proceeds spherically under the edges of the mask. The undercut of the etch mask equals the etch depth. Therefore, the maximum aspect ratio (width:height) is isotropically etched structures is 2:1. Wet etching of amorphous materials is always isotropic. Wet etching of crystalline materials, on the other hand, may be anisotropic due to crystal orientation dependent etch rates. For example, with caustic etch solutions, such as potassium hydroxide (KOH), the $\{111\}$ planes of silicon are etched slowly compared to the other crystal planes. Thus, etched cavities are defined by $\{111\}$ sidewalls as shown in Figure 2.2 (b). Plasma etching can be either isotropic or anisotropic. If the etching is purely chemical the profile is usually isotropic as in wet etching. Physical etching is directional and results in anisotropic etch profile. However, purely physical etching has low selectivity against the masking materials and, therefore, for deep structures with high aspect ratios and vertical sidewall profiles special processes are required. DRIE methods for silicon and glass will be discussed in Sections 2.3.2 and 2.4.2, respectively. Powder blasting produces an anisotropic channel profile with maximum aspect ratios around 1:3. Powder blasting is further discussed in Section 2.4.3.

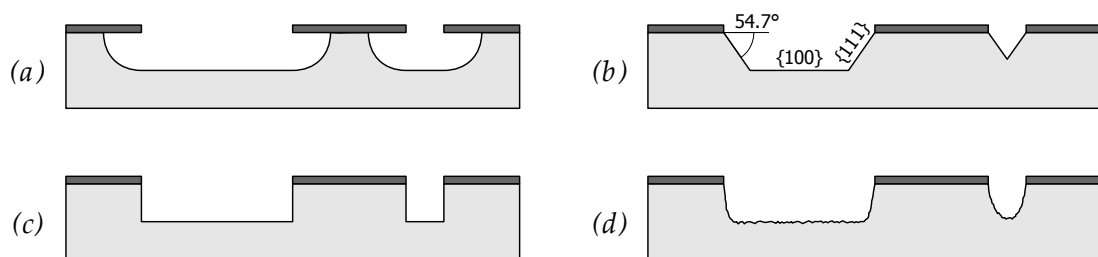


Figure 2.2: Etch profiles with different etch processes: (a) isotropic, (b) anisotropic wet etching of $\langle 100 \rangle$ silicon, (c) ideally anisotropic DRIE and (d) powder blasting.

2.2.3 Lift-off patterning and shadow masks

In lift-off patterning lithography is done before thin-film deposition. The material that is deposited over the photoresist will be removed during resist stripping (Figure 2.1 (c)). In general, negative tone photoresists provide negative sidewall profile for lift-off patterning than positive tone ones. Positive tone photoresist have typically slightly slanted sidewalls leading to continuous film with thin connection between the deposited film on the substrate and over the resist. Naturally, this makes resist stripping difficult and the pattern quality may deteriorate due to the tearing of flakes at the pattern edges. Because the lifted-off thin-film will end up as particles and flakes in the resist stripping solution there is a danger of contaminating the sample, especially with microfluidic chips with channels.

Therefore, etch patterning is generally preferred and lift-off patterning is only applied to materials that are difficult to etch.

Lift-off patterning is practically limited to evaporated and sputtered metals, because the deposition temperature has to be close to room temperature in order to avoid damage to the photoresist. Even with these deposition methods there is a chance that the wafer surface will overheat because photoresists have poor thermal conductivity. Therefore, the deposition power or time may need to be limited in order to avoid damage to the photoresist. Otherwise the photoresist may become very difficult to remove or it may crack leading to metal deposition to unwanted areas. Also, there may be outgassing from the photoresist that affects the properties of the deposited film, for example, the sheet resistance of the metal film may become higher.

Lift-off patterning is particularly useful for metals that are difficult to etch, such as platinum. Lift-off patterning the thin-film heaters of the HN chips will be discussed in Section 3.1.4.

Shadow mask deposition is a special kind of lift-off process where an external mask with through-holes is used and no lithography is needed. Extremely high resolution (down to 10 nm) can be achieved with the most advanced shadow masks [68]. In addition to masked deposition, shadow masks can be applied to masking of plasma etching [69] as done in publication III. If needed, the shadow mask can be accurately aligned in a bond aligner and temporarily bonded with a small amount of photoresist, glue, vacuum grease, or wax.

2.2.4 Polymer micromachining

Different polymers are frequently used for the fabrication of microfluidics. Polymers offer a range of chemical, mechanical and optical properties and polymer microfluidic devices they can be much cheaper compared to silicon and glass devices. There are several micromachining techniques available for polymers.

Master replication techniques are used with thermoplastics and curable polymers. Figure 2.1 (f) illustrates the casting of liquid pre-polymers, such as PDMS [70]. The inverse topography of the mould is copied to the cured polymer. Publication I uses a wet-etched silicon mould for the PDMS connectors. In hot-embossing, the temperature is increased over the glass transition point of the thermoplastic and then the master is compressed against the polymer substrate. Then the temperature is decreased below glass transition point and the master is released. The embossed substrate will have the inverse topography of the master. Injection moulding is used on a massive scale in the manufacturing of compact disks for digital audio and data storage. Microinjection moulding processes and master fabrication were recently reviewed [71]. The moulding approach is also feasible for glasses given the moulding temperature is high enough [72].

Photoresists are polymers and in addition to their typical use as an etch mask they can also be used as structural materials. SU-8 is chemically quite stable and transparent in the visible and near-ultraviolet range. Layering of several SU-8 films enables complex 3D structures made entirely of SU-8 [32]. In addition, SU-8 is frequently used to make masters for PDMS moulding.

2.2.5 Other micromachining methods

Several other approaches can be used for machining in micro and nano scale. Conventional machining methods can be scaled down. Very small diameter tools and mechanical positioning stages with sub-nanometre resolution are available off-the-shelf. Milling with rotating abrasive or cutting tool tips and electric (EDM) or electrochemical (ECDM) [73] discharge machining can be used for machining with down to a few micrometres' resolution. Atomic force microscope (AFM) tips provide the ultimate resolution enabling the manipulation of single atoms as demonstrated twenty years ago by IBM researchers [74]. However, all these methods lack the batch nature of lithography and etching and, therefore, the throughput is low and the expense of a single device will be high.

Laser machining has potential for high throughput machining of patterning with dimensions in the microscale [75]. Through-holes, trenches and even embedded 3D structures are possible [76].

Powder blasting is mostly utilized for cleaning and surface texturing, but is suitable for micromachining as well. In this context, the method is sometimes called as abrasive jet machining with additional methods such as water jet machining [77] also falling within the category. The resolution of powder blasting is determined by the size of the abrasive particles that are readily available down to a few micron size. Elastic and ductile materials can be used for masking of brittle and hard workpieces. Powder blasting of glass will be further discussed in Section 2.4.3.

Focused ion beam (FIB) is a true nanomachining method. It is similar to EBL but instead of electrons, it uses heavy ions, such as gallium [78]. FIB can do both physical ion-milling and direct writing of an etch mask by doping the surface layer. FIB machining is suited for practically any material, including glasses [79].

2.3 Silicon micromachining

This section reviews the basics of bulk micromachining of silicon using both wet and dry etching methods. Further information can be found in several books [58-60,80] and review articles [81].

2.3.1 Wet etching of silicon

Silicon wafers are single crystals and exhibit anisotropic wet etching in alkaline etch solutions, such as KOH, tetra methyl ammonium hydroxide (TMAH) and ethylenediamine pyrocatechol (EDP). The etch rate in $\langle 100 \rangle$ directions is tens or hundreds of times faster than in $\langle 111 \rangle$ direction. The $\{110\}$ and higher order planes are etched even faster. In addition to the crystal plane, the etch rate depends on concentration, temperature, the wafer's doping, mechanical agitation, masking layer stress and possible additives and applied electric fields [82-88]. High levels of p-type doping can be used to slow down the etch rate of the surface layer which enables etching of membranes with good thickness control. An etch-stop to a p-type silicon can also be obtained by applying a voltage over a diffused pn-junction. Addition of isopropyl alcohol (IPA) in KOH or TMAH reduces the surface roughness and changes the crystal plane selectivity [88]. Changes in crystal plane selectivity have significant implications. For example, mask undercutting is significantly reduced for islands on $\langle 100 \rangle$ wafers as shown in Figure 2.3. KOH+IPA etching has also

been applied to make capillary tube stopper structures in the nebulizer chip channel which will be further discussed in Section 3.1.2.

There are also isotropic wet etchants for silicon. They are based on mixtures of nitric (HNO_3) and hydrofluoric (HF) acids. The nitric acid oxidises the silicon surface and the HF etches the oxide away. The properties of HNO_3 -HF- H_2O and HF- HNO_3 - CH_3COOH silicon etch systems have been thoroughly documented in [89].

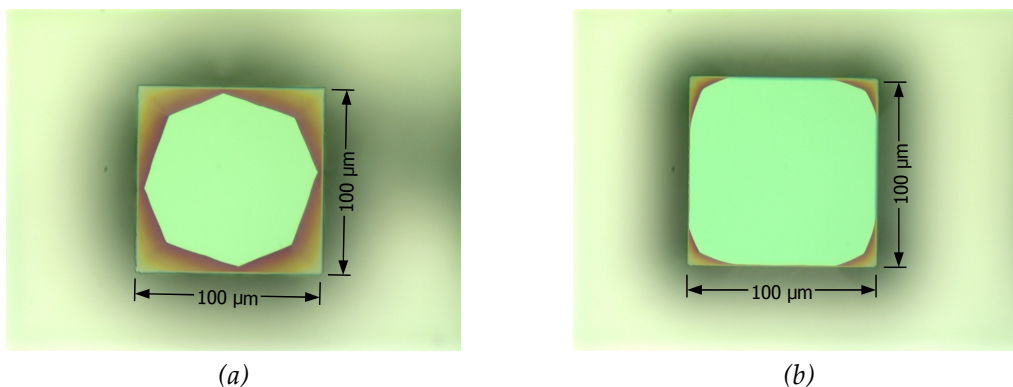


Figure 2.3: Square masked silicon island etched for 30 minutes in 82 °C (a) 20% KOH and (b) 20% KOH + 5% IPA. (Micrographs courtesy of Kestas Grigoras.)

2.3.2 Dry etching of silicon

Dry etching of silicon can be done with fluorine or chlorine containing atmospheres with [90] or without [91,92] plasma. Deep anisotropic etching requires sidewall passivation to prevent underetching by chemical etching. Two approaches can be used for this: the pulsed Bosch process and the cryogenic process. Two reviews of silicon DRIE technology were recently published [93,94].

The patented Bosch process uses alternating etch and passivation steps repeatedly [95]. A similar gas chopping etch technique had previously been presented for etching polyimide [96]. During the passivation step a fluoropolymer layer is deposited on the sample. The passivation layer is removed from the bottom of trenches due to physical etching. Both PECVD and RIE are equipment-wise very close to each others and, in principle, both deposition and etching can easily be done using the same equipment just by changing the process gasses, pressure and plasma power. The pulsed passivation and etch process leads to characteristic ripple at the sidewalls of Bosch DRIE etched structures as shown in Figure 2.4 (a). The size of the ripple depends on the exact process parameters, such as the pulse lengths. Parameter optimization requires multivariate analysis [97,98]. However, minimal sidewall scallop is obtained at the expense of etch rate or mask selectivity [99]. Alternatively, the ripple can be reduced by post processing, for example, by wet etching in KOH+IPA [100] or using a doped silicate glass deposition and reflow annealing [101].

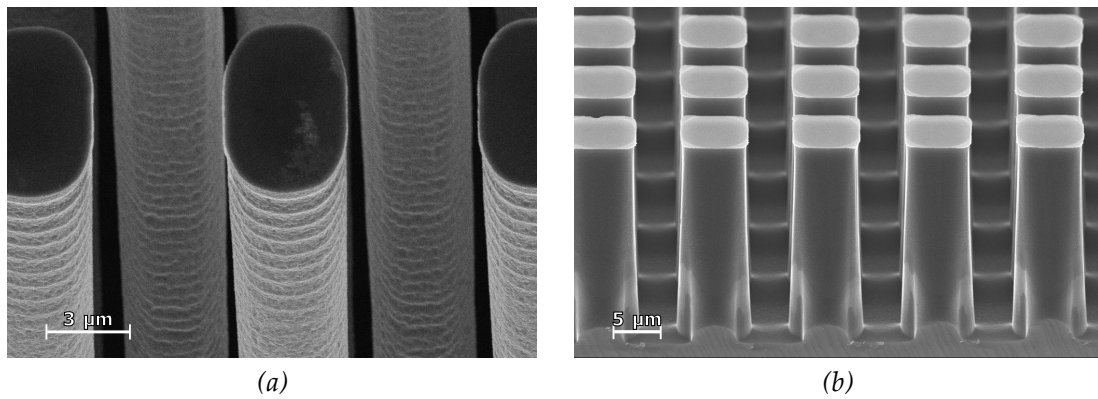


Figure 2.4: Silicon DRIE sidewall profiles with different processes: (a) the pulsed-mode Bosch process and (b) the cryogenic etch process (courtesy of Lauri Sainiemi).

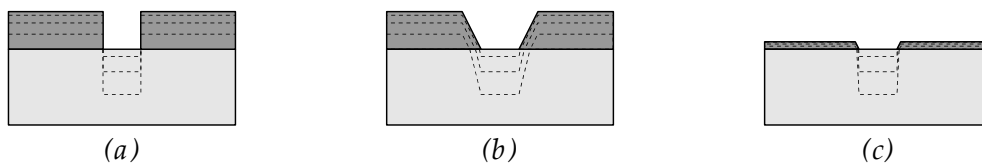


Figure 2.5: Effect of mask profile on the etch profile in a perfectly anisotropic etch process but finite selectivity between substrate and mask. (a) Vertical mask sidewalls can provide vertical channel sidewalls but (b) slanted sidewalls or mask undercutting lead to slanted channel profile. (c) Having higher etch selectivity helps.

Another approach for silicon DRIE uses a non-pulsed process at cryogenic temperatures around $-110\text{ }^{\circ}\text{C}$ [102]. The process gasses are SF_6 and O_2 . The process gasses form a thin passivating SiO_xF_y layer on silicon surfaces but due to physical etching the layer is removed from the bottom leaving only the sidewalls protected. The process is sensitive to the oxygen flow rate. Too little oxygen leads to insufficient sidewall protection and mask undercutting whereas too much oxygen will lead to silicon nanograss — black silicon — at the bottom because the physical etching is not capable of removing the passivation layer fast enough. With cryogenic DRIE it is easier to get smooth sidewalls compared to the Bosch process, as shown in Figure 2.4 (b).

Even for a perfectly anisotropic etch profile the resulting sidewall profile is affected by the sidewall profile of the etch mask. There is never an infinite etch selectivity between the mask and substrate. Therefore, the exposed area can change along the thinning or undercutting of the mask layer as illustrated in Figure 2.5.

Three important phenomena that lead to variations in etched depths with the same plasma etching process are loading, the RIE lag and aspect ratio dependent etching (ARDE) [103,104]. The ratio between the etched and protected surface area determine the loading. The etch rate may decrease if loading increases. Small features are etching slower than large ones because of RIE lag. This is due to the dynamics of the process, i.e. the ion bombardment and gas transport rates. ARDE is similar to RIE lag, but it is related to changes in etch rate of a chosen linewidth as the etch proceeds and aspect ratio of the feature increases, whereas RIE lag is for a specific etch time and different linewidths. It is possible to take advantage of RIE lag to fabricate channels with custom depth profile [105]. However, uniform etch depth are generally more favourable. It requires careful process

optimization and may require settling for lower etch rates [106]. Ramping the process parameters during the etch run can also improve the results [107].

2.4 Glass micromachining

This section will cover the literature about the three most typical glass micromachining methods: wet etching, dry etching and powder blasting. In addition, other off-mainstream glass micromachining methods are briefly discussed and compared. Recently, a book on glass microfabrication was published [57].

2.4.1 Wet etching of glass

Because most glasses compose mostly of silicon dioxide, they are etched in HF-based solutions. The etch rate depends on the concentration of the solution and can vary from tens of nanometres per minute with buffered HF [108] close to $10 \mu\text{m min}^{-1}$ with concentrated HF [109,110]. Because glass is amorphous, the etching is isotropic. However, there are some special glasses that do exhibit anisotropic wet etching. These include single crystal quartz and photoactive glasses, such as Foturan [111].

Relatively shallow, up to a few tens of micrometer, etches can be done using a photoresist mask [112,113]. Deeper etches require the use of a hard mask. There are several suitable hard mask materials that are not etched in HF [114]. Silicon is one obvious choice. Both LPCVD [115] and PECVD deposited [116] silicon thin-films and even bonded silicon wafers [117] with through etched patterns have been used. In addition, different combinations of layers of chromium, gold, copper and photoresist [118-123] and PECVD silicon carbide [109] have been successfully applied as etch masks for glass.

For defect free etching the masking layer stresses have to be low [118]. Otherwise there will be pinholes and cracking of the under etched hard mask. These defects are illustrated in Figure 2.6. Tensile stress in the hard mask layer often results in pinhole defects at the surface where the etchant has penetrated through the mask through a microscopic hole.

Several glasses — including Pyrex — have constituents (e.g. K_2O , CaO , MgO or Al_2O_3) that do not produce soluble etch products with HF. During etching they lead to micromasking and added surface roughness. The problem can be overcome by the addition of H_2SO_4 or HCl in the etch solution [110,124]. Alternatively, the precipitated particles can be removed by periodical 10 second immersion of the wafer in HCl solution after every 5 minutes of etching in BHF [112].

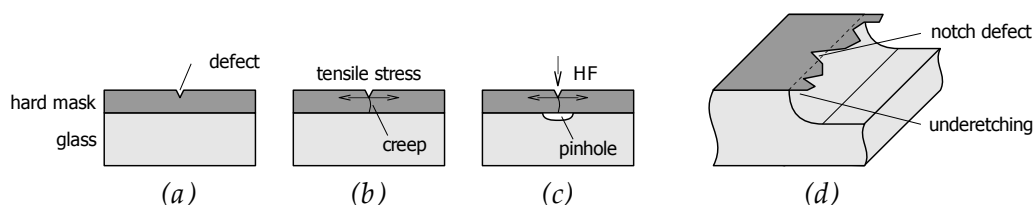


Figure 2.6: Mechanisms for mask induced etch defects. Pinhole formation (a-c) and notch defects (d). Redrawn from [118].

2.4.2 Dry etching of glass

Isotropic vapour phase etching of SiO_2 and glasses can be done with HF vapours, which can be used, for example, in the release etch of MEMS devices with sacrificial oxide [125]. However, anisotropic etching is often desirable due to inherent limitations of isotropic etching. Anisotropic profiles can be obtained with RIE.

In general, fluorine chemistry is used in plasma etching of glasses. Various combinations of process gasses have been studied: CF_4 [126-128], CF_4/O_2 [129], CF_4/Ar [129,130], CF_4/CHF_3 [126,127], CHF_3/Ar [129,130], CHF_3 [131], SF_6 [132-135], SF_6/Ar [130,132,133,136], SF_6/CHF_3 [137], $\text{SF}_6/\text{C}_4\text{F}_8$ [137], C_4F_8 [131,137], $\text{C}_4\text{F}_8/\text{Ar}$ [138], $\text{C}_4\text{F}_8/\text{Ar}/\text{CHF}_3$ [139], $\text{C}_4\text{F}_8/\text{O}_2$ [138], $\text{C}_4\text{F}_8/\text{O}_2/\text{He}$ [140], $\text{C}_4\text{F}_8/\text{He}$ [140], $\text{C}_4\text{F}_8/\text{CH}_4$ [141] and Ar [126,127].

Etch reaction products from SiO_2 are highly volatile SiF_4 , CO , CO_2 and H_2O [127]. Many glasses contain B_2O_3 with volatile reaction products BF_3 and B_2F_4 [126]. However, several other compounds that are used in glasses and that may be as trace impurities also in high purity silica glasses have non-volatile etch products: AlF_3 , BaF_2 , CaF_2 , KF , LiF and NaF [126,127]. The removal of these non-volatile species is achieved with physical etching, but process optimization is required for good surface quality, profile control and etch selectivity between masking material and the glass substrate. The glass compositions which were studied include different quartz glasses [126,127,130,132,137,138,140], Pyrex and similar borosilicate glasses [127,128,131-134,136,139,140], soda-lime glass [129] and several other silica-based glasses [126,127,132].

The etch mask materials used include standard photoresist [127,129,138], thick SU-8 resist [128,130], aluminium [129], chromium [126,132], evaporated [136] and electroplated [133-135] nickel, sputtered aluminium nitride [137], ALD deposited Al_2O_3 [137], LPCVD amorphous silicon [140], polysilicon [138,141] and through etched silicon wafers – either anodically bonded [131,139] or as reusable shadow masks [140]. Publication III shows the use of different $\text{C}_4\text{F}_8/\text{He}/\text{O}_2$ plasma etches with four different mask materials: electroplated Ni, LPCVD a-Si, SU-8 and a silicon shadow mask.

DRIE of glass with etched depths over 100 μm deep is shown in [128,131,135,139,140]. In contrast to silicon DRIE with the pulsed Bosch process dominating, glass DRIE processes are continuous. Glass DRIE etch rates are about an order of magnitude lower (up to a few hundred nm min^{-1}) compared to silicon DRIE. Major challenge is obtaining good etch selectivity between the etch mask and glass. Fairly high selectivity (30:1) AlN and Al_2O_3 masks have been demonstrated for silica [137]. However, selectivity reduces with other glasses that require significant physical etching for the non-volatile etch products. The non-volatile etch products are sputtered on the sidewalls affecting the resulting etch profile [134]. The sidewall taper angle depends on both mask opening width and glass composition. In general, thick masking layers are needed for glass DRIE. For deposited films, stress-related problems may limit the maximum mask thickness. Also, the thicker the mask is the more difficult it is to make small patterns due to an increased aspect ratio which contributes to RIE lag and ARDE of both the mask and subsequent glass etching. As already illustrated in Figure 2.5 the sidewall profile of the mask affects the sidewall profile of the etched trench. The optimal etch process depends on the used masking material. For example, SF_6 is not a good choice with silicon masks, because it rapidly etches silicon. Instead, polymer forming etch gasses – such as C_4F_8 or CHF_3 – should be used with silicon masks to reduce the mask erosion.

2.4.3 Powder blasting

Since the mid-1990s powder blasting has become a fairly well established micromachining method [142-145]. In powder blasting, high velocity particles (e.g. fine grain alumina sand) erode the surface via cracking upon impact. It is well suited for brittle and hard materials, such as glass. Powder blasting is anisotropic and the etch rate depends on the mass flow rate of the particles and their velocity, that is, the applied kinetic energy.

Large areas are etched fairly uniformly but the resulting side wall profile of the pattern edges is dependent on aspect ratio, the used particle size, shape and velocity [146]. The profile changes with depth. An example of a powder blasted glass structure is shown in Figure 2.7 (a).

As a rule of thumb, the minimum linewidth is about three times the particle diameter. However, ARDE is much more significant compared to RIE and linewidths up to a few tens of times the particle size are affected. With 30 μm particles the etched depth starts reducing below 400 μm linewidth as shown in Figure 2.7 (b). Of course, also the mask thickness contributes and thinner masking layer can be used alleviate ARDE to some extent. Although in general ARDE is considered an unwanted side effect, it is possible to utilize ARDE to implement channels with varying depth [147]. The etch profile can be tailored by varying the incident angle of the powder jet [142,148]. This enables, for example, the fabrication of released bridges and high aspect ration structures [149].

Various metal and polymer masks can be used with powder blasting [150,151]. These include laser machined steel stencils [145], laminated and spin-on elastomer photoresists [152,153], PDMS [154] and laser ablation patterned polyurethane with gold nanoparticles [155].

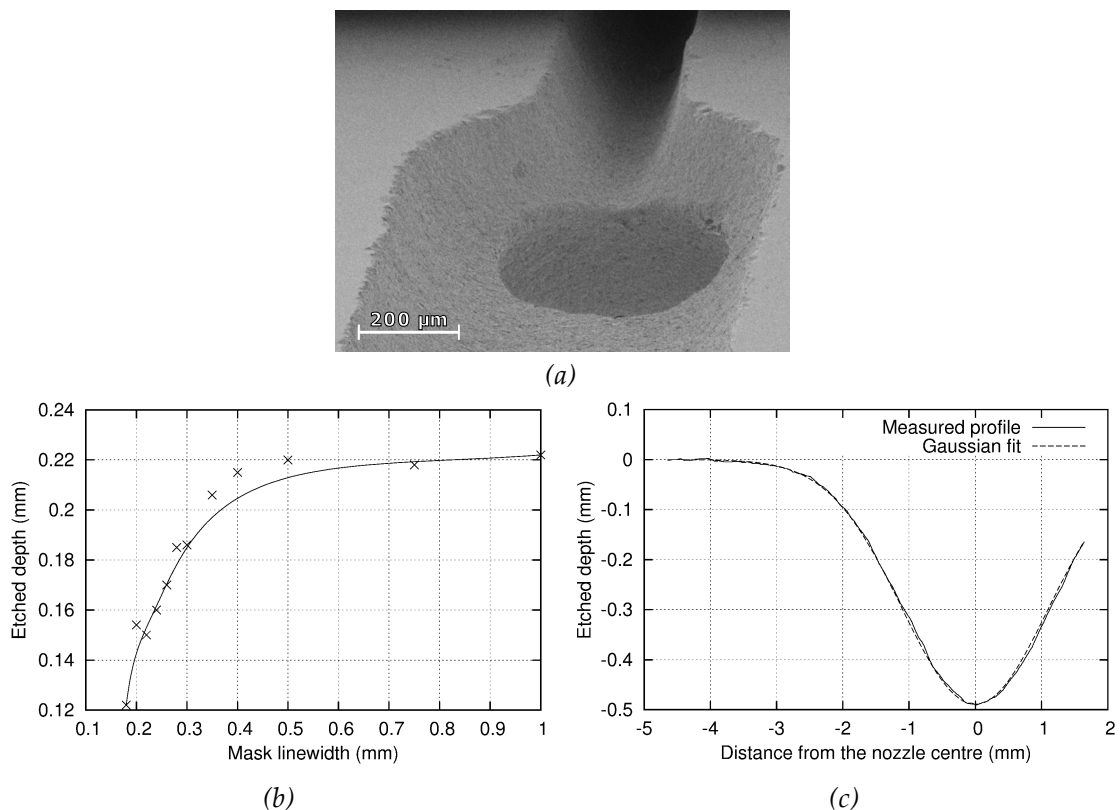


Figure 2.7: Powder blasting with 30 μm alumina particles. (a) SEM of a powder blasted channel with through-hole. (b) ARDE with 0.4 mm thick steel stencil mask. (c) Maskless etch profile of a single sweep with 2 mm diameter blasting nozzle.

Scanning of the powder jet is required to etch large surfaces. For uniform etch depth the scanning path needs to be considered. In addition, the erosion rate should remain constant. However, there are several factors that can lead to variance in the erosion rate. First of all, the blast powder quality should be uniform which means little variation in the size and shape distribution of the grains. Secondly, the feed rate of the powder should not vary. The moisture content in the powder and compressed air plays an important role here. Too much moisture leads to agglomeration of the powder causing unstable powder feed and clogging of the transport lines and nozzle. To avoid moisture-related problems low dew point ($-30\text{ }^{\circ}\text{C}$) air dryers in the compressed air line and optional heating should be used.

Maskless sub-millimetre resolution patterning is possible with small powder blasting nozzles that are available at least down to $250\text{ }\mu\text{m}$ diameter [156]. However, maskless powder blasting has limited applicability. A circular powder blasting nozzle results in Gaussian etch depth with a single sweep (Figure 2.7 (c)) and, therefore, the pattern edges are not sharp unless a masking layer is used.

Powder blasting is very useful for making through-holes for fluidic interconnections. For example, a cryogenic cooler made of a stack of three bonded glass wafers has been made using HF etching for the channels and powder blasting for the fluidic inlet and outlet holes [157]. However, in several fluidic applications powder blasting cannot be used to make the fluidic channels due to high surface roughness which affects both fluid flow and optical properties. Surface roughness of powder blasted surfaces depends on the process parameters, such as particle size and velocity, but typically the roughness is on the order of $1\text{ }\mu\text{m}$ [143,144]. Different approaches, such as wet etching and thermal annealing, have been studied to reduce the roughness of a glass surface [158,159] but their effect is rather a removal of the damaged and porous surface layer without a significant reduction in the magnitude of the surface roughness. To conclude, a powder blasted surface cannot compete with the smoothness of wet or plasma etched channels that result in nanometre scale roughness when properly optimized. Variation of roughness in glass wet etching has been studied in [110].

2.4.4 Discussion about glass machining

Other glass micromachining methods in addition to wet etching, RIE and powder blasting include micro-ultra-sonic machining [111], ECDM and similar spark-assisted etching methods [73,160,161], laser machining [162-165], FIB [79], embossing [166,167], moulding [72] and glass blowing [168]. Wafer dicing saws can be set to cut only a part of the substrate thickness, resulting in straight grooves and crossings that can be used as simple fluidic channels [169,170]. Width of the channel is determined by the width of the saw blade.

Price, throughput, available aspect ratio and surface quality are important factors for comparing between the methods. For pricing one has to consider the whole process flow. For example, wet etching may seem like a cheap approach but the equipment needed for high quality masking, e.g. a LPCVD silicon furnace, may render the method very expensive for small production volumes. Powder blasting is a very convenient and economical way of making through-holes in glass. Wet etching requires expensive masking and the cross-section of isotropically etched hole is hardly optimal. Glass DRIE can provide high quality through-holes, but it is expensive and not yet mature technology. However, due to the mechanical nature of powder blasting there is chipping of larger flakes near the edges of the hole as seen in the cross-section in Figure 2.8. Therefore, DRIE might be the only choice if

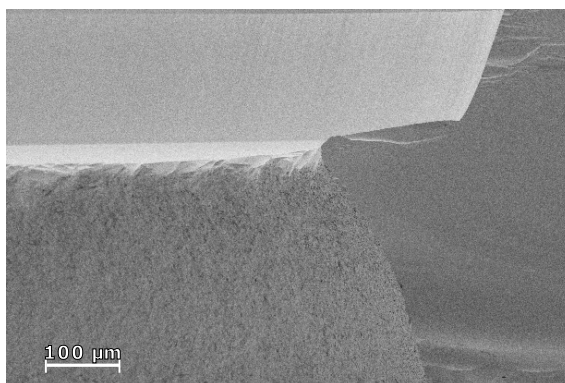


Figure 2.8: Cross-section of a glass wafer etched with DRIE from top and by powder blasting from bottom.

smooth surfaces and anisotropy are required. Mechanical drilling of glass with diamond coated drill tips usually induces large cracks at the surface near the entrance and exit points and the wafer needs grinding and polishing afterwards. Also, the lifetime of the tool is limited to tens or hundreds of holes at most.

In general, mechanical machining methods cannot compete with the surface quality achieved with chemical etching. The etch selectivity in photopatternable glasses is based on change in crystal structure, i.e. the development of polycrystalline regions. The surface roughness at the pattern edges is proportional to the crystal size and might be several micrometers [57]. Rough surfaces are generally not good either for microfluidic or optical applications. Increased surface roughness of fluidic channels increase surface area and adsorption which results in band broadening (i.e. reduced resolution) in chromatographic and electrophoretic separation channels. Planar surfaces can be polished to reduce surface roughness. However, the roughness of features below the surface plane is determined by the selected machining method and very little can be done to reduce the roughness afterwards.

2.5 Wafer bonding

In wafer bonding, two substrates are attached together (Figure 2.1 (g)). There are applications for both permanent and temporary bonds. Wafer bonding is used to make advanced substrates, such as silicon-on-insulator (SOI) wafers [171], layer transfer [172], 3D microstructures [173] and wafer-level packaging [174]. Several MST devices are impractical or impossible to implement with mere bulk or surface microfabrication. By attaching two or more substrates together the device complexity can be easily increased.

There are various wafer bonding methods — anodic, fusion, glass frit, eutectic, thermocompression, solder, ultrasonic and (polymer) adhesive bonding — to name a few. Wafer bonding procedure starts with cleaning of the wafers followed with alignment and contacting of the wafers. Depending on the bonding method there may be additional steps involved such as application of adhesive layers. The choice of the bonding method depends on the used materials and requirements from the application: temperature tolerance (formation and service), thermal expansion, surface chemistry, price, throughput, yield, hermetic or non-hermetic, electrically conductive or insulating. Wafer bonding methods can be divided in two categories: bonding with or without an intermediate layer.

Two mirror polished surfaces will spontaneously bond to each others with van der Waals force. Van der Waals bonding is relatively weak but thermal annealing can lead to formation of strong covalent bonds provided that the substrates have sufficiently matching coefficients of thermal expansion, the surface chemistry is suitable, the surface polish and the planarity are good enough and that the trapped particles are few enough.

Different adhesives can be used to fix the substrates together. Low temperature melting glass paste or metal solders are frequently used when hermetic seals are required. Polymer adhesives are useful when high temperatures (>200 °C) have to be avoided, but they are quite permeable to gasses and hence are not applicable when a hermetic seal is required. Water glass bonding enables low temperature bonding of glass wafers [175].

The next subsections will present silicon and glass wafer bonding techniques that are also applied to the nebulizer and LC chips of this dissertation (further discussed in Section 3.1.3). Comprehensive information about bonding can be found in a historical review [176], a semiconductor direct bonding review [177], an adhesive bonding review [178], a bond characterization review [179] and several books dedicated to wafer bonding [180-182].

2.5.1 Direct bonding

Polishing methods for silicon wafers provide sub-nanometre surface roughness on a routine basis and, therefore, silicon direct bonding or fusion bonding of silicon wafers is fairly straightforward. There are two different mechanisms in silicon-to-silicon fusion bonding [183]. In hydrophilic bonding there is an oxide layer on the wafers or the last washing solution leaves the silicon surface hydroxyl group terminated. This will lead to covalent bonding with an insulating oxide layer between the wafers. Heating of the sample promotes rearrangement of trapped water and transformation of silanol groups (Si-O-H) into covalent siloxane (Si-O-Si) bonds at the interface. Siloxane formation reaction produces water which further oxidises silicon near the interface zone. The remaining hydrogen can diffuse out through the silicon [184]. In hydrophobic bonding all oxide layers are removed in HF solution from the bonding surfaces of the silicon wafers prior to bonding resulting in direct Si-Si bonds during annealing. The necessary annealing temperature for fully developed bond strength in silicon fusion bonding is similar to thermal oxidation temperature (around 1000 °C). The high process temperatures required limit the applicability of fusion bonding. For example, no organic matter or metals are allowed and ICs with sub-micron transistors are likely to be destroyed by the diffusion of the dopants.

Fusion bonding of two glass wafers is also widely applied. The typical annealing temperature for Pyrex 7740 wafers is around 650 °C [160,185]. This is above the annealing point of Pyrex (560 °C) allowing small glass flow to compensate for surface roughness. Slow cooling rate is required to relieve strain induced by the temperature change. Typical glass wafer surface roughness is about 2 nm. Practical considerations in fusion bonding of glass include elimination of unwanted deformation of the wafers and avoidance of voids. The wafers should be placed in the annealing furnace on top of a horizontal supporting plate to prevent wafer bow and also because room temperature bond strength is too weak to hold the wafers together.

Conventional fusion bonding requires thermal annealing to promote bond strength. However, bulk comparable bond strengths can also be achieved near room temperature by chemically activating the surfaces prior to contacting. However, the activation and

contacting has to be done in a vacuum chamber because the activation will rapidly degrade at room atmosphere with very rapid adsorption of, for example, moisture. A cluster tool with chambers for O₂ and N₂ plasma cleaning and surface activation for room temperature glass-to-glass bonding is presented in [186]. Compared to conventional fusion bonding, surface activated low-temperature bonding is more sensitive to surface imperfections because there is no thermal annealing that allows some material flow to compensate small surface mismatch. For glass wafers with generally higher surface roughness compared to silicon wafers this is problematic and thermal annealing is still required for the highest bond strengths.

2.5.2 Anodic bonding

Anodic bonding is a well established method for bonding silicon to glass. The bonding is done at elevated temperature where the Na₂O in glass is dissociated into sodium and oxygen ions with Na⁺ having the highest mobility. A negative voltage is applied on the glass outer surface causing electrophoretic drift of Na⁺ ions away from the interface between silicon and glass wafers creating a strong electrostatic force and leading to permanent bonding between the substrate. Covalent siloxane bonds are formed at the interface. Typical bonding conditions for silicon and Pyrex 7740 glass are approximately 350 °C and 600 V. At this temperature the thermal expansion of glass and silicon is well matched leading to low stresses at room temperature. The cathode electrode contacting the glass is subject to corrosion due to accumulating sodium which also reacts with moisture to form NaOH caustic [182]. Cathodic corrosion of deposited platinum film at the glass surface will be discussed in Section 3.2.

With proper intermediate layers anodic bonding can also be applied to bond materials that are not anodically bonded as such. Silicon-to-silicon anodic bonding is possible with a sputtered borosilicate glass layer on the other bonding surface [187,188]. Glass-to-glass anodic bonding is possible with thin-films that prevent electrostatic drift of sodium and thus enable the formation of the depletion layer. Possible materials include standard thin-films, such as polysilicon, amorphous silicon, nitride and carbide [189,190]. Oxide layer does not work as a sodium barrier, but it can be used in some multilayer configurations [189].

2.6 Packaging and chip-to-world interfacing

After everything is ready on the cleanroom processed wafer, it is diced to separate individual chips (Figure 2.1 (*h*)). Dicing is a dirty process and it is thus done outside the cleanroom. Before dicing, the wafer is attached to a frame with a sticky film. The dicing is done with a fast spinning thin resin blade with 3-axis automated motion. Thin silicon wafers can be cut with a 20 μm-thick blade, but other materials and thicker samples require thicker, e.g. 150 μm blades.

After dicing the chips are usually packaged before they are ready to be shipped to the customer. The purpose of packing is to protect the chip from the environment, ease the handling and to provide chip-to-world interconnections. For ICs, the packaging involves attaching the die to a carrier, wire bonding the die's contact pads to the carriers metal leads and final encapsulation. This is illustrated in Figure 2.1 (*i*). However, MEMS and microfluidic devices can seldom use standard IC packaging. Special modifications to the

standard packages or even completely custom made solutions are required. For example, a pressure sensor cannot be fully encapsulated because its sensing element must be in contact with the ambient air in order to get the pressure reading.

In contrast to electrical circuits, there is no standard packaging solution for microfluidic devices. Depending on the application, the requirements may include uncovered surfaces, connections to tubing, electrical connections and optical viewports. Several microfluidic chip companies have developed their own connection solutions. The quartz chips of Affymetrix DNA microarrays are packaged in plastic cartridges that ease the handling of the chips and contain identification data [191]. Optical fluorescence detection is done after incubating the chip in hybridization and washing solutions. Agilent's LC-ESI chips are packed in metal cartridges [41]. Dolomite offers a set of microfluidic standard chips with a range of matching top and edge connectors [192]. Micronit Microfluidics offers a connector frame for use with different chips with both fluidic and electrical connectors [193]. Microfluidic ChipShop uses different kinds of commercial fittings, including Luer taper ports that are glued on the chip [194]. The next section reviews different methods for fluidic interconnections in more detail.

2.6.1 Fluidic interconnections

Microfluidic devices operate on liquids and gasses and fluidic interconnections are required to introduce them to the chip and extract them out. Sometimes open sample reservoirs are sufficient for introducing liquids by pipetting. Open sample wells also allow the use of electric probe needles for applying electric potentials needed, for example, with CE chips. Sometimes open sample wells are sufficient but very often capillary tubes are connected to the chip. Figure 2.9 illustrates these basic approaches.

Several aspects need consideration when planning fluidic interconnections: influence on the chip fabrication process, pressure tolerance, dead volume, material properties such as chemical compatibility and temperature tolerance, required space, ease of operation, reusability and price. Due to the nature of the machining processes, the available inlet port geometries are different depending on whether it is located on the top or edge surface of the chip. Dead volume — unnecessary channel volume — has detrimental effect to the device performance and it needs to be minimized. For example, if the composition of the inflow is changed, the earlier composition stored in the dead volume will slowly mix to the new one through diffusion. In chromatography, dead volumes lead to band broadening and peak tailing.

Different fittings for tube connectors for industrial and chromatography applications are available from various manufacturers, such as Svalgelok [195], Upchurch Scientific¹ [196] and Valco Instruments [197]. Some of these fittings and the applied principles are also applicable to making fluidic connections to chips. A typical fitting consists of a nut that compresses a ferrule against the tubing and the body of the connector for gripping the tube in place and for sealing the connection. There are various types of nuts and ferrules available. In general, coned fittings offer higher pressure tolerance compared to flat-bottom fittings. The pressure tolerance depends on the properties of the used materials. Higher pressures mean that harder materials have to be used because of the pressure induced deformation of soft tubing and ferrules. Metal tubing and fittings offer the highest pressure tolerance, but on the other hand plastic ones have several benefits, too [198]. A variety of

¹ Part of IDEX Health & Science LLC.

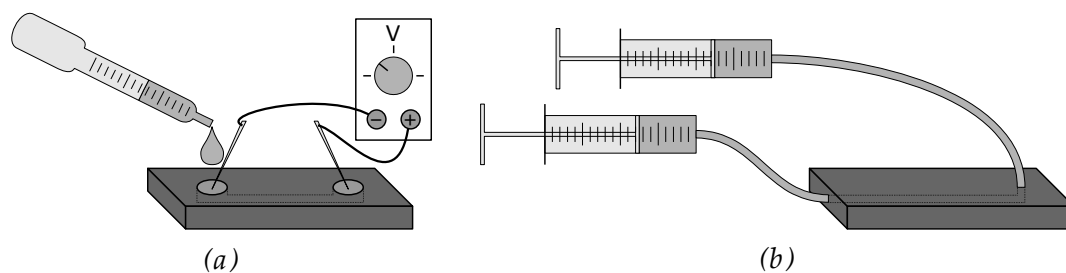


Figure 2.9: (a) Open sample wells allow simple application of liquid droplets and the use of probe needles for electrical connections. (b) Tubing can be connected from the edge or surface of the chip.

different polymer fittings are available with extensive chemical compatibility range, reusability and competitive pricing. In addition, polymer tubing is easy to cut.

There are various approaches for chip-to-world interfacing as shown in a review [199]. Exemplary approaches for connecting tubes with microfluidic chips are illustrated in Figure 2.10. A simple approach is to push the tube against an inlet hole on the chip surface (Figure 2.10 (a)). Gluing is usually required for making the connection leak-tight provided that the glue is chemically compatible with the application. However, gluing is laborious manual work and involves a great chance of miss-alignment or clogging the tube or chip with the glue. The inevitable loss in the yield of glued connections renders the approach unsuitable for microfluidic devices with high number of fluidic connections. In addition, the permanent nature of gluing prevents alterations in the configuration. Gluing can be avoided by using pliant silicone tubing and a special fixture that compresses the tubes against the chip [200]. Polymer films can be used for sealing [201]. There are also different connectors that can be attached on the chip either by gluing [202], anodic bonding [203], or ultrasonic welding [204].

Problems with alignment and clogging by glue can be alleviated by making a recess in the chip which closely matches the outer diameter of the tubing as shown in Figure 2.10 (b). Hourglass shaped holes have been machined to glass using ECDM [205]. Different flanging

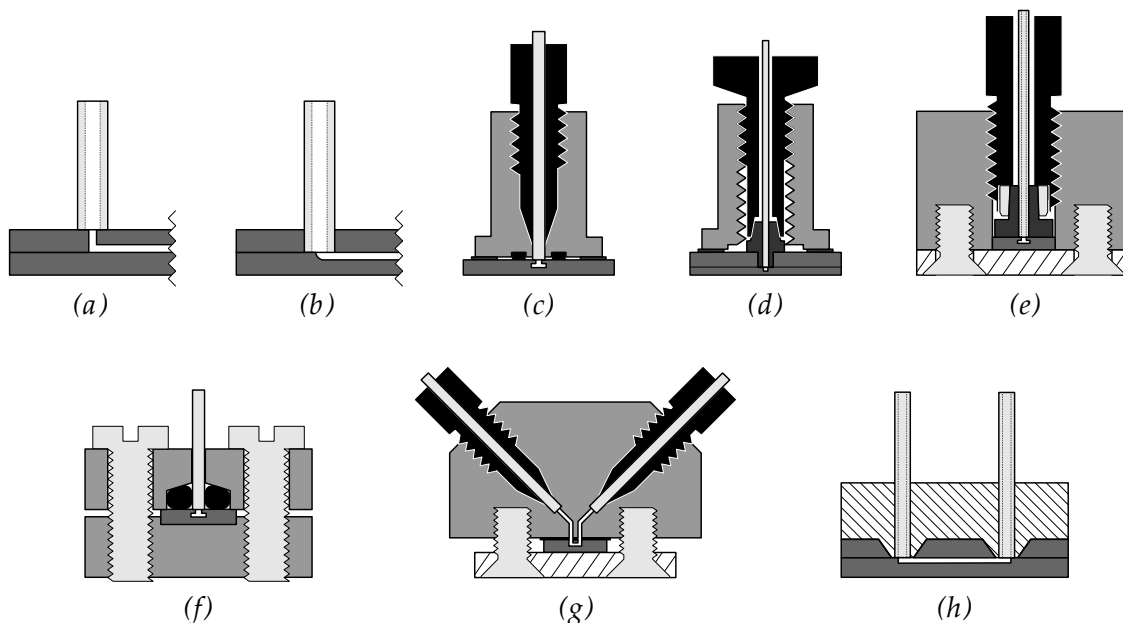


Figure 2.10: Examples of different solutions for connecting tubing to chip: direct coupling (a, b), NanoPort connectors (c, d), custom made fixtures (e–f) and a PDMS connector.

processes can be used to reshape the end of the tube for sealing [206,207]. Thermoplastic cyclic polyolefin² (COC) has been used to make direct sealing with metal needles [208]. Unfortunately, depending on the fabrication process it is not always possible to make tightly fitting slots for the tubing. Also, a simple slot might not provide sufficient grip to hold the tubing in place.

One of the few commercial general purpose off-the-shelf solutions for microfluidic interconnections are the NanoPort connectors from Upchurch Scientific [209]. Two different NanoPort configurations are shown in Figure 2.10 (c) and (d). They compose of a cylinder block with internal threading that is glued on the chip surface. Different NanoPort assembly configurations allow the use of either coned or flat-bottom fittings and they can also be used as sample reservoirs. NanoPort connectors enable repeated attachment and release of the tubing, but because they are glued on the chip they usually have to be discarded with the chip. Therefore, NanoPorts can be expensive solution if the lifetime of the chip is short. With the preformed adhesive ring the NanoPort connectors take up about a 10 mm diameter area on the chip surface. With this and the general issues with gluing in mind, NanoPorts are not feasible for high density inlets.

An alternative to gluing of fluidic ports to the chip is to use custom made chip holders. Typically, a two part approach is used with top and bottom plates accommodating a housing for the chip and fixed positions for the fittings. The same fittings can be used as with NanoPort connectors, but there is no need for gluing and less surface area is required for the connection possibly enabling reduction of the chip size and the fabrication of more chips per wafer. On the other hand, a chip holder might take up more space than a NanoPort connector which may be of importance in some applications. Figure 2.10 (e) shows a chip holder with a flat-bottom fitting and (f) with an o-ring. Reusable magnetic connectors were recently published [210]. They offer a freely configurable alternative to dedicated holders for each chip design that can also be used with whole wafers.

Density of inlets using standard nut fittings is limited by the diameter of the nuts. For higher density connections the tubes cannot be brought in direct contact with the chip as shown in Figure 2.10 (g). A thin sealing membrane between the frame and chip offers higher pressure tolerance [211]. Alternatively, o-rings can be used [212-214].

Edge connections can potentially greatly simplify the fabrication process because there is no need for the through-holes. Fairly good edge surface quality can be achieved in wafer dicing. Standard fittings require some space and can be only be used with fairly thick chips. For example, Dolomite uses 4 mm thick chips with their edge connectors. A more universal approach is to insert the capillary inside the channel and settle for gluing. UV curable glue can be used to accurately control the penetration depth of the glue into the capillary insertion channel [215]. Reversible edge connections using PDMS as the sealant and small metal wire to prevent clogging have been demonstrated [216] but this method is hardly universal.

The PDMS connector of publication I introduced in Section 1.4.1 utilizes the self-sealing nature of PDMS that provides reversible seals between PDMS and tubing, and PDMS and the chip. The PDMS connector is moulded on a master with matching surface textures of the PDMS connector and the fluidic chip enabling easy alignment of multiple tubes simultaneously. The inverted pyramid profile of KOH etched <100> silicon is particularly useful for this purpose. The matching surfaces of silicon pyramids are also used in the

2 Also known as cyclo olefin polymer (COP).

fluidic couplers [202]. In publication I the holes for the capillary tubes are made using dummy capillaries during moulding. Others have made PDMS connector blocks with punctured holes [217] or machined pillars on a PMMA mould [218].

Interconnection schemes for the HN chips will be further discussed in Section 3.3.

3 Heated nebulizer chips

The HN chips are used to introduce a vaporized and ionized sample to a mass spectrometer. This chapter will cover the different fabrication processes used and discuss the different chip designs. Also the chip lifetime, jet shape and the different analytical applications will be discussed.

3.1 Different chip designs and fabrication processes

The HN chips have been implemented using various layouts, materials and fabrication processes. Photographs of four different nebulizer chips are shown in Figure 3.1. The author has made the chip in some 40 different variations since taking over their development work. Before this, the chips had been made from wet etched [52] and DRIE etched [56] silicon with anodically bonded glass cover. During this dissertation work, different glass microfabrication processes were explored resulting in all-glass HN chips. Different nozzles and their influence on the jet shape were studied. A meander pre-heating channel for the nebulizer gas was realized. Chip size was reduced thanks to new interconnection methods.

The fabrication of all the different versions of the nebulizer chips follows the same process outline with two main process stages: (1) double sided through-wafer etching of a wafer with nebulizer channel, nozzle and fluidic interconnections and (2) bonding to a

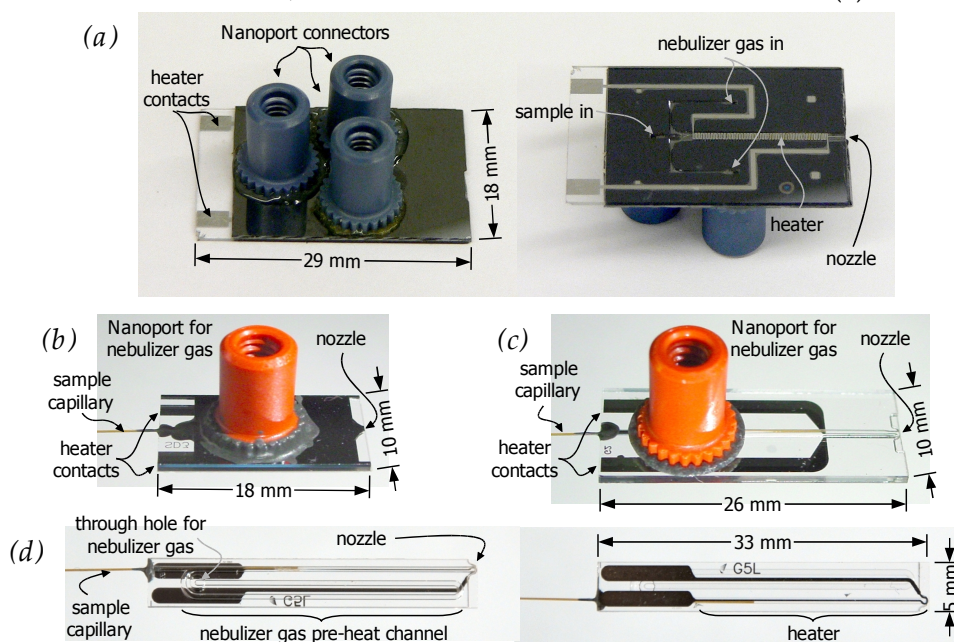


Figure 3.1: Different heated nebulizer chips: (a) original silicon–glass nebulizer chip (top and bottom views), (b) improved silicon–glass chip, (c) wet etched glass chip and (d) glass chip without NanoPort for use with a chip holder (top and bottom views). (Photos courtesy of Markus Haapala.)

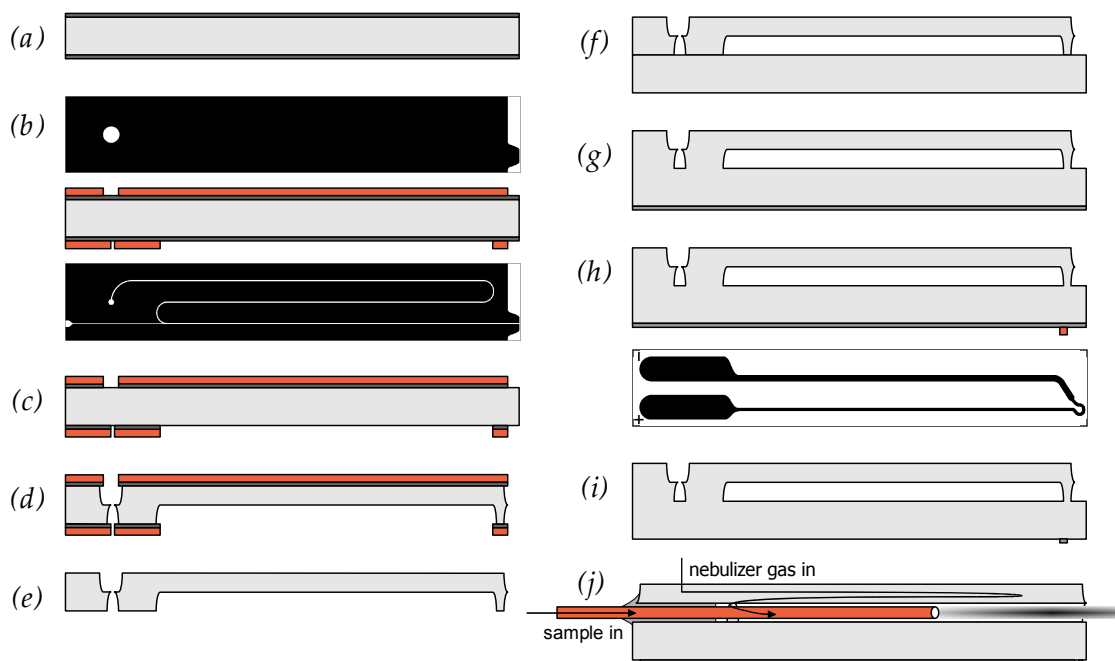


Figure 3.2: Fabrication process of wet etched glass nebulizer chip: (a) LPCVD silicon deposition, (b) double sided lithography, (c) silicon wet etching, (d) glass wet etching, (e) photoresist and silicon stripping, (f) bonding to another glass wafer, (g) platinum sputtering, (h) lithography, platinum etching, (i) photoresist stripping and (j) dicing. A sample capillary is inserted from the edge of the chip and sealed with high temperature epoxy glue.

cover wafer with a heater element. Figure 3.2 illustrates the fabrication process using wet etching of a glass wafer. The upcoming subsections will discuss the different materials and fabrication processes used for the nebulizer chips.

3.1.1 Substrate materials

The nebulizer chips have been fabricated using either one silicon and one glass wafer anodically bonded together or two glass wafers. Because the on-chip operating temperatures of the nebulizer chip typically range from 300 °C to 500 °C polymers substrates are out of the question. For silicon and borosilicate glass this temperature range is suitable.

Surface chemistry and chemical compatibility of silicon and glass are similar. However, thermal conductivity values are very different. Thermal conductivity of silicon is about two order of magnitudes higher than that of glass. Thermal images of silicon–glass and all-glass chips are shown in Figure 3.3. Glass allows much more localized heating with high on-chip temperature gradients whereas silicon will efficiently spread out the heat over the whole surface. This has implications, for example, for the durability of fluidic interconnections that may involve the use of materials with lower temperature tolerance than silicon and glass. Even though all the chips in Figure 3.3 are heated with the same power and the same amount of gas flows through the channels, there are considerable differences with the peak temperatures of the chips. In addition to the material choice, the layout of the heater also affects the peak temperature. On the meander channel chip the heating power is distributed over a larger area resulting in much lower peak temperature compared to the chip with the straight channel chip with a narrow heater. A photo of the meandering chip is shown in Figure 1.5 on the left.

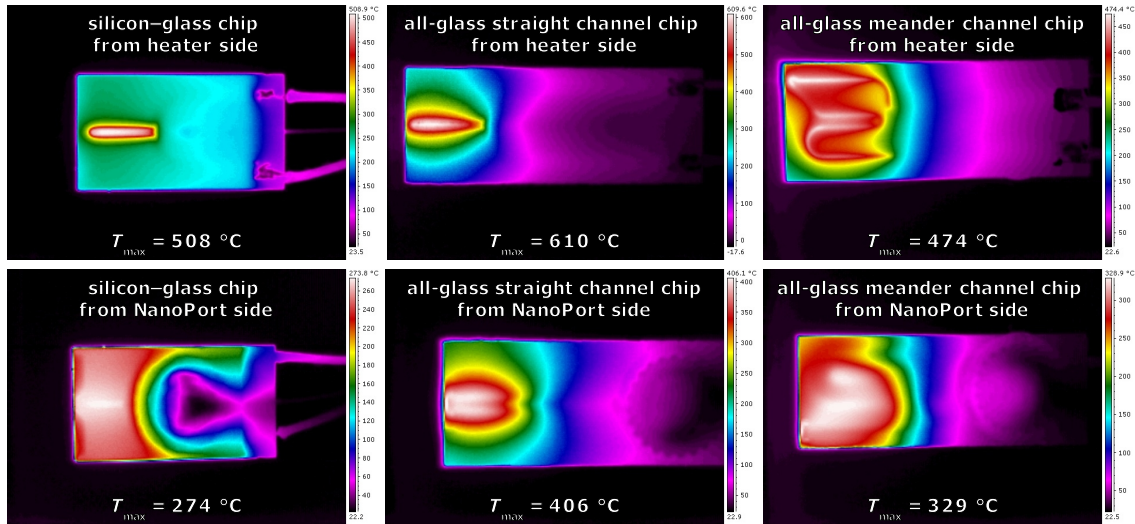


Figure 3.3: Infrared thermal images with peak temperatures (T_{max}) of HN chips with 4 W heating power and 150 sccm nitrogen flow. Silicon-glass chip size is 18 mm \times 10 mm and both all-glass chips are 26 mm \times 10 mm.

3.1.2 Channel fabrication processes

Different etch processes can be applied to both silicon and glass wafers as discussed in Sections 2.3 and 2.4. Figure 3.4 shows scanning electron microscope (SEM) images of nebulizer chip nozzles produced by different fabrication methods. This subsection compares the different methods applied for making the nebulizer chips.

Wet etched glass

Fabrication process for nebulizer chips with wet etched channels are described in publication II. Chips made with a similar process are also used in [1-6] and in the jet shape measurements of publication IV. The process is outlined in Figure 3.2. LPCVD silicon hard

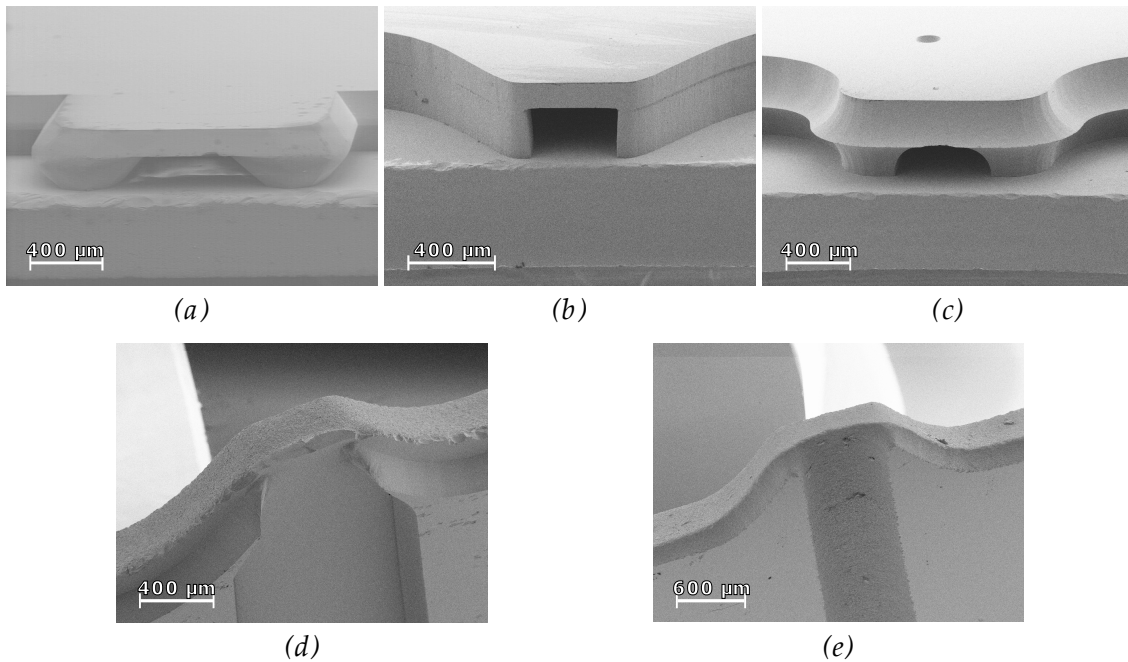


Figure 3.4: Nebulizer chip nozzles produced with various fabrication processes: (a) anisotropic wet etching of silicon, (b) DRIE of silicon, (c) wet etched glass, (d) powder blasted glass and (e) DRIE etched glass channel with powder blasted through-holes.

mask deposition (about 400 nm thick) was ordered from CSEM (Neuchâtel, Switzerland). Standard double sided lithography (AZ5214E resist, AZ Electronic Materials GmbH, Germany) follows with wet etching of the silicon hard mask ($\text{HNO}_3/\text{NH}_4\text{F}/\text{H}_2\text{O}$, 44:1:18), glass wet etching (HF/HCl , 10:1), photoresist stripping (ultrasonic acetone bath) and hard mask removal (25% TMAH, 80 °C). Alternatively the photoresist can be removed after the silicon etching prior to glass etching, but the photoresist layer can potentially help to reduce pinhole defects. The isotropic silicon etchant also etches glass and leads to higher surface roughness compared to stripping with TMAH [108]. Without stirring of the glass etch solution visible waviness on the channel surface will result. The etch process is endothermic and the magnitude of natural convection in the solution depends on the area of the exposed surface. Therefore, continuous stirring of the solution is important for uniform etch depth. Ultra- or mega-sonic agitation can also be used for improving etch uniformity [219].

The nozzle shape obtained with this process is shown in Figure 3.4 (c). The isotropy is very good with almost perfect radial etch profile. Using this process with simultaneous two sided etching the wafer thickness defines the channel depth and minimum channel width. Some over-etching is required to ensure proper through-etching throughout the wafer. For standard 500 μm thick glass wafers the channel depth will be about 250 μm and the channels will be about 500 μm wider at the wafer surface compared to the channel width on the mask. If the mask openings are too small the etch rate may be locally reduced because of limited transport of fresh etchant to the surface. For the 250 μm deep etch 50 μm wide openings are large enough to be reproduced without problems. Isotropic etching can produce at best 1:2 (height:width) aspect ratio which gives little room to play with nozzle shape and possible extra structures monolithically integrated to the channels.

Wet etched silicon

The first nebulizer chips were fabricated using anisotropic wet etching of silicon. Both TMAH [52,53,56] and KOH [220] etching was used with 600 nm...1 μm thermal oxide hard mask material. The oxide mask was patterned on both sides via lithography and etching. Typically, about 90% of the oxide thickness was first etched with RIE and then the remainder with BHF. Compared to etching fully with BHF this approach results in better edge profile which has some effect on the resulting channel profile as discussed in Section 2.3.2. However, the nebulizer chips do not have very high aspect ratio structures so this phenomena has little practical significance. Alternatively, LPCVD Si_3N_4 (~100 nm) was sometimes used as the hard mask instead of thick thermal oxide. Nitride has a lower etch rate in both TMAH and KOH compared to oxide. However, nitride has to be patterned using RIE and nitride stripping requires either RIE or 160 °C phosphoric acid, which is complicated compared to oxide stripping in HF. Also, for good etch results a thin oxide layer underneath nitride is required to reduce stress and to improve nitride adhesion. All and all, the use of a simple thick enough oxide hard mask is favoured over nitride.

For typical 380 μm thick DSP wafers, the maximum outer diameter (OD) of the sample capillary is 190 μm . Although capillaries with OD less than 90 μm are available there was an interest to use commercially available 220 μm OD deactivated capillaries that minimize the possibility of unwanted surface effects involved with untreated capillaries. However, the use of thick capillaries would have required either the use of thicker DSP wafers or two phase etching to enable other than half wafer thickness channel depth. Alternatively, the

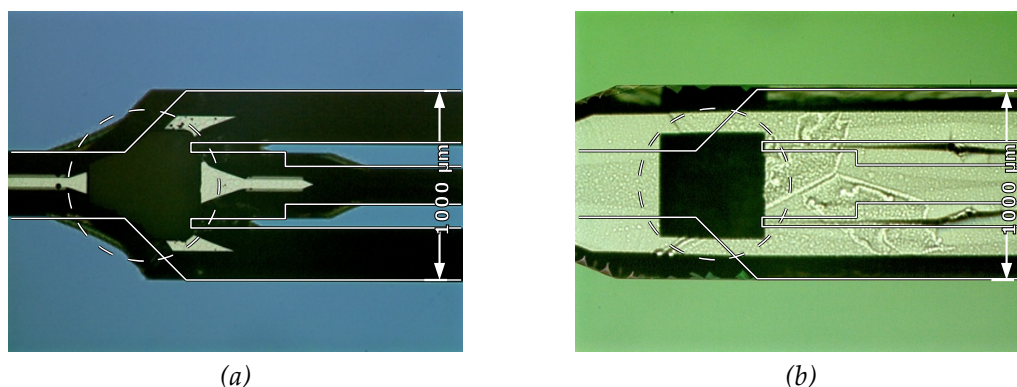


Figure 3.5: Nebulizer gas inlet hole and capillary stopper structure etched in (a) KOH+IPA and (b) TMAH. The dashed and the solid lines indicate the original etch mask edges on the inlet and channel sides of the wafer, respectively. (Micrographs courtesy of Kestas Grigoras.)

etching can be continued after penetration of the wafer but this adds to the undercutting of the nozzle and other convex corners. KOH with added IPA has smaller undercutting and it was used to etch 240 μm deep structures from both sides of 380 μm thick silicon wafer [218]. Reduced undercutting of KOH+IPA also enabled a capillary stopper structure in the nebulizer channel which could not be made with TMAH as shown in Figure 3.5. The purpose of the capillary stopper was to provide repeatable positioning of the sample capillary. However, the capillary stoppers were left out after a couple of chip generations because the influence of the capillary positioning was yet to be determined and the structures could interfere with the sample and the nebulizer gas flow at the capillary tip with an effect on the stability of the mixing. Unfortunately, it is very difficult to get definite experimental verification of these and many other effects. The absolute ion intensity in the mass spectra is affected by a plethora of different factors, such as, ambient conditions, exact positioning of the ion source with respect to the ion inlet of the mass spectrometer and the electrical drift of the detector. In quantitative analysis with mass spectrometers calibration is established by a reference standard with known composition and concentration mixed in the sample.

DRIE etched silicon

The DRIE etched silicon process is very similar to the wet etched silicon process except the etching is done using DRIE. Again, thermal oxide is good masking material but there is no need to remove the photoresist after oxide patterning. DRIE etched silicon-glass nebulizer chips are used in [7-10,56].

Anisotropic DRIE etching offers freedom of layout because there will be very little etching under the mask. The channels have rectangular cross-section. Especially the nozzle design can be easily tailored and there is no need for corner compensation structures like in anisotropic wet etching. Sharp and tapering nozzles are easy. As DRIE is one sided process, there is no problem to etch different depths from each side. For the 220 μm OD deactivated capillaries, the target depth of the channels was 250 μm to give some tolerance.

Powder blasted glass

A nebulizer chip nozzle etched with powder blasting is shown in Figure 3.4 (d). A photopatternable LF55GN elastomer was used as masking material and powder blasting was done in a custom-made chamber equipped with sample stage and nozzle oscillators. A

Texas Airsonics, Model HP-2 powder blasting machine was used with 30 μm alumina particles (EKF 320, Strahltechnik Bachmann AG).

Compared with wet etching of glass, powder blasting allows higher aspect ratios. This, combined with possibilities from oblique angle blasting, enables the micromachining of more complex structures. Also, powder blasting is economical compared to wet etching thanks to easy masking processes available. However, for the nebulizer chips the rough surface of the powder blasted nebulizer channel could be detrimental to the analytical performance of the chip. Sample droplets from the inlet capillary are pushed to the sidewalls where they spread on the rough surface and are flash evaporated by nucleate boiling. The analytes with the highest boiling point may desorb slowly causing a memory effect. Also, the hot surface may cause thermal degradation of the analytes temporarily dried on it. A smooth inner surface of the nebulizer channel is better because if the surface is hot enough it can provide vapour film boiling of the sample droplets where the droplets bounce off the channel surface due to the Leidenfrost effect. Much less thermal degradation of the analytes will result as most of the droplet evaporation will take place in gas phase with heat transfer from the nebulizer gas. These issues are further discussed in [16]. Unfortunately, no powder blasted chips were made ready for testing with a mass spectrometer to get experimental verification whether the added surface roughness makes a difference or not.

DRIE etched glass

The DRIE of glass was also applied for making nebulizer chip channel wafers as presented in publication III and Figure 3.4 (e). Out of the three glass micromachining methods used in this work, glass DRIE offers the highest aspect ratios and most flexible channel and nozzle geometries similar to silicon DRIE. A silicon wafer shadow mask was used to mask the DRIE etching from the channel side. Etching from the other side was done with powder blasting. Back side alignment for LF55GN lithography for powder blasting masking was easier compared to alignment of a shadow mask for DRIE. Also, through-etching with DRIE would require additional protection for the sample stage, for example, a dummy wafer underneath the sample wafer.

Glass DRIE can provide very low surface roughness and there are no apparent reasons why nebulizer chips would not perform well in their applications. Unfortunately, the prepared wafer broke during bonding and no chips could be made ready for testing with a mass spectrometer. For the current nebulizer chip designs there are no foreseeable advantages resulting from using glass DRIE and the process is expensive and cumbersome compared to wet etching of glass. In contrast, for a nebulizer chip with integrated LC column glass DRIE could be advantageous as will be discussed in Section 4.2.

3.1.3 Cover wafer bonding

For nebulizer chips with the channel wafer made of silicon anodic bonding of a glass cover wafer is an obvious choice as it is a fairly routine microfabrication process as discussed in Section 2.5. Anodic bonding provides very strong bonding and it is not too sensitive to surface roughness or minor particle contamination on the bonding surfaces. For the nebulizer chips an RCA-1 cleaning step was done to both silicon and glass wafers prior to bonding. Anodic bonding can also conform to thin (~100 nm) heater elements between the wafers. The on-chip heater will be further discussed in Section 3.1.4. Anodic bonding often

results in minor corrosion (visible staining) on the glass (cathode) surface. The corrosion depends on the local electrical contact quality between the glass and the bonder electrode. Corrosion results from sparking due to poor contact and from sodium agglomeration.

Fusion bonding of two glass wafers was used for all glass nebulizer chips. The wafers are RCA-1 cleaned, dried, contacted and thermally annealed at 650 °C resulting in very strong bonding, comparable to bulk glass. During annealing the glass wafers are placed in a horizontal position on a quartz plate with a non-polished surface. Polished surface quartz plates would bond with glass and the wafers would break during chamber cool down due to about one order of magnitude difference in thermal expansion between silicon and quartz. If cleaned wafers are directly put on top of each other for annealing there will be a varying amount of voids between the wafers. To reduce the voids a pre-bond step in a vacuum bonding chamber with compression and heating up to 500 °C was found to provide good results. Using higher temperatures with compression would result in imprinting of the bonder platen patterns (the alignment view ports, for example) on the glass. Furnace annealing at 650 °C after the pre-bond step was still required to increase the bond strength.

Also anodic bonding experiments between two glass wafers with intermediate silicon thin-film were conducted as mentioned in publication II. Initial experiments with PECVD deposited a-Si lead to poor bond strength presumably due to out gassing from the film. The LPCVD silicon could provide stronger bonding but the over hanging silicon hard mask on channel edges imposes some problems. During water rinsing after glass etching the hanging silicon tends to crack away with poor edge quality affecting the bond interface at channel edges. Overall, fusion bonding is preferred.

3.1.4 On-chip heater

The nebulizer chips have thin-film metal resistors that are used for heating. In initial prototypes aluminium was used but these heaters had a very short lifetime even with low heating powers. In addition, the heater was directly in the vaporization channel of the chip and was exposed to the vapours of the sample. Some analytical applications use dilute caustics as a solvent which is not a good combination with aluminium because they are aluminium etchants. Therefore, the heater material was changed to platinum which provided much longer heater lifetime. Typically, the platinum heaters of the all-glass HN chips have lifetimes of one to a couple of weeks corresponding to operating times from tens to hundreds of hours, which can be considered sufficiently long.

Typically, a 300 nm thick sputtered platinum with a 17 nm thick chromium adhesion layer was used as the heater. The sheet resistance of this kind of heater is around 1 Ω/sq providing a reasonable heater resistance from 100 Ω to 200 Ω depending on the heater layout. This resistance range is suitable for the typical 3 W...5 W heating powers with ordinary 60 V laboratory DC power sources.

Thin-film platinum heater elements are used in various MEMS devices, because platinum tolerates high temperatures well and has fairly constant temperature coefficient of resistivity over wide temperature range. However, platinum is also used as a catalyst for various chemical reactions. With this in mind it did not seem like a good idea to have platinum in contact with the sample flow. Therefore, the heater was moved away from the channel to the outer surface of the chip. Naturally, this slightly reduces the energy

efficiency of the heater because the heat must be conducted through the glass cover wafer to the nebulizer channel.

Another benefit of having the heater on the outer surface is that the heater can be made after wafer bonding. Anodic bonding can easily conform to approximately 100 nm thick heater film between the wafers, but a thicker film – that would have both lower resistivity and longer lifetime – would result in voids. This problem can be solved by embedding the heater in the surface level of the wafer by etching a recess before deposition but this adds the process complexity and requires good film thickness uniformity [122]. Patterning the heater elements after the bonding has the advantage that no alignment is needed for the bonding. Also, anodic bonding causes cathodic corrosion (further discussed in Section 3.2) and spark erosion of platinum.

Both lift-off and etch patterning were applied to the platinum heater. Typically, etch patterning was used and it was done in diluted aqua regia (3:1:2 HCl:HNO₃:H₂O, 70 °C, etch rate some tens of nm min⁻¹) with AZ5214E photoresist. A chromium adhesion layer was etched in a ceric ammonium nitrate-based etchant (200 g of Ce(NH₄)₂(NO₃)₆ + 50 ml of HClO₄ + 1090 ml of H₂O). Wet etching of platinum is quite a sensitive process because even a small amount of oxidized platinum at the surface inhibits dissolution of platinum in aqua regia [221]. A sputtered platinum film would usually etch without problems, but evaporated platinum had such a slow etch rate that the photoresist was dissolved faster. This could be due to some remaining oxygen in the evaporation chamber. Also, wet etching of platinum that was deposited prior to anodic bonding was unsuccessful. With lift-off it is important to have suitable photoresist and avoid its overheating during deposition. If lift-off patterning is done after bonding there is a danger that the channels will be contaminated with released platinum particles. By using etch patterning particle contamination of the channels is avoided, but the channels are filled with the etchant and it is somewhat laborious to properly rinse them.

For glass-to-glass fusion bonding the coefficient of thermal expansion between glass and platinum poses a problem. An experiment to bond glass wafer with platinum resulted in large voids throughout the wafer due to the deformation of the glass with the platinum heaters. The problem could be overcome with low temperature glass-to-glass bonding or by using compression during the annealing, but the necessary machinery was not available in our facilities. The surface texture of the platens of the compressing machine will be imprinted in the surface of glass and surface polishing may be required after the bonding if the surface quality is an issue. Fortunately, the performance of the HN chips is not affected by the added roughness on the outer surface. Integrated metal electrodes between glass wafers have been demonstrated in [122] with a block of alumina placed on top of the aligned wafers during annealing.

In addition to platinum, also aluminium, copper, tungsten, chromium and gold thin-film heaters were tried out. Out of these metals, gold was the only one that showed a similar temperature tolerance and lifetime as platinum. However, pure gold is soft and susceptible to scratching. With ordinary handling gold heaters would often fail prematurely because of scratching. Therefore, platinum seems like the best choice.

3.2 Lifetime and failure mechanism of the platinum heater

Earlier studies have identified different phenomena that play a role in the failure of platinum heaters: electromigration, stress-induced morphological changes (recrystallization), interlayer diffusion and chemical reactions [213]. For investigating the failure mechanism and the lifetime of the platinum heater used in the HN chips a set of test wafers were prepared. The layout of the heater test chips is shown in Figure 3.6 (a). The influence of three different adhesion layers (Cr, Ti, Ta) and different thermal annealing temperatures (no annealing, 450 °C, 600 °C) were tested for platinum heaters on Pyrex glass wafers. Annealing time was 30 minutes and it was done in nitrogen atmosphere with $\pm 10\text{ }^\circ\text{C min}^{-1}$ temperature rampings. The test chips were operated with a computer controlled power source with data logging of the current, voltage and the the chip temperature measured with a thermocouple. The chips were operated at ambient air with 6 W power corresponding a temperature of about 550 °C at the centre of the chip. This is higher than the typical operating temperature of the chips and it was chosen to accelerate testing. The measured lifetimes are shown in Figure 3.6 (b) and various other properties of the samples in Table 3.1.

The rate of corrosion depends on the applied electric field. The resistances of the tested Cr/Pt films were lowest resulting in lowest operating voltages and longest lifetimes. 150 μm wide heaters were also tested and their lifetimes were only 20 %...40 % of the lifetime of the 300 μm wide heaters. The narrow heaters have higher resistance and they require higher operating voltage for the same heating power. In all chips the failure of the heater took place near the contact pad for negative electrode, i.e. the cathode end. There was visible smudge on the platinum film around the failure point. Figure 3.7 shows an SEM and an energy dispersive spectroscopy (EDS) elemental analysis map of a failed platinum heater. The EDS analysis revealed the smudge crystals are mainly composed of sodium, carbon and oxygen – probably in the form of sodium carbonate (Na_2CO_3). Other sodium compound such as Na_2O , Na_2O_2 and NaOH may also be present but eventually they should react with the atmospheric CO_2 to form sodium carbonate. Unfortunately, EDS does not provide reliable quantification of light elements (carbon, hydrogen and oxygen) and other measurements would be needed to get verification of the exact composition of the smudge. A few microlitre drop of phenolphthalein pH indicator solution turned pink on the corroded platinum surface indicating an increase in the pH of the drop. This is in good agreement with the proposed composition of the smudge as all of the above mentioned sodium compounds are bases. It is well known that at elevated temperatures Na^+ ions in glass become mobile and will drift in an applied electric field. This phenomenon is the basis of anodic bonding as discussed in Section 2.5. Sodium ions migrate towards the cathode, diffuse through platinum film and react with ambient air at the surface causing corrosion on the platinum. Galvanic corrosion of platinum in molten Na_2CO_3 around 500 °C has been reported and oxidation of the platinum at the cathode, transport to the anode and reduction to metallic platinum at the anode was proposed as an explanation [222]. Because in the case of the heater there is no separate anode, this can also be interpreted to be electromigration or recrystallization of platinum. Naturally, there is also considerable compressive stress in the platinum film which can be relieved through hillock formation. However, because the heaters always fails at the cathode end, the sodium agglomeration undoubtedly plays an important part in the failure mechanism.

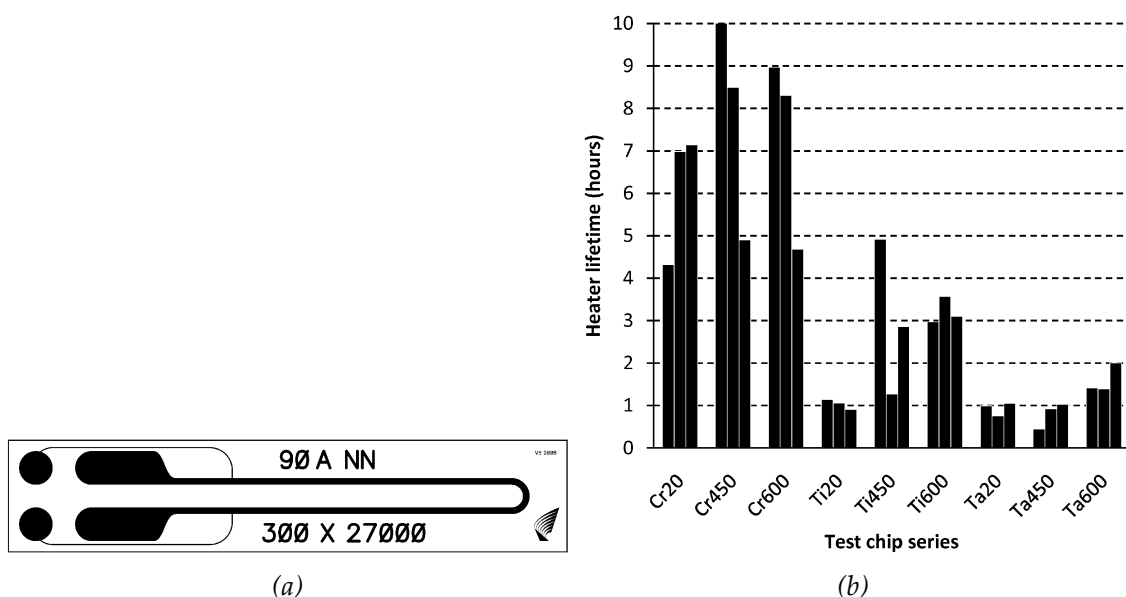


Figure 3.6: (a) Heater test chip layout (5 mm x 25 mm). DC power source was connected to large contact pads and voltage was measured via reference electrodes to determine the resistance of the heater outside the contact area. (b) Lifetime of the individual 300 μm wide Pt-heaters (three of a kind) at 6 W operating power with different adhesion layers (Cr, Ti, Ta) and post deposition annealing temperatures (20 $^{\circ}\text{C}$, 450 $^{\circ}\text{C}$, 600 $^{\circ}\text{C}$).

Table 3.1: Prepared test chips: Cr/Pt by sputtering, Ti/Pt and Ta/Pt by e-beam evaporation.

	Cr/Pt	Ti/Pt	Ta/Pt
Nominal adhesion layer thickness	17 nm	10 nm	10 nm
Nominal Pt layer thickness	200 nm	150 nm	150 nm
Profilometer measured total thickness	211 nm	180 nm	208 nm
Average resistance ^(a) of chips without thermal annealing	197 Ω	302 Ω	313 Ω
Average resistance ^(a) of chips annealed at 450 $^{\circ}\text{C}$	197 Ω	286 Ω	338 Ω
Average resistance ^(a) of chips annealed at 600 $^{\circ}\text{C}$	200 Ω	273 Ω	345 Ω

^(a) at 6 W operation

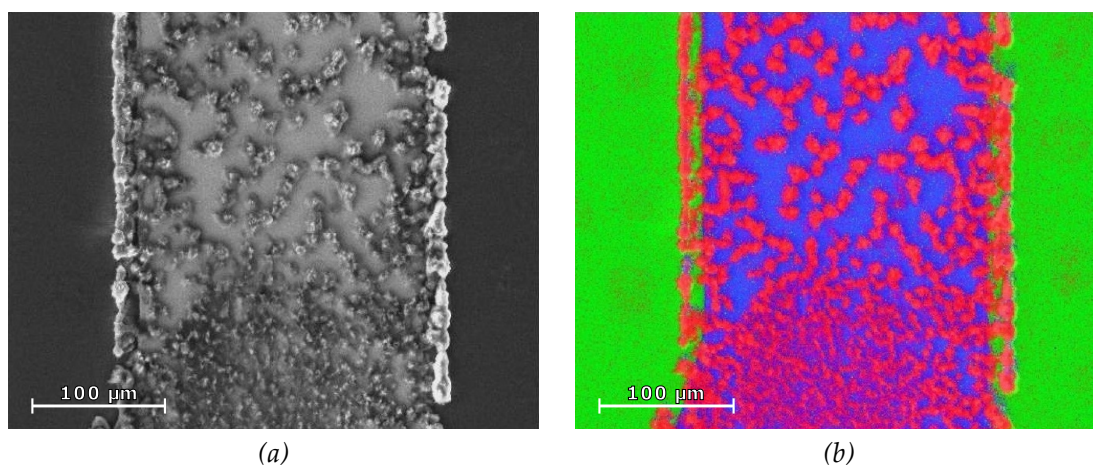


Figure 3.7: (a) SEM of a platinum heater after operation showing small agglomerated crystals and (b) EDS map from the same area with silicon showing in green, sodium in red and platinum in blue.

The electrophoretic agglomeration of sodium could be avoided by using sodium-free or low sodium containing glass. For example, quartz glass is pure SiO₂ and has much higher softening temperature compared to Pyrex which, theoretically, should enable the use of higher operating temperatures. However, the thermomechanical properties of quartz glass are inferior to Pyrex. Heater test chips made on quartz glass would spontaneously break during heating due to stresses from on-chip temperature gradients or due to phase transition that takes place for single crystalline α -quartz at 573 °C. Redesigning a heater that would provide better temperature uniformity might enable the use of quartz glass. However, quartz-to-quartz bonding is more difficult than glass-to-glass bonding [223,224]. Alternatively, sodium diffusion from glass can be reduced with a diffusion barrier layer (e.g. Si, SiN_x or SiC_x) between glass and heater as in glass-to-glass anodic bonding [189,225,226].

With the conducted test set, no decisive conclusions can be drawn regarding the effect of the adhesion layer or annealing. For sputtered Cr/Pt films the annealing had no effect, evaporated Ti/Pt film shows reduction in resistance and Ta/Pt film increase in resistance. For titanium adhesion, the average lifetime shows approximately three-fold increase for chips annealed at 600 °C compared to chips without any post deposition annealing.

To maximize the lifetime of a platinum heater on a glass substrate one should use as thick a platinum layer as possible, minimize local electric fields in the layout of the heater and make the cathode end wider so that it takes longer to fail by corrosion. A diffusion barrier either for the sodium from the glass or the oxygen from the air might help, but could also lead to issues with adhesion or film stress.

3.3 Fluidic and electrical interconnections

The nebulizer chip requires connections for sample and nebulizer gas flows and electrical connection to the heaters. Various approaches for making the chip-to-world connections have been applied. The first nebulizer chips had three NanoPort connectors (Figure 3.1 (a)): one for the sample flow and two for the nebulizer gas. This was not an economical approach for two reasons. Firstly, NanoPort assemblies are fairly expensive (around €20 each) and they are difficult to reuse. Secondly, three NanoPorts take plenty of surface area reducing the number of chips per wafer. A two NanoPort design with only one NanoPort for nebulizer gas connection behind the sample NanoPort was demonstrated in [56] but it was almost immediately replaced with a single NanoPort design.

In the single NanoPort design a sample capillary is inserted directly into the nebulizer channel from the chip edge and sealed with high temperature tolerant epoxy glue (Duralco 4703, Cotronics). The NanoPort is used for the nebulizer gas. A glass nebulizer chip with the single NanoPort approach is shown in Figure 3.8 (a).

As discussed in Section 2.6.1 there are several possibilities to make top surface fluidic connections. Different chip holders that used flat-bottom connectors were used to replace the NanoPort connector for nebulizer gas. The reversible nut-and-ferrule gas connection eases the use of the nebulizer chips as only the sample capillary needs to be glued to the chip and the chip can easily be replaced in the set-up, when needed. The holder material has to tolerate the on-chip temperatures, preferably up to 500 °C. Also, it must not short circuit the heater on the chip surface. A monolithic holder made of machinable glass ceramic (MACOR, Corning Inc.) is shown in Figure 3.8 (a). MACOR is a non-porous high

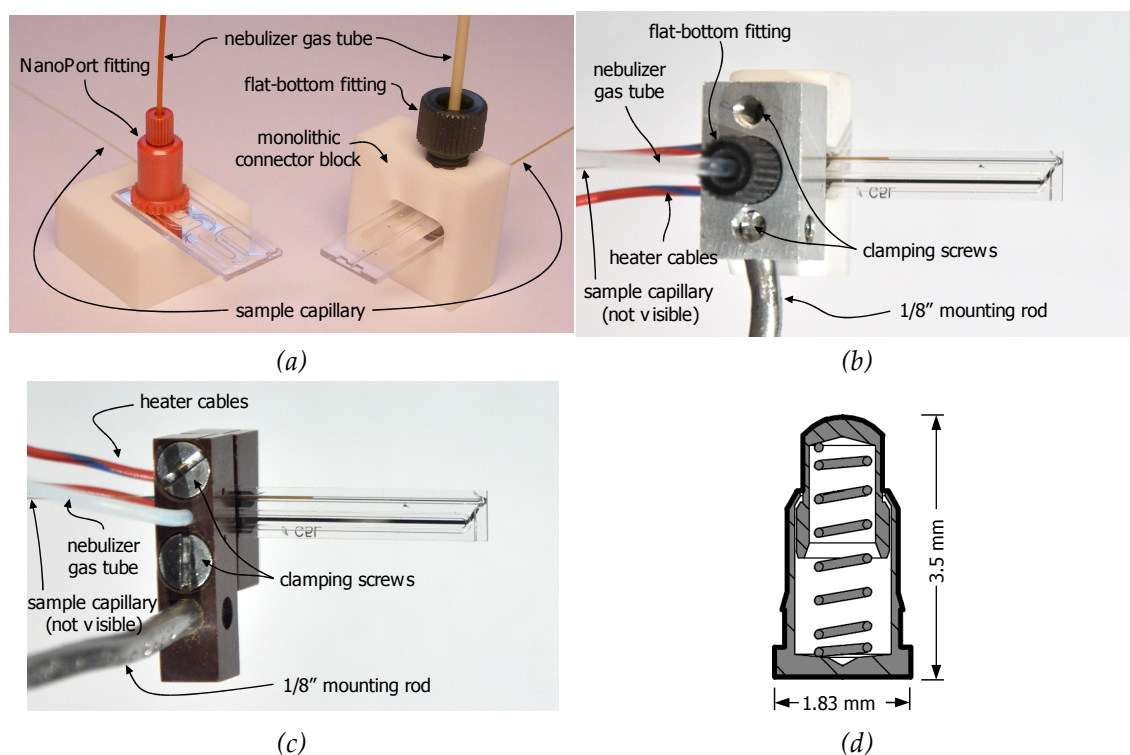


Figure 3.8: Different interconnection schemes for the nebulizer chips. (a) NanoPort connector and a monolithic ceramic holder with flat-bottom fitting. (b) Aluminium holder with flat-bottom connector. (c) Polyimide holder with integrated o-ring seal. (d) Cross-section of the spring loaded electrical connector used in (b) and (c).

end material that can be machined with ordinary metal working tools and it withstands continuous use at 800 °C. However, it is brittle and requires careful machining whereas metals, such as aluminium, are much easier to machine. An aluminium-MACOR two piece holder is shown in Figure 3.8 (b). The latest chip holders (Figure 3.8 (c)) are made from high temperature tolerant polyimide polymer (Sintimid NT, Ensinger Sintimid GmbH) and they have an o-ring (Perlast G75B, Perlast Ltd.) seal for the tubing. A schematic cross-section of this holder is shown in Figure 2.10 (f).

For electrical connection to the heater it is possible to solder wires directly to the heater. Although the peak temperature on the chip is higher than a typical solder melting point, the inlet end of the chip remains cooler. Nevertheless, it may be necessary to use a high melting point solder depending on the chip layout and operating power. For solder-less connections the recent chip holders are equipped with gold plated spring loaded connectors (90041, Preci-Dip SA; cross-section in Figure 3.8 (d)) that provide easy and reversible heater contacts.

Publication I presents a fluidic inlet scheme that used PDMS to seal the tubing against the chip. Unfortunately, this approach was not compatible with the heated chips as the outgassing from the PDMS leads to a significant increase in the signal background noise and contaminates the mass spectra.

3.4 Jet shape and temperature

The jet shape produced by the nebulizer chips influence both ionization and ion collection efficiencies. Therefore, knowing and controlling the jet shape is important. However, it is

not trivial to measure the shape of a small gaseous jet. Optical contrast between ambient air is too weak for direct photography. Liquid fluorescent droplets containing spray can be imaged with fluorescence microscopy, but fluorescence intensity from a fully gaseous jet is too weak for conventional fluorescence image sensors. Methods demonstrated for measuring gaseous jets are planar laser-induced fluorescence (PLIF) [227,228], infrared imaging [56,229] and microcantilever sensors attached to a computer controlled xyz stage [230].

Infrared imaging has been applied for measuring the jet shape of the nebulizer chip by capturing the heat trace of the jet on a piece of paper along the jet [56]. As such, the hot gas would not stand out from the background. However, the capture sheet distorts the jet reducing spatial and temperature accuracy of the measurement. The method is also very sensitive to the positioning and deformation of the capture sheet. Despite the limitations of the applied infrared jet shape measurement the results clearly showed that a narrow plume can be produced by the nebulizer chip. However, the apparent difference between DRIE and wet etched silicon nozzles is probably exaggerated by measurement artefacts and in reality the jet shapes are much closer to each other.

Publication IV presents a method for measuring 3D temperature distribution of the jet. A miniature thermocouple is attached to a computer-controlled xyz table and an array of data points is measured at different positions. A schematic of the measurement set-up is shown in Figure 3.9 (a). The thermocouple has a sharp about 7 mm long V-shaped tip (Figure 3.9 (b)) made of 25 μm diameter wire with the junction at the apex. A set of 2D temperature scans is shown in Figure 3.10. The measurements were done under a box that provided some protection from the random air flows in the laboratory, but nevertheless some thermal noise is seen around the jet due to fluctuations in the ambient air.

The measured temperature is the temperature of the thermocouple junction and that temperature depends on the sum of heat fluxes. The gas jet induces fairly rapid convective heat transfer and thermal conduction of heat takes place along the thermocouple wires. Depending on the position of the thermocouple either heat flux can be either positive or negative. Thermal conduction along the wires depends on the cross-sectional area of the wires and the temperature gradient along the wire. To study the effect of thermocouple size three different thermocouple wire diameters (13 μm , 25 μm and 50 μm) were compared. The measured temperature profiles along a line scan across the jet are shown in Figure 3.11 (a). The 13 μm and 25 μm diameter thermocouples provided practically identical results, but the measured peak temperature was lower with the 50 μm diameter thermocouple. This experiment shows that with sufficiently small thermocouple the conduction along the thermocouple wires can be neglected. The 25 μm thermocouple was used in other

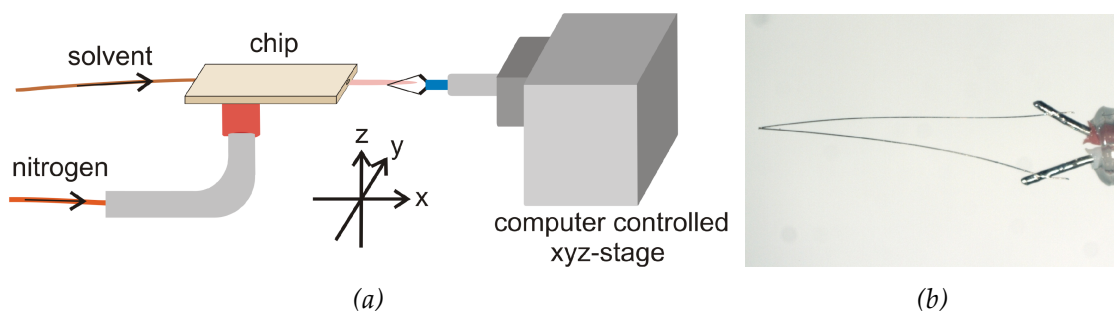


Figure 3.9: (a) Schematic measurement set-up. (b) Close-up of the 25 μm wire diameter thermocouple tip. [IV]

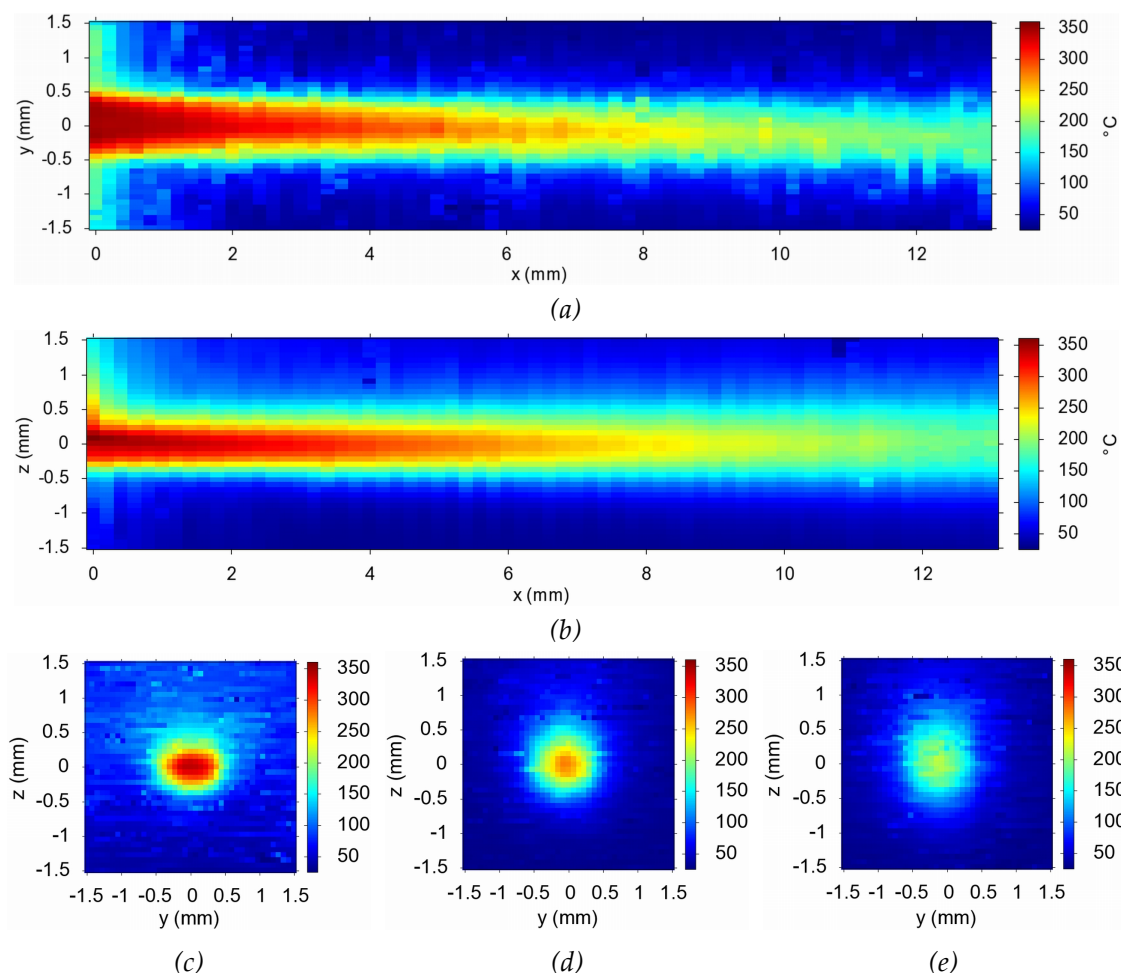


Figure 3.10: Temperature maps of a heated nitrogen jet produced by an all-glass nebulizer chip. The chip nozzle is at the origin and gas flow is to the right. (a) xy cross-section, (b) xz cross-section and yz cross-sections at (c) 1 mm, (d) 5 mm and (e) 10 mm distances from the nozzle. Nitrogen flow rate 100 sccm, $10 \mu\text{L min}^{-1}$ water/methanol (50/50) and 3 W heating power. [IV]

measurements because it was small enough for accurate measurements but mechanically more rigid than the $13 \mu\text{m}$ one.

It takes a while for the thermocouple temperature and the heat fluxes to reach equilibrium. The measurement programme has a stabilization algorithm, which allows the user to adjust stabilization parameters. There is a trade-off between the measurement time and accuracy. Longer temperature signal averaging would allow more accurate results but would increase the overall measurement time. Too fast measurements result in a hysteresis effect in a reciprocating scan as seen in Figure 3.10 (a). The measurement time of a single data point was about 0.5 s on average, but it varied between different temperature regions. All in all, the thermocouple can be assumed to have reached equilibrium in this time as the measured 63 % rise and fall time constants of the thermocouple were 28 ms and 60 ms, respectively. Naturally, the exact time constants depend on the velocity of the jet, but the order of magnitude should remain the same. Figure 3.11 (b) shows the measured temperature as a function of gas flow rate. The measured temperature is highest at 120 sccm nitrogen flow rate. With higher flow rates the temperature decreases, which is natural because the energy needed to heat the increased mass flow of the gas increases but the heating power is kept constant. Also, the velocity of the gas is increasing and there might be insufficient time to reach thermal equilibrium with the channel wall temperature

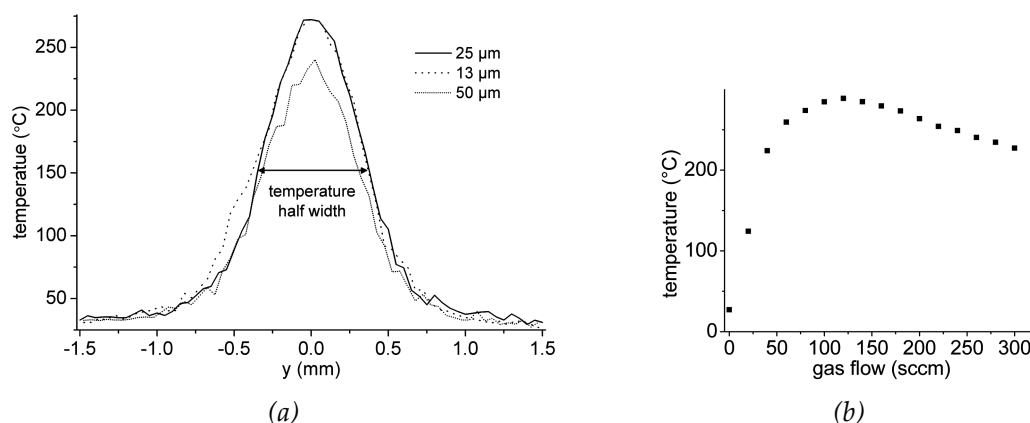


Figure 3.11: (a) Temperature profile along the y -axis at a distance of 5 mm from the nozzle with different size thermocouples (100 sccm N_2 , 3 W heating power). (b) The measured peak temperature of the jet 5 mm from the nozzle as a function of gas flow rate (25 μm thermocouple, 3 W heating power). [IV]

due to decreasing residence time in the channel. At lower flow rates the measured temperature also decreases which can be explained by the more rapid spreading of the low velocity jet and decreased heat flux to the thermocouple which might be insufficient to overpower the conduction losses via thermocouple wires.

The thermocouple scanning method provides temperature distribution but velocity distribution of the jet is also of considerable interest. The different physical and chemical magnitudes are interconnected by the laws of physics. To get an idea of the correlation between temperature and velocity profiles an axial symmetry 2D computer simulation model was made using the COMSOL Multiphysics 3.5 program with a non-isothermal flow application mode. The boundary conditions were selected to provide peak temperature and mass flow analogous to the thermocouple measured jets. The simulation results are shown in Figure 3.12.

The simulated velocity profile is parabolic throughout the jet, which is characteristic for a laminar flow. The jet exits the nozzle with uniform temperature but after some 2 mm from the nozzle also the temperature profile has a Gaussian profile and after this both temperature and velocity decrease at similar rate as shown in Figure 3.12 (c). The heat of the jet is dissipated to the ambient air mostly by conduction because convection is small due to laminar flow. Velocity decreases due to viscous friction and due to decreasing gas volume with decreasing temperature. Based on the simulation results, it can be concluded that an approximate velocity profile is obtained by measuring the temperature profile of a heated jet.

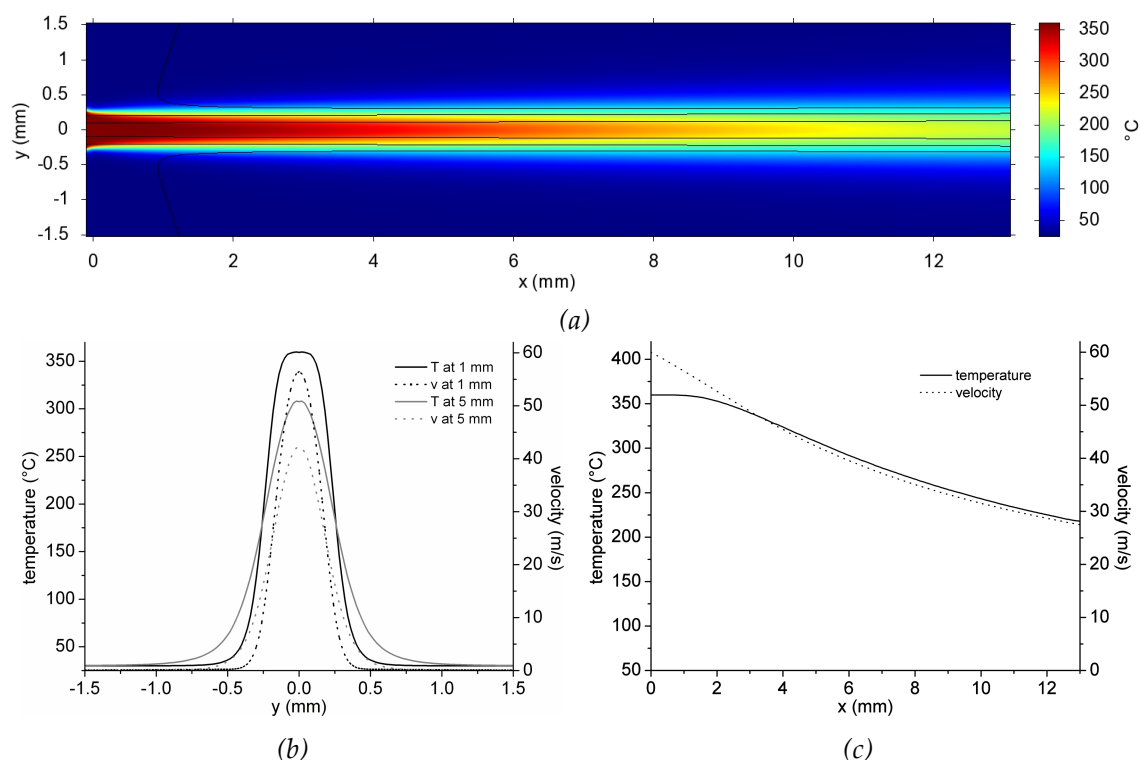


Figure 3.12: (a) 2D axial symmetry computer simulation of the temperature distribution of a heated nitrogen gas jet. The black velocity streamlines follow the temperature profile closely. (b) Axial temperature and velocity profile at distances of 1 mm and 5 mm from the nozzle. (c) Temperature and velocity along the centreline. [IV]

3.5 Applications of the heated nebulizer chips

The nebulizer chips can be applied to several ionization methods and used in various configurations (e.g. in combination with different separation methods). Table 3.2 lists all the ionisation principles that have so far been demonstrated with the nebulizer chips. The first demonstrations were with APCI [52] and APPI [53]. In APPI, a dopant (e.g. toluene) is mixed in vaporized sample. The dopant has an important role in the photoionization process.

Performance of APCI using the nebulizer chip as the source has been found better compared to a commercial macroscopic APCI source [52] enabling much lower sample flow rates without compromising the detection limits. This can be explained with the shape of the nebulizer chip's plume. The chip provides a very narrow and confined jet compared to the commercial APCI, which has roughly one order of magnitude larger tubular nozzle. As the range of a corona discharge is in the order of a few hundred micrometers the analytes in a jet with the similar diameter are ionized much more efficiently compared to a larger plume. The jet shape also determines how efficiently the ions are collected to the MS inlet. The nozzle shape of the chip and the resulting jet shape can easily be varied and, therefore, knowing the jet shape is important. Publication IV and Section 3.4 shows that the jet is sharp and it spreads out very little in the measured 13 mm distance which is similar to the distance between the chip and the inlet of MS.

In addition to APCI and APPI, the nebulizer chip can be used for other API techniques. Sonic spray ionization (SSI) is demonstrated in [7] and atmospheric pressure thermospray ionization (APTSI) in [1]. In SSI the nebulizer gas flow is much higher than with APCI and

Table 3.2: Summary of different ionization methods demonstrated with the heated nebulizer chips.

Method	Description	Applicability
APCI	Atmospheric pressure chemical ionization; heated jet, high voltage applied to a needle electrode for corona discharge	For thermally stable polar and less polar analytes, $m/z \leq 1.000$
APPI	Atmospheric pressure photoionization; heated jet, dopant mixed to nebulizer gas	For thermally stable polar and nonpolar analytes, $m/z \leq 1.000$
APTSI	Atmospheric pressure thermospray ionization; heated jet	Thermally stable very polar analytes
DAPPI	Desorption APPI; hot jet with dopant applied towards sample surface	Analysis of surfaces and solid samples with little or no preparation; suitable for same analytes as APPI
IS	Ionspray; room temperature, voltage applied to the liquid sample, nebulizer gas flow	Biomolecules and other (polar) analytes similar to ESI; allows higher flow rates and more water in solvent than ESI (thanks to the nebulizer gas, which is not used in ESI)
SSI	Sonic spray ionization; room temperature, high nebulizer gas flow	Biomolecules and other polar or ionic analytes; more gentle than ESI

the velocity of the jet is near the speed of sound, i.e. sonic speed. No heating of the chip is required. SSI is best suited for analytes that are already ionized in the solution whereas ionization of nonpolar compounds is inefficient. Nevertheless, SSI is a robust and soft ionization technique, which makes it suitable for thermolabile compounds. APTSI differs from APCI and APPI by the lack of additional excitation. Only heating and nebulizer gas are used. Certain analytes are ions already in the solution or may be spontaneously protonated in the gas phase after vaporization. Out of the the above mentioned API techniques, APPI is the most universal one providing efficient ionization of the widest range of analytes.

Direct sample infusion has limited applicability in practical applications, but it can be useful, for example, with crude oil analysis with extremely powerful Fourier transform ion cyclotron resonance mass spectrometry (FT-ICR MS) as shown in [2]. Using the nebulizer chip instead of a conventional APPI source has clear advantages. Similar sensitivity is obtained with much lower sample flow rates and the contamination of the mass spectrometer chamber is reduced. In addition, the nebulizer chips are easy to replace after accumulation of non-volatile crude oil components inside the chip.

The optimal sample flow rate range with the nebulizer chip is similar to the flow rates used in capillary liquid chromatography. External LC systems have been connected with the nebulizer chip via capillary tubing [6,8,9]. Commercial ion sources offer only ESI for capillary LC whereas the HN chip enables other ionization methods extending the range of suitable analytes.

The nebulizer chips can also be used with gaseous samples as shown in [9,10,12] where a gas chromatograph is connected to the chip via a heated transfer line for APPI-MS analysis. When coupling the chips to gas chromatography (GC) it is important that there

are no cold spots in the part between the GC oven and the chip. Cold spots are problematic because analytes with higher boiling point will condense compromising the GC separation. The beginning of the chip where the transfer capillary is glued is a potential cold spot and, therefore, silicon–glass chips were preferred for use with GC because they have less temperature gradients compared to all-glass chips. However, in order to have suitable all-glass HN chips for GC, a new heater layout was designed to provide more heating at the beginning of the chip thus preventing the possibility of a cold spot.

The nebulizer chip can also be used for desorption ionization to analyse the composition at the surfaces of the sample. Desorption atmospheric pressure photoionization (DAPPI) has been used to analyse pharmaceutical tablets, illicit drugs, environmental soil and food samples [3-5,11]. In DAPPI, a heated dopant containing gas jet from the nebulizer chip and photons from a photoionization lamp is directed towards a surface. Analytes on the surface are desorbed, ionized and the ions are collected into a mass spectrometer.

Just recently, the silicon–glass nebulizer chip was demonstrated for the ionspray (IS) technique where a high voltage is applied to the silicon part of the chip and no heating is required [231]. IS is suitable for similar analytes as ESI – that is for polar molecules and large and thermolabile biomolecules – but it can operate on higher flow rates and tolerates a higher water proportion in the solvent.

4 On-chip liquid chromatography

This chapter reviews the literature about on-chip LC and discusses the LC chips developed in this dissertation project.

4.1 Review of LC chips

Liquid chromatography is a very versatile and powerful separation method. However, LC has gained less attention in the miniaturization community compared to CE, capillary electrochromatography (CEC) and related separation methods [30,232-234]. There are, nevertheless, quite a few publications dealing with microchip based LC. Various substrate materials, stationary phases and detection methods have been applied. A fully integrated LC system consists of pumps, a sample injector, a column and a detector. However, most of the LC chip development is still concerning the miniaturization of one or a few subcomponents and the devices still rely on external – and usually regular size – components.

4.1.1 Materials

Silicon substrates with etched channels and anodically bonded glass cover have been used by many [235-239] – also in publications V and VI. Silicon dioxide based materials are dominant in laboratory glassware and capillary tubing and they have been also applied to LC chips in the form of glass [38,240,241], fused silica [242] and quartz [243] wafers. The Agilent LC-ESI chip is made from laminated polyimide films machined by laser ablation [35]. Other polymers that have been used include hot-embossed [244-246] or injection moulded [247] COC, PDMS [248], SU-8 [37] and parylene-C [249].

4.1.2 Columns

There are four different types of the LC columns: open-tubular [235,236,250], particle packed [35,36,38,248,251,249], monolith [37,240-242,244-247,252,253] and pillar array columns [237,238,243,254-256].

Open-tubular columns have a small cross-sectional area (dimensions 0.5 μm ... 250 μm) and they are quite long (10 cm ... 16 cm). The channel walls are coated with the desired stationary phase which is typically hydrophobic saturated carbon chains. Open-tubular columns are limited in injection capacity and subject to blocking [234]. For the best separation performance long channels and, subsequently, high pumping pressures are required. In general, the separation quality is proportional to the separation time.

More frequently, the column channel is filled with solid media to increase the surface area of the column and thus to improve the capacity and to reduce the necessary column length. Channels can be filled with particles by pumping the channel with a slurry with the

particles mixed in a solvent. In order to stop the particles from going through the channel a frit or a tapering channel is needed at the column end. Although the cross-section of a tapering channel end would be larger than the particle size the keystone-effect leads to blocking of the particles at the column [248,257,251]. Elastic columns can block the particles also by a clamping effect where the channel expands and contracts due to pressure change or an anchoring effect with particles adhering to the sidewalls [248]. The LC chips in publications V and VI use a high aspect ratio pillar array as a frit etched in silicon (see Figure 4.1) to stop particles during column packing. The pillar frit works fine for 2.5 μm particles even though the distance between neighbouring pillars is at most 6 μm .

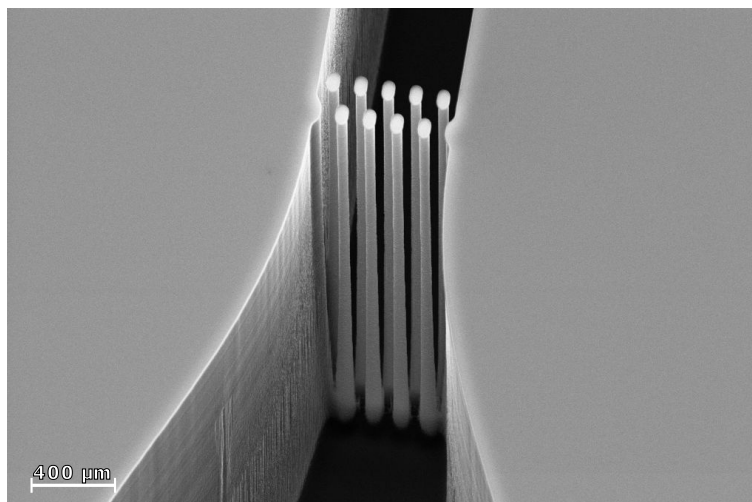


Figure 4.1: Detail from the LC chip.

Porous solid media filled columns are called monolithic columns. They are made by first filling the column with a precursor which is then cured during which the solvent in the precursor evaporates leaving a solid backbone which is then coated with the desired functional coating (e.g. hydrophobic octadecylsilica, C18, for reversed-phase LC).

A different kind of monolithic column which also utilises the batch fabrication nature of microfabrication is the pillar array column which consists of lithographically defined regular array of etched pillars. The integrated pillars eliminate the need for a separate packing step and offer higher capacity compared to open-tubular columns. With properly optimized distances between pillars and channel sidewalls a flat flow profile can be obtained for minimal band broadening [258]. A perfect LC column is perfectly ordered, i.e. the porosity is uniform [232]. However, it is difficult to eliminate all non-idealities that decrease the theoretical performance. The pillars always have some variation in size, shape and sidewall profile. Again, the column needs to be coated and the quality of the coating affects the separation performance. The pillar array column has a limited capacity because of limited surface area. Surface area of the silicon pillars can be increased by electrochemical anodization [238,259].

Temperature of the LC column affects the retention properties of the analytes and heating of the column can potentially provide better and faster separation results. The LC chip in publication VI has a separate platinum heater element for the column, but so far it has not been used. An LC column heater has also been presented in [235].

4.1.3 Interconnections, sample injection and pumping

Fluidic interconnections for microchip LC are challenging because they need to tolerate the high pumping pressures required by the small channels. Depending on the column dimensions and the packing density the pumping pressures can be several hundreds of atmospheres. Gluing of capillary tubing is a straightforward solution [240], but it has its weaknesses, as discussed in Section 2.6.1. If the chip is not made of brittle and hard material syringe needles can be pressed in providing tight connections up to 200 bar without additional gluing [245]. Alternatively, the chip can be compressed inside a custom made connector block [260]. In the LC chips of publication V, the capillaries were inserted and glued from the edge of the chip directly in the column. A custom made holder with standard flat-bottom fittings was used with integrated LC-nebulizer chip of publication VI. The connections did not show leakage with the maximum 150 bar pumping pressure used in the experiments.

In LC, the column is filled with eluent and then a small volume of sample is injected and the eluent pumping is continued. The two main principles of sample injection are shown in Figure 4.2. Sample injection can be done using crossing channels with the injection volume determined by the channel volume at the crossing [240,261]. Simple crossing of two channels or a double-T configuration are frequently used. This method is ideal for microchip CE where the direction of the flows is determined simply by the applied voltage at each inlet. However, mechanical valves are needed to avoid leakage between the additional injection channels in LC because the flow is pressure driven. Therefore, many LC chips rely on external valves for the injection [245]. The injection volume is determined by the volume of the injection loop. The unique feature of the Agilent chip is that it is placed between the stator and rotor of the injection valve [35]. This enables high pressure tolerant connections, low dead volumes and eliminates possible cross-talk between different inlets thanks to physical separation between them.

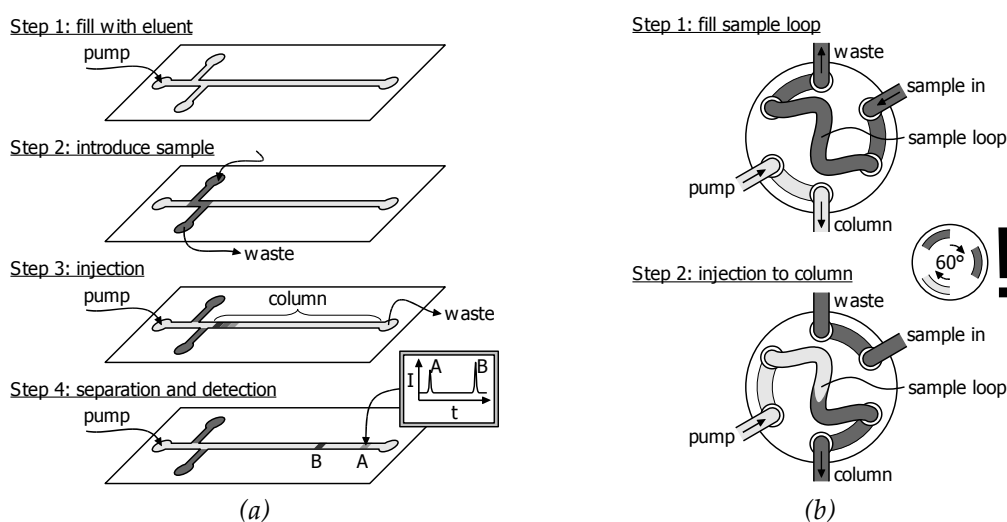


Figure 4.2: Different sample plug injection schemes: (a) on-chip injection using crossing channels and (b) off-chip injection with a mechanical 6-way injection valve.

Unlike CE, LC is based on pressure driven flow which is more challenging to miniaturize. Integrated pumps can rely on a separate electroosmotic flow (EOF) pump [261] or on electrochemical pumping via electrolysis in a closed chamber [36]. However,

frequently external pumps are applied with LC chips. Syringe pumps or commercial LC pumps can provide high pressures and stable flow rates. A moving cover lid can provide shear driven flow [256]. In practical LC applications the composition of the mobile phase eluent is usually changed during the run. This is achieved by using gradient pumps that can generate a desired mixture from several sources. A clever on-chip gradient generator channel network has been demonstrated to create gradient flow using only a single pump [39].

4.1.4 Detection

Several detection methods are applicable to LC. Mass spectrometric detection with an on-chip ESI source is frequently applied [35-38]. On-chip detection methods that rely heavily on external instrumentation include fluorescence [242,245] and UV absorbance [261] detections. Detection methods that can be integrated inside the chip include amperometric [236], heat transfer based [262], conductometric [250] and electrochemical [263] detectors. Naturally, external control electronics and data analysis software are required even with these detection methods. Although some of these methods may be highly sensitive or specific, none can provide the performance, versatility and identification capability of MS. The integrated LC–HN of publication VI chip extends the applicability of LC chips by enabling other API-MS techniques than ESI to be used for the ionization of a wider range of analytes as discussed in Section 3.5.

4.2 All-glass LC-nebulizer chip

A major problem with the integrated LC–HN chip of publication VI is the conduction of heat from the hot (up to 500 °C) nebulizer section to the LC column. For good separation efficiency the column temperature should be as uniform as possible. The high thermal conductivity of silicon ($150 \text{ W m}^{-1} \text{ °C}^{-1}$) is a problem when trying to keep different parts of the chip at different temperatures. Minimizing the silicon cross-sectional area will improve thermal insulation, but this was insufficient to provide the frit and column temperatures low enough in publication VI. Therefore, an external cooler block was used in to eliminate excess heating of the column. Similar problems with thermal conductivity of silicon have been encountered by others, too. For efficient thermal isolation the silicon is completely removed and replaced with a thermally isolating material. Parylene-C has very low thermal conductivity ($0.08 \text{ W m}^{-1} \text{ °C}^{-1}$) and it can be conformally coated which makes it a feasible choice [263] but only for temperatures up to its glass transition point around 100 °C. Suspended low stress silicon nitride is applicable also for higher temperatures [264]. The thermal conductivity of glass is roughly two orders of magnitude lower than that of silicon. Therefore, a process for making the LC-nebulizer chip out of two glass wafers was developed.

An LC-nebulizer chip made entirely out of glass should eliminate the need for active cooling between the LC and HN chip parts that was required with the silicon–glass chip. In addition, the all-glass design has reduced flushed volume after the LC column prior to the mixer with nebulizer gas implemented with double layer masking process with aluminium nitride and SU-8 was used for making different channel depths for the pillar frit and the column portions of the chip. In theory, the LC column channel depth would smoothly decrease prior to the frit due to aspect ratio dependent etch phenomenon.

The fabrication process of the all glass LC HN chip is illustrated in Figure 4.3. First, reactive sputtering (Von Ardenne Anlagentechnik GmbH, Dresden, Germany) of 1.3 μm thick AlN hard mask layer is done on a clean glass wafer. AlN is patterned with channel and pillar frit structures using standard lithography (AZ5214E resist) and RIE (STS AOE). After resist removal, a 50 μm thick layer of SU-8 is applied over the patterned AlN. The photomask for SU-8 is otherwise the same as that for AlN except that the LC column channel tapers down just prior to the frit and the frit and narrow optical detection channel are covered with SU-8. DRIE of glass is done in two steps. First the SU-8 is used as the mask to etch part of the desired channel depth (100 μm). Then SU-8 is stripped in O_2/CF_4 plasma and glass DRIE is continued with AlN as the masking layer. The AlN mask was necessary as the pillar size structures could not be patterned by the thick SU-8. Because the glass DRIE process is not optimal for making through-wafer etching, the necessary fluidic interconnections would be made via the bonded glass cover wafer with through-holes.

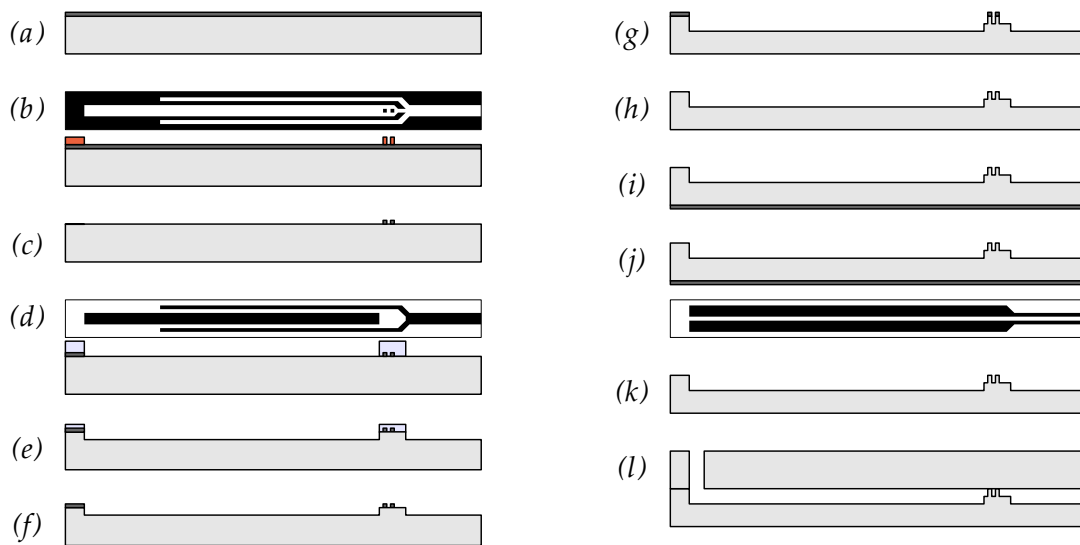


Figure 4.3: All-glass LC-nebulizer chip fabrication process: AlN deposition and patterning on a glass wafer (a-c), SU-8 (d), glass DRIE (e), SU-8 strip (f), continued glass DRIE for pillar frit (g), AlN stripping (h), Pt sputtering & patterning (i-k) and bonding with cover wafer with inlet holes (l).

Unfortunately, there were issues that could not be overcome and no chips could be completed for testing with LC and MS. The AlN to glass etch selectivity was too small which limited the channel depth to about 5 μm . Unfortunately, process optimization could not be carried out properly due to a limited number of samples. The AlN sputter had poor availability and there were repeatability issues involving AlN film or wafer cracking and problems with adhesion. The high selectivity glass DRIE process with AlN masking that had worked well for fused silica wafers [137] was not compatible with Pyrex glass because of the non-volatile etch products. Therefore, a process with higher ion bombardment was used with the expense of rapid wearing of the masking layer. Figure 4.4 shows an example of the obtained structures.

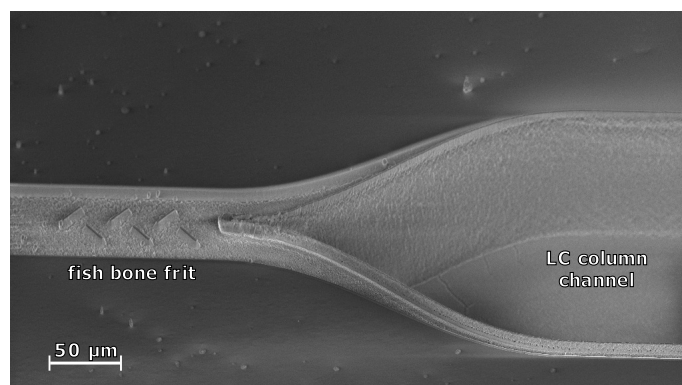


Figure 4.4: Fish bone shaped pillar frit structure in Pyrex glass made with double mask layer mask and DRIE. (SEM by Kai Kolari)

5 Conclusions and outlook

The HN chips have shown several advantages over conventional API mass spectrometer ion sources. The chip sources can be operated at a fraction of the sample flow rates without compromising sensitivity. This leads to reduced sample, solvent and nebulizer gas consumption and allows higher mass spectrometer uptime thanks to less frequent need to clean the chamber from accumulated contamination from the sample flow. All these lead to cost savings. The HN chips cover all the most used API techniques (APCI, APPI, SSI, APTSI and SI) and it can be applied to desorption ionization (DAPPI) as well. The nebulizer chips can operate with any API mass spectrometer whereas commercial ion sources are dedicated to a single model or brand. However, there is still work to be done before the chips can be commercialized. Most important, it should be easy to equip a mass spectrometer with the necessary mountings required by the chips and the routine operation of the chips must be straightforward. Custom fixtures and power sources can be used in experimental research environments but this is unacceptable for routine mass spectrometer users. For added operator safety and reduction of the risk of contamination of the mass spectra from compounds in the laboratory air, the ion source has to be enclosed inside a casing. Chip design, its lifetime and the production economics can still be improved. Different ionization methods have different requirements for electric conductivity and temperature of the chip as well as the nozzle and the jet shape. The channel and the nozzle dimensions used in the HN chips so far, are quite large from the microfabrication point of view and their further miniaturization could be worth further studies. Combined ionization modes such as simultaneous or alternating ESI and APPI are also subject to future study. For this, some ideas could be taken from the silicon micropillar ESI chip developed in our group [33].

The LC–HN chip was the first published demonstration of this kind of integrated LC chip for MS, but so far its analytical performance has been less impressive and the reasons for the suboptimal chromatographic peak shapes need to be investigated. Other future studies will include channel sidewall deactivation coating and high temperature LC with the use of the separate column heater element. One advantage of the current integrated chip is that post column dead volume is minimal. However, the post column dead volume can be negligible even with a conventional capillary LC connected to a HN chip and, as such, the current LC–HN chip has little advantage to offer. However, integration of further functionality could take the usefulness of the chip up to a higher level. Integration of a pre-column or a sample injector could be one possibility. Changing the column from the particle packed one to a microfabricated pillar array column would reduce the required post-processing of the chips after wafer dicing. Despite the faced challenges during our attempt to make one, the all-glass integrated LC–HN chip is still an intriguing prospect as it should solve the issues concerning excess heating of the LC column part of the chip

without resorting to an active cooling element. A parallel LC chip with multiple columns could be useful for high throughput analysis. Multidimensional separations [265] or transformation into a CEC [266,267] chip which combines both CE and LC in a single column could open up interesting new separation capabilities.

Another future prospect could be the integration of a GC column and a heated nebulizer. The LC–HN chip would be a good starting point for such a GC–HN chip. As GC is typically done at a similar temperature as the HN operating temperature there should be no problems with the heat transport even with a silicon–glass design.

A lot of know-how about silicon and glass microfabrication, on-chip heaters, chip-to-world interconnection schemes and jet shape measurements was acquired during this work. The HN chips and LC columns discussed in this dissertation have only scratched the surface of the possible applications where this kind of microfabrication could be applied to. The multidisciplinary nature of the field is both a challenge and an opportunity. Successful collaboration between experts with different backgrounds can lead to innovations having a revolutionizing impact on health care, security and the environment.

References

- [1] P. Keski-Rahkonen, M. Haapala, V. Saarela, S. Franssila, T. Kotiaho, R. Kostiainen, and S. Auriola, Atmospheric pressure thermospray ionization using a heated microchip nebulizer, *Rapid Communications in Mass Spectrometry* **23** (2009) 3313-3322. doi:10.1002/rcm.4252
- [2] M. Haapala, J.M. Purcell, V. Saarela, S. Franssila, R.P. Rodgers, C.L. Hendrickson, T. Kotiaho, A.G. Marshall, and R. Kostiainen, Microchip Atmospheric Pressure Photoionization for Analysis of Petroleum by Fourier Transform Ion Cyclotron Resonance Mass Spectrometry, *Analytical Chemistry* **81** (2009) 2799-2803. doi:10.1021/ac802427m
- [3] L. Luosujarvi, V. Arvola, M. Haapala, J. Pól, V. Saarela, S. Franssila, T. Kotiaho, R. Kostiainen, and T. Kauppila, Desorption and ionization mechanisms in desorption atmospheric pressure photoionization, *Analytical Chemistry* **80** (2008) 7460-7466. doi:10.1021/ac801186x
- [4] M. Haapala, J. Pól, V. Saarela, V. Arvola, T. Kotiaho, R. Ketola, S. Franssila, T. Kauppila, and R. Kostiainen, Desorption atmospheric pressure photoionization, *Analytical Chemistry* **79** (2007) 7867-7872. doi:10.1021/ac071152g
- [5] T. Kauppila, V. Arvola, M. Haapala, J. Pól, L. Aalberg, V. Saarela, S. Franssila, T. Kotiaho, and R. Kostiainen, Direct analysis of illicit drugs by desorption atmospheric pressure photolonization, *Rapid Communications in Mass Spectrometry* **22** (2008) 979-985. doi:10.1002/rcm.3461
- [6] L.L. Ahonen, M. Haapala, V. Saarela, S. Franssila, T. Kotiaho, and R. Kostiainen, Feasibility of capillary liquid chromatography-microchip atmospheric pressure photoionization-mass spectrometry in analyzing anabolic steroids in urine samples, *Rapid Communications in Mass Spectrometry* **24** (2010) 958-964. doi:10.1002/rcm.4468
- [7] J. Pól, T. Kauppila, M. Haapala, V. Saarela, S. Franssila, R. Ketola, T. Kotiaho, and R. Kostiainen, Microchip sonic spray ionization, *Analytical Chemistry* **79** (2007) 3519-3523. doi:10.1021/ac070003v
- [8] P. Östman, S. Jäntti, K. Grigoras, V. Saarela, R. Ketola, S. Franssila, T. Kotiaho, and R. Kostiainen, Capillary liquid chromatography-microchip atmospheric pressure chemical ionization-mass spectrometry, *Lab on a Chip* **6** (2006) 948-953. doi:10.1039/b601290f
- [9] M. Haapala, L. Luosujarvi, V. Saarela, T. Kotiaho, R.A. Ketola, S. Franssila, and R. Kostiainen, Microchip for combining gas chromatography or capillary liquid chromatography with atmospheric pressure photoionization-mass spectrometry, *Analytical Chemistry* **79** (2007) 4994-4999. doi:10.1021/ac070157a
- [10] L. Luosujarvi, M. Karikko, M. Haapala, V. Saarela, S. Huhtala, S. Franssila, R. Kostiainen, T. Kotiaho, and T. Kauppila, Gas chromatography/mass spectrometry of polychlorinated biphenyls using atmospheric pressure chemical ionization and atmospheric pressure photoionization microchips, *Rapid Communications in Mass Spectrometry* **22** (2008) 425-431. doi:10.1002/rcm.3379
- [11] L. Luosujärvi, S. Kanerva, V. Saarela, S. Franssila, R. Kostiainen, T. Kotiaho, and T.J. Kauppila, Environmental and food analysis by desorption atmospheric pressure photoionization-mass spectrometry, *Rapid Communications in Mass Spectrometry* **24** (2010) 1343-1350. doi:10.1002/rcm.4524
- [12] L. Luosujärvi, M. Haapala, M. Thevis, V. Saarela, S. Franssila, R.A. Ketola, R. Kostiainen, and T. Kotiaho, Analysis of selective androgen receptor modulators by gas chromatography-microchip atmospheric pressure photoionization-mass spectrometry, *Journal of the American Society for Mass Spectrometry* **21** (2010) 310-316. doi:10.1016/j.jasms.2009.10.019
- [13] G.E. Moore, Cramming more components onto integrated circuits, *Electronics* **38** (1965) 114.
- [14] Silicon Technology from Intel, http://www.intel.com/technology/architecture-silicon/silicon.htm?iid=tech_as_lhn+silicon
- [15] ITRS Starting Materials Sub-TWG, *Advantages and Challenges Associated with the Introduction of 450mm Wafers*, 2005.
- [16] T.R. Covey, B.A. Thomson, and B.B. Schneider, Atmospheric pressure ion sources, *Mass Spectrometry Reviews* **28** (2009) 870-897. doi:10.1002/mas.20246

- [17] Inkjet Head Market flyer, Yole Développement, http://www.yole.fr/pagesAn/products/pdf/Ink_jet_head_market.pdf
- [18] M.C. Louwerse, H.V. Jansen, M.N.W. Groenendijk, and M.C. Elwenspoek, Nozzle fabrication for micropropulsion of a microsatellite, *Journal of Micromechanics and Microengineering* **19** (2009) 045008.
- [19] J.D.J.S. Samuel, R. Steger, G. Birkle, R. Zengerle, P. Koltay, and J. Ruhe, Modification of Micronozzle Surfaces Using Fluorinated Polymeric Nanofilms for Enhanced Dispensing of Polar and Nonpolar Fluids, *Analytical Chemistry* **77** (2005) 6469-6474. doi:10.1021/ac050878e
- [20] W.G. Gardner, J.W. Jaworski, A.P. Camacho, and J.M. Protz, Experimental results for a microscale ethanol vapor jet ejector, *Journal of Micromechanics and Microengineering* **20** (2010) 045019. doi:10.1088/0960-1317/20/4/045019
- [21] S. Zimmermann, S. Wischhusen, and J. Müller, Micro flame ionization detector and micro flame spectrometer, *Sensors and Actuators B* **63** (2000) 159-166. doi:10.1016/S0925-4005(00)00353-1
- [22] S. Terry, J. Jerman, and J. Angell, A gas chromatographic air analyzer fabricated on a silicon wafer, *IEEE Transactions on Electron Devices* **26** (1979) 1880-1886.
- [23] A. Manz, N. Graber, and H. Widmer, Miniaturized total chemical analysis systems: A novel concept for chemical sensing, *Sensors and Actuators B* **1** (1990) 244-248. doi:10.1016/0925-4005(90)80209-I
- [24] J. West, M. Becker, S. Tombrink, and A. Manz, Micro Total Analysis Systems: Latest Achievements, *Analytical Chemistry* **80** (2008) 4403-4419. doi:10.1021/ac800680j
- [25] M.A. Burns, Everyone's a (Future) Chemist, *Science* **296** (2002) 1818-1819. doi:10.1126/science.1073562
- [26] M.A. Burns, B.N. Johnson, S.N. Brahmasandra, K. Handique, J.R. Webster, M. Krishnan, T.S. Sammarco, P.M. Man, D. Jones, D. Heldsinger, C.H. Mastrangelo, and D.T. Burke, An Integrated Nanoliter DNA Analysis Device, *Science* **282** (1998) 484-487. doi:10.1126/science.282.5388.484
- [27] W.R. Vandaveer IV, S.A. Padas-Farmer, D.J. Fischer, C.N. Frankenfeld, and S.M. Lunte, Recent developments in electrochemical detection for microchip capillary electrophoresis, *Electrophoresis* **25** (2004) 3528-3549. doi:10.1002/elps.200406115
- [28] K.B. Mogensen, H. Klank, and J.P. Kutter, Recent developments in detection for microfluidic systems, *Electrophoresis* **25** (2004) 3498-3512. doi:10.1002/elps.200406108
- [29] T. Sikanen, S. Franssila, T.J. Kauppila, R. Kostianen, T. Kotiaho, and R.A. Ketola, Microchip technology in mass spectrometry, *Mass Spectrometry Reviews* **29** (2010) 351-391. doi:10.1002/mas.20238
- [30] S. Koster and E. Verpoorte, A decade of microfluidic analysis coupled with electrospray mass spectrometry: An overview, *Lab on a Chip* **7** (2007) 1394-1412. doi:10.1039/b709706a
- [31] J. Lee, S.A. Soper, and K.K. Murray, Microfluidic chips for mass spectrometry-based proteomics, *Journal of Mass Spectrometry* **44** (2009) 579-593. doi:10.1002/jms.1585
- [32] S. Tuomikoski, T. Sikanen, R.A. Ketola, R. Kostianen, T. Kotiaho, and S. Franssila, Fabrication of enclosed SU-8 tips for electrospray ionization-mass spectrometry, *Electrophoresis* **26** (2005) 4691-4702. doi:10.1002/elps.200500475
- [33] L. Sainiemi, T. Nissilä, V. Jokinen, T. Sikanen, T. Kotiaho, R. Kostianen, R.A. Ketola, and S. Franssila, Fabrication and fluidic characterization of silicon micropillar array electrospray ionization chip, *Sensors and Actuators B* **132** (2008) 380-387. doi:10.1016/j.snb.2007.09.077
- [34] T. Sikanen, S. Tuomikoski, R.A. Ketola, R. Kostianen, S. Franssila, and T. Kotiaho, Fully Microfabricated and Integrated SU-8-Based Capillary Electrophoresis-Electrospray Ionization Microchips for Mass Spectrometry, *Analytical Chemistry* **79** (2007) 9135-9144. doi:10.1021/ac071531+
- [35] H. Yin, K. Killeen, R. Brennen, D. Sobek, M. Werlich, and T. van de Goor, Microfluidic Chip for Peptide Analysis with an Integrated HPLC Column, Sample Enrichment Column, and Nanoelectrospray Tip, *Analytical Chemistry* **77** (2005) 527-533. doi:10.1021/ac049068d
- [36] J. Xie, Y. Miao, J. Shih, Y. Tai, and T.D. Lee, Microfluidic Platform for Liquid Chromatography-Tandem Mass Spectrometry Analyses of Complex Peptide Mixtures, *Analytical Chemistry* **77** (2005) 6947-6953. doi:10.1021/ac0510888
- [37] J. Carlier, S. Arscott, V. Thomy, J.C. Camart, C. Cren-Olivé, and S. Le Gac, Integrated microfabricated systems including a purification module and an on-chip nano electrospray ionization interface for biological analysis, *Journal of Chromatography A* **1071** (2005) 213-222.
- [38] I.M. Lazar, P. Trisiripisal, and H.A. Sarvaiya, Microfluidic liquid chromatography system for proteomic applications and biomarker screening, *Analytical Chemistry* **78** (2006) 5513-5524.
- [39] R.A. Brennen, H. Yin, and K.P. Killeen, Microfluidic Gradient Formation for Nanoflow Chip LC, *Analytical Chemistry* **79** (2007) 9302-9309. doi:10.1021/ac0712805

- [40] C.S. Chu, M.R. Niñonuevo, B.H. Clowers, P.D. Perkins, H.J. An, H. Yin, K. Killeen, S. Miyamoto, R. Grimm, and C.B. Lebrilla, Profile of native N-linked glycan structures from human serum using high performance liquid chromatography on a microfluidic chip and time-of-flight mass spectrometry, *Proteomics* **9** (2009) 1939-1951. doi:10.1002/pmic.200800249
- [41] K. Cottingham, Nano-LC/ESI on a chip, *Analytical Chemistry* **77** (2005) 51A. doi:10.1021/ac0533321
- [42] S. Ehlert, K. Kraiczek, J.A. Mora, M. Dittmann, G.P. Rozing, and U. Tallarek, Separation Efficiency of Particle-Packed HPLC Microchips, *Analytical Chemistry* **80** (2008) 5945-5950.
- [43] K. Reinsberg, U. Effelsberg, and U. Tallarek, Microchip electrospray performance during gradient elution with bulk conductivity changes, *Lab on a Chip* **9** (2009) 2914-2923. doi:10.1039/b905052c
- [44] H. Yin and K. Killeen, The fundamental aspects and applications of Agilent HPLC-Chip, *Journal of Separation Science* **30** (2007) 1427-1434. doi:10.1002/jssc.200600454
- [45] T.J. Kauppila, T. Kuuranne, E.C. Meurer, M.N. Eberlin, T. Kotiaho, and R. Kostiainen, Atmospheric Pressure Photoionization Mass Spectrometry. Ionization Mechanism and the Effect of Solvent on the Ionization of Naphthalenes, *Analytical Chemistry* **74** (2002) 5470-5479. doi:10.1021/ac025659x
- [46] S. Tuomikoski, K. Huikko, K. Grigoras, P. Ostman, R. Kostiainen, M. Baumann, J. Abian, T. Kotiaho, and S. Franssila, Preparation of porous n-type silicon sample plates for desorption/ionization on silicon mass spectrometry (DIOS-MS), *Lab on a Chip* **2** (2002) 247-253.
- [47] A. Sen, J. Darabi, and D. Knapp, Design, fabrication and test of a microfluidic nebulizer chip for desorption electrospray ionization mass spectrometry, *Sensors and Actuators B* **137** (2009) 789-796. doi:10.1016/j.snb.2009.02.002
- [48] S. Tuomikoski, K. Huikko, K. Grigoras, P. Ostman, R. Kostiainen, M. Baumann, J. Abian, T. Kotiaho, and S. Franssila, Preparation of porous n-type silicon sample plates for desorption/ionization on silicon mass spectrometry (DIOS-MS), *Lab on a Chip* **2** (2002) 247-253. doi:10.1039/b207634a
- [49] Z. Ouyang and R.G. Cooks, Miniature mass spectrometers, *Annual Review of Analytical Chemistry* **2** (2009) 187-214. doi:10.1146/annurev-anchem-060908-155229
- [50] Torion Technologies Inc., <http://www.torion.com/>
- [51] Z. Ouyang, R.J. Noll, and R.G. Cooks, Handheld Miniature Ion Trap Mass Spectrometers, *Analytical Chemistry* **81** (2009) 2421-2425. doi:10.1021/ac900292w
- [52] P. Östman, S. Marttila, T. Kotiaho, S. Franssila, and R. Kostiainen, Microchip atmospheric pressure chemical ionization source for mass spectrometry, *Analytical Chemistry* **76** (2004) 6659-6664. doi:10.1021/ac049345g
- [53] T. Kauppila, P. Ostman, S. Marttila, R. Ketola, T. Kotiaho, S. Franssila, and R. Kostiainen, Atmospheric pressure photoionization-mass spectrometry with a microchip heated nebulizer, *Analytical Chemistry* **76** (2004) 6797-6801. doi:10.1021/ac049058c
- [54] S. Marttila, *Micromechanical ion source made of silicon and glass*, Master's thesis, Helsinki University of Technology, Finland, 2003.
- [55] R. Kostiainen, S. Franssila, T. Kotiaho, and S. Marttila, *Method and apparatus for mass spectrometric analysis*, Patent #WO2005047848 (A3)
- [56] S. Franssila, S. Marttila, K. Kolari, P. Ostman, T. Kotiaho, R. Kostiainen, R. Lehtiniemi, C. Fager, and J. Manninen, A microfabricated nebulizer for liquid vaporization in chemical analysis, *Journal of Microelectromechanical Systems* **15** (2006) 1251-1259. doi:10.1109/JMEMS.2006.879671
- [57] D. Hülsenberg, A. Harnisch, and A. Bismarck, *Microstructuring of glasses*, Springer, 2008.
- [58] S. Franssila, *Introduction to Microfabrication*, Wiley, 2004.
- [59] G.T.A. Kovacs, *Micromachined Transducers Sourcebook*, McGraw-Hill Science/Engineering/Math, 1998.
- [60] M.J. Madou, *Fundamentals of Microfabrication: The Science of Miniaturization, Second Edition*, CRC, 2002.
- [61] V. Lindroos, M. Tilli, A. Lehto, and T. Motooka, *Handbook of silicon based MEMS materials and technologies*, William Andrew/Elsevier, 2010.
- [62] H. Becker and C. Gärtner, Polymer microfabrication technologies for microfluidic systems, *Analytical and Bioanalytical Chemistry* **390** (2008) 89-111. doi:10.1007/s00216-007-1692-2
- [63] A.N. Tiwari, A. Romeo, D. Baetzner, and H. Zogg, Flexible CdTe solar cells on polymer films, *Progress in Photovoltaics: Research and Applications* **9** (2001) 211-215. doi:10.1002/pip.374
- [64] Heidelberg Instruments Mikrotechnik GmbH, <http://www.himt.de/>
- [65] A.E. Grigorescu and C.W. Hagen, Resists for sub-20-nm electron beam lithography with a focus on HSQ: state of the art, *Nanotechnology* **20** (2009) 292001. doi:10.1088/0957-4484/20/29/292001
- [66] H. Schiff, Nanoimprint lithography: An old story in modern times? A review, *Journal of Vacuum Science & Technology B* **26** (2008) 458-480. doi:10.1116/1.2890972

- [67] SU-8 Resists, MicroChem Corp., http://www.microchem.com/products/su_eight.htm
- [68] G.M. Kim, M.A.F. van den Boogaart, and J. Brugger, Fabrication and application of a full wafer size micro/nanostencil for multiple length-scale surface patterning, *Microelectronic Engineering* **67-68** (2003) 609-614. doi:10.1016/S0167-9317(03)00121-7
- [69] S.W. Pang, M.W. Geis, W.D. Goodhue, N.N. Efremow, D.J. Ehrlich, R.B. Goodman, and J.N. Randall, Pattern transfer by dry etching through stencil masks, *Journal of Vacuum Science & Technology B* **6** (1988) 249-252. doi:10.1116/1.584016
- [70] Y. Xia and G.M. Whitesides, Soft Lithography, *Annual Review of Materials Science* **28** (1998) 153-184. doi:10.1146/annurev.matsci.28.1.153
- [71] J. Giboz, T. Copponnex, and P. Mélé, Microinjection molding of thermoplastic polymers: a review, *Journal of Micromechanics and Microengineering* **17** (2007) R96-R109. doi:10.1088/0960-1317/17/6/R02
- [72] C. Lin, Y. Lee, C. Chang, W. Hsu, Y. Chang, and W. Fang, Novel glass microprobe arrays for neural recording, *Biosensors and Bioelectronics* **25** (2009) 475-481. doi:10.1016/j.bios.2009.08.006
- [73] V. Fascio, R. Wuthrich, D. Viquerat, and H. Langen, 3D microstructuring of glass using electrochemical dischargemachining (ECDM), *1999 International Symposium on Micromechatronics and Human Science* (1999) 179-183.
- [74] D.M. Eigler and E.K. Schweizer, Positioning single atoms with a scanning tunnelling microscope, *Nature* **344** (1990) 524-526. doi:10.1038/344524a0
- [75] A.K. Dubey and V. Yadava, Laser beam machining--A review, *International Journal of Machine Tools and Manufacture* **48** (2008) 609-628. doi:10.1016/j.ijmachtools.2007.10.017
- [76] Cunxia Li et al, Fabrication of three-dimensional microchannels inside silicon using a femtosecond laser, *Journal of Micromechanics and Microengineering* **19** (2009) 125007. doi:10.1088/0960-1317/19/12/125007
- [77] D.S. Miller, Micromachining with abrasive waterjets, *Journal of Materials Processing Tech.* **149** (2004) 37-42.
- [78] N. Chekurov, K. Grigoras, A. Peltonen, S. Franssila, and I. Tittonen, The fabrication of silicon nanostructures by local gallium implantation and cryogenic deep reactive ion etching, *Nanotechnology* **20** (2009) 065307. doi:10.1088/0957-4484/20/6/065307
- [79] C. Chao, S. Shen, and J. Wu, Fabrication of 3-D Submicron Glass Structures by FIB, *Journal of Materials Engineering and Performance* **18** (2009) 878-885. doi:10.1007/s11665-008-9318-1
- [80] M. Elwenspoek and H.V. Jansen, *Silicon Micromachining*, Cambridge University Press, 2004.
- [81] G.T. Kovacs, N.I. Maluf, and K.E. Petersen, Bulk micromachining of silicon, *Proceedings of the IEEE* **86** (1998) 1536-1551. doi:10.1109/5.704259
- [82] K. Biswas and S. Kal, Etch characteristics of KOH, TMAH and dual doped TMAH for bulk micromachining of silicon, *Microelectronics Journal* **37** (2006) 519-525.
- [83] J. Chen, L. Liu, Z. Li, Z. Tan, Q. Jiang, H. Fang, Y. Xu, and Y. Liu, Study of anisotropic etching of (1 0 0) Si with ultrasonic agitation, *Sensors and Actuators A* **96** (2002) 152-156.
- [84] K. Sato, M. Shikida, T. Yamashiro, K. Asaumi, Y. Iriye, and M. Yamamoto, Anisotropic etching rates of single-crystal silicon for TMAH water solution as a function of crystallographic orientation, *Sensors and Actuators A* **73** (1999) 131-137.
- [85] M. Decarli, V. Guarnieri, R. Pal, F. Giacomozzi, B. Margesin, and M. Zen, Influence of masking layer stress on anisotropic silicon etching in TMAH solutions, *International Conference on Microelectronic Test Structures* (2003) 25-28.
- [86] C.R. Yang, P.Y. Chen, Y.C. Chiou, and R.T. Lee, Effects of mechanical agitation and surfactant additive on silicon anisotropic etching in alkaline KOH solution, *Sensors and Actuators A* **119** (2005) 263-270.
- [87] E. Van Veenendaal, K. Sato, M. Shikida, and J. Van Suchtelen, Micromorphology of single crystalline silicon surfaces during anisotropic wet chemical etching in KOH and TMAH, *Sensors and Actuators A* **93** (2001) 219-231.
- [88] I. Zubel and M. Kramkowska, The effect of isopropyl alcohol on etching rate and roughness of (1 0 0) Si surface etched in KOH and TMAH solutions, *Sensors and Actuators A* **93** (2001) 138-147. doi:10.1016/S0924-4247(01)00648-3
- [89] B. Schwartz and H. Robbins, Chemical Etching of Silicon, *Journal of The Electrochemical Society* **123** (1976) 1903-1909. doi:10.1149/1.2132721
- [90] D.L. Flamm, Mechanisms of silicon etching in fluorine-and chlorine-containing plasmas, *Pure and Applied Chemistry* **62** (1990) 1709-1720.
- [91] D.E. Ibbotson, J.A. Mucha, D.L. Flamm, and J.M. Cook, Plasmaless dry etching of silicon with fluorine-containing compounds, *Journal of Applied Physics* **56** (1984) 2939-2942. doi:10.1063/1.333834

- [92] L.R. Arana, N. de Mas, R. Schmidt, A.J. Franz, M.A. Schmidt, and K.F. Jensen, Isotropic etching of silicon in fluorine gas for MEMS micromachining, *Journal of Micromechanics and Microengineering* **17** (2007) 384–392. doi:10.1088/0960-1317/17/2/026
- [93] F. Lärmer, S. Franssila, L. Sainiemi, and K. Kolari, Deep reactive ion etching, in V. Lindroos, M. Tilli, A. Lehto, and T. Motooka (Eds.), *Handbook of Silicon Based MEMS Materials and Technologies*, William Andrew/Elsevier, 2010.
- [94] H.V. Jansen, M.J.D. Boer, S. Unnikrishnan, M.C. Louwerse, and M.C. Elwenspoek, Black silicon method X: a review on high speed and selective plasma etching of silicon with profile control: an in-depth comparison between Bosch and cryostat DRIE processes as a roadmap to next generation equipment, *Journal of Micromechanics and Microengineering* **19** (2009) 033001. doi:10.1088/0960-1317/19/3/033001
- [95] F. Laermer and A. Schilp, *Method of anisotropically etching silicon*, Patent #US5501893, March 26, 1996.
- [96] I.W. Rangelow, High-resolution tri-level process by downstream-microwave rf-biased etching, *Proceedings of SPIE* **1392** (1991) 180-184. doi:10.1117/12.48912
- [97] S. Chen, Y. Lin, J. Wu, L. Horng, and C. Cheng, Parameter optimization for an ICP deep silicon etching system, *Microsystem Technologies* **13** (2007) 465-474. doi:10.1007/s00542-006-0211-2
- [98] M. Brunet, P. Dubreuil, H. Mahfoz-Kotb, A. Gouantes, and A. Dorthe, Factorial experimental design applied to DRIE for optimised process in power electronics applications requiring high-aspect ratio trenches, *Microsystem Technologies* **15** (2009) 1449-1457. doi:10.1007/s00542-009-0893-3
- [99] B. Volland, F. Shi, P. Hudek, H. Heerlein, and I.W. Rangelow, Dry etching with gas chopping without rippled sidewalls, *Journal of Vacuum Science & Technology B* **17** (1999) 2768-2771. doi:10.1116/1.591061
- [100] D. Nilsson, S. Jensen, and A. Menon, Fabrication of silicon molds for polymer optics, *Journal of Micromechanics and Microengineering* **13** (2003) S57-S61. doi:10.1088/0960-1317/13/4/309
- [101] K. Weng, M. Wang, and P. Tsai, Planarize the Sidewall Ripples of Silicon Deep Reactive Ion Etching, *Technical Proceedings of the 2004 NSTI Nanotechnology Conference and Trade Show* **1** (2004) 473-476.
- [102] M. de Boer, J. Gardeniers, H. Jansen, E. Smulders, M. Gilde, G. Roelofs, J. Sasserath, and M. Elwenspoek, Guidelines for etching silicon MEMS structures using fluorine high-density plasmas at cryogenic temperatures, *Journal of Microelectromechanical Systems* **11** (2002) 385-401. doi:10.1109/JMEMS.2002.800928
- [103] R.A. Gottscho, C.W. Jurgensen, and D.J. Vitkavage, Microscopic uniformity in plasma etching, *Journal of Vacuum Science & Technology B* **10** (1992) 2133-2147. doi:10.1116/1.586180
- [104] J. Kiihamaki and S. Franssila, Pattern shape effects and artefacts in deep silicon etching, *Journal of Vacuum Science and Technology A* **17** (1999) 2280-2285. doi:10.1116/1.581761
- [105] T. Humphreys, J. Andersson, U. Södervall, and T. Melvin, Microfluidic interconnects for DNA loading, *Journal of Micromechanics and Microengineering* **19** (2009) 105024. doi:10.1088/0960-1317/19/10/105024
- [106] J. Kiihamäki and S. Franssila, Deep Silicon Etching in Inductively Coupled Plasma Reactor for MEMS, *Physica Scripta* **T79** (1999) 250-254. doi:10.1238/Physica.Topical.079a00250
- [107] A.M. Hynes, H. Ashraf, J.K. Bhardwaj, J. Hopkins, I. Johnston, and J.N. Shepherd, Recent advances in silicon etching for MEMS using the ASE(TM) process, *Sensors and Actuators A* **74** (1999) 13-17. doi:10.1016/S0924-4247(98)00326-4
- [108] K.R. Williams, K. Gupta, and M. Wasilik, Etch rates for micromachining processing-Part II, *Journal of Microelectromechanical Systems* **12** (2003) 761-778. doi:10.1109/JMEMS.2003.820936
- [109] H. Zhang, H. Guo, Z. Chen, G. Zhang, and Z. Li, Application of PECVD SiC in glass micromachining, *Journal of Micromechanics and Microengineering* **17** (2007) 775-780. doi:10.1088/0960-1317/17/4/014
- [110] C. Iliescu, J. Jing, F.E. Tay, J. Miao, and T. Sun, Characterization of masking layers for deep wet etching of glass in an improved HF/HCl solution, *Surface and Coatings Technology* **198** (2005) 314-318. doi:10.1016/j.surfcoat.2004.10.094
- [111] C. Khan Malek, L. Robert, J. Boy, and P. Blind, Deep microstructuring in glass for microfluidic applications, *Microsystem Technologies* **13** (2007) 447-453. doi:10.1007/s00542-006-0185-0
- [112] C.H. Lin, G.B. Lee, Y.H. Lin, and G.L. Chang, Fabrication of microfluidic systems on soda-lime glass, *Journal of micromechanics and microengineering* **11** (2001) 726–732. doi:10.1088/0960-1317/11/6/316

- [113] A. Grosse, M. Grewe, and H. Fouckhardt, Deep wet etching of fused silica glass for microfluidic devices, *Journal of Micromechanics and Microengineering* **11** (2001) 257–262. doi:10.1088/0960-1317/11/3/315
- [114] C. Iliescu, B. Chen, and J. Miao, On the wet etching of Pyrex glass, *Sensors and Actuators A* **143** (2008) 154–161. doi:10.1016/j.sna.2007.11.022
- [115] M.A. Grétilat, F. Paoletti, P. Thiebaud, S. Roth, M. Koudelka-Hep, and N.F. de Rooij, A new fabrication method for borosilicate glass capillary tubes with lateral inlets and outlets, *Sensors and Actuators A* **60** (1997) 219–222.
- [116] C. Iliescu, J. Miao, and F.E.H. Tay, Optimization of an amorphous silicon mask PECVD process for deep wet etching of Pyrex glass, *Surface and Coatings Technology* **192** (2005) 43–47. doi:10.1016/j.surfcoat.2004.03.043
- [117] T. Corman, P. Enoksson, and G. Stemme, Deep wet etching of borosilicate glass using an anodically bonded silicon substrate as mask, *Journal of micromechanics and microengineering* **8** (1998) 84–87. doi:10.1088/0960-1317/8/2/010
- [118] C. Iliescu, J. Miao, and F.E.H. Tay, Stress control in masking layers for deep wet micromachining of Pyrex glass, *Sensors and Actuators A* **117** (2005) 286–292. doi:10.1016/j.sna.2004.03.004
- [119] I. Steingoetter and H. Fouckhardt, Deep fused silica wet etching using an Au-free and stress-reduced sputter-deposited Cr hard mask, *Journal of Micromechanics and Microengineering* **15** (2005) 2130–2135. doi:10.1088/0960-1317/15/11/019
- [120] F. Ceysens and R. Puers, Deep etching of glass wafers using sputtered molybdenum masks, *Journal of Micromechanics and Microengineering* **19** (2009) 067001.
- [121] M. Bu, T. Melvin, G.J. Ensell, J.S. Wilkinson, and A.G.R. Evans, A new masking technology for deep glass etching and its microfluidic application, *Sensors and Actuators A* **115** (2004) 476–482. doi:10.1016/j.sna.2003.12.013
- [122] R.S. Keynton, T.J. Roussel, M.M. Crain, D.J. Jackson, D.B. Franco, J.F. Naber, K.M. Walsh, and R.P. Baldwin, Design and development of microfabricated capillary electrophoresis devices with electrochemical detection, *Analytica Chimica Acta* **507** (2004) 95–105.
- [123] C. Iliescu, F.E. Tay, and J. Miao, Strategies in deep wet etching of Pyrex glass, *Sensors and Actuators A* **133** (2007) 395–400. doi:10.1016/j.sna.2006.06.044
- [124] T. Arakawa, Y. Sato, T. Ueno, T. Funatsu, and S. Shoji, Pinhole-free Pyrex glass etching using HF-H₂SO₄ mixed acid and its applications for a PDMS microflow system, *TRANSDUCERS '05, Digest of Technical Papers* **2** (2005) 1489–1492.
- [125] W.I. Jang, C.A. Choi, M.L. Lee, C.H. Jun, and Y.T. Kim, Fabrication of MEMS devices by using anhydrous HF gas-phase etching with alcoholic vapor, *Journal of Micromechanics and Microengineering* **12** (2002) 297–306. doi:10.1088/0960-1317/12/3/316
- [126] P.W. Leech, Reactive ion etching of quartz and silica-based glasses in CF₄/CHF₃ plasmas, *Vacuum* **55** (1999) 191–196. doi:10.1016/S0042-207X(99)00146-3
- [127] E. Metwalli and C.G. Pantano, Reactive ion etching of glasses: Composition dependence, *Nuclear Instruments and Methods in Physics Research Section B* **207** (2003) 21–27. doi:10.1016/S0168-583X(03)00517-2
- [128] A. Baram and M. Naftali, Dry etching of deep cavities in Pyrex for MEMS applications using standard lithography, *Journal of Micromechanics and Microengineering* **16** (2006) 2287–2291. doi:10.1088/0960-1317/16/11/006
- [129] S. Ronggui and G.C. Righini, Characterization of reactive ion etching of glass and its applications in integrated optics, *Journal of Vacuum Science & Technology A* **9** (1991) 2709–2712. doi:10.1116/1.577229
- [130] H. Chen and C. Fu, An investigation into the characteristics of the deep reactive ion etching of quartz using SU-8 as a mask, *Journal of Micromechanics and Microengineering* **18** (2008) 105001. doi:10.1088/0960-1317/18/10/105001
- [131] T. Akashi and Y. Yoshimura, Deep reactive ion etching of borosilicate glass using an anodically bonded silicon wafer as an etching mask, *Journal of Micromechanics and Microengineering* **16** (2006) 1051–1056. doi:10.1088/0960-1317/16/5/024
- [132] T. Ichiki, Y. Sugiyama, R. Taura, T. Koidesawa, and Y. Horiike, Plasma applications for biochip technology, *Thin Solid Films* **435** (2003) 62–68. doi:10.1016/S0040-6090(03)00370-5
- [133] J. Park, N. Lee, J. Lee, J. Park, and H. Park, Deep dry etching of borosilicate glass using SF₆ and SF₆/Ar inductively coupled plasmas, *Microelectronic Engineering* **82** (2005) 119–128. doi:10.1016/j.mee.2005.07.006
- [134] X. Li, T. Abe, and M. Esashi, Deep reactive ion etching of Pyrex glass using SF₆ plasma, *Sensors and Actuators A* **87** (2001) 139–145. doi:10.1016/S0924-4247(00)00482-9

- [135] X. Li, T. Abe, Y. Liu, and M. Esashi, Fabrication of high-density electrical feed-throughs by deep-reactive-ion etching of Pyrex glass, *Journal of Microelectromechanical Systems* **11** (2002) 625-630. doi:10.1109/JMEMS.2002.805211
- [136] H.C. Jung, W. Lu, S. Wang, L.J. Lee, and X. Hu, Etching of Pyrex glass substrates by inductively coupled plasma reactive ion etching for micro/nanofluidic devices, *Journal of Vacuum Science & Technology B* **24** (2006) 3162-3164. doi:10.1116/1.2388959
- [137] K. Kolari, High etch selectivity for plasma etching SiO₂ with AlN and Al₂O₃ masks, *Microelectronic Engineering* **85** (2008) 985-987. doi:10.1016/j.mee.2007.12.037
- [138] X. Li, L. Ling, X. Hua, M. Fukasawa, G.S. Oehrlein, M. Barela, and H.M. Anderson, Effects of Ar and O₂ additives on SiO₂ etching in C4F₈-based plasmas, *Journal of Vacuum Science & Technology A* **21** (2003) 284-293. doi:10.1116/1.1531140
- [139] T. Akashi and Y. Yoshimura, Profile control of a borosilicate-glass groove formed by deep reactive ion etching, *Journal of Micromechanics and Microengineering* **18** (2008) 105004. doi:10.1088/0960-1317/18/10/105004
- [140] K. Kolari, Deep plasma etching of glass with a silicon shadow mask, *Sensors and Actuators A* **141** (2008) 677-684. doi:10.1016/j.sna.2007.09.005
- [141] M. Pavius, C. Hibert, P. Fluckiger, P. Renaud, L. Rolland, and M. Puech, Profile angle control in SiO₂ deep anisotropic dry etching for MEMS fabrication, *Proceedings of IEEE MEMS 2004* (2004) 669-672.
- [142] D.S. Park, M.W. Cho, and H. Lee, Effects of the impact angle variations on the erosion rate of glass in powder blasting process, *The International Journal of Advanced Manufacturing Technology* **23** (2004) 444-450.
- [143] P.J. Slikkerveer, P.C.P. Bouten, F.H. in't Veld, and H. Scholten, Erosion and damage by sharp particles, *Wear* **217** (1998) 237-250. doi:10.1016/S0043-1648(98)00187-2
- [144] M. Buijs and J.M.M. Pasmans, Erosion of glass by alumina particles: transitions and exponents, *Wear* **184** (1995) 61-65. doi:10.1016/0043-1648(94)06560-8
- [145] E. Belloy, A. Sayah, and M.A.M. Gijs, Powder blasting for three-dimensional microstructuring of glass, *Sensors and Actuators A* **86** (2000) 231-237. doi:10.1016/S0924-4247(00)00447-7
- [146] P.J. Slikkerveer, P.C.P. Bouten, and F.C.M. de Haas, High quality mechanical etching of brittle materials by powder blasting, *Sensors and Actuators A* **85** (2000) 296-303. doi:10.1016/S0924-4247(00)00343-5
- [147] A. Sayah, P. Thivolle, V.K. Parashar, and M.A.M. Gijs, Fabrication of microfluidic mixers with varying topography in glass using the powder-blasting process, *Journal of Micromechanics and Microengineering* **19** (2009) 085024. doi:10.1088/0960-1317/19/8/085024
- [148] E. Belloy, A. Sayah, and M.A.M. Gijs, Oblique powder blasting for three-dimensional micromachining of brittle materials, *Sensors and Actuators A* **92** (2001) 358-363.
- [149] E. Belloy, A. Pawlowski, A. Sayah, and M. Gijs, Microfabrication of high-aspect ratio and complex monolithic structures in glass, *Journal of Microelectromechanical Systems* **11** (2002) 521-527.
- [150] H. Wensink, H.V. Jansen, J.W. Berenschot, and M.C. Elwenspoek, Mask materials for powder blasting, *Journal of Micromechanics and Microengineering* **10** (2000) 175-180. doi:10.1088/0960-1317/10/2/313
- [151] A. Sayah, V.K. Parashar, A.G. Pawlowski, and M.A.M. Gijs, Elastomer mask for powder blasting microfabrication, *Sensors and Actuators A* **125** (2005) 84-90.
- [152] A. Sayah, V.K. Parashar, and M.A.M. Gijs, LF55GN Photosensitive Flexopolymer: A New Material for Ultrathick and High-Aspect-Ratio MEMS Fabrication, *Journal of Microelectromechanical Systems* **16** (2007) 564-570.
- [153] D. Park, M. Cho, H. Lee, and W. Cho, Micro-grooving of glass using micro-abrasive jet machining, *Journal of Materials Processing Technology* **146** (2004) 234-240. doi:10.1016/j.jmatprotec.2003.11.013
- [154] A. Pawlowski, A. Sayah, and M. Gijs, Precision poly-(dimethyl siloxane) masking technology for high-resolution powder blasting, *Journal of Microelectromechanical Systems* **14** (2005) 619-624. doi:10.1109/JMEMS.2005.844745
- [155] H. Yagyu, K. Sugano, S. Hayashi, and O. Tabata, Micropowder blasting with nanoparticles dispersed polymer mask for rapid prototyping of glass chip, *Journal of Micromechanics and Microengineering* **15** (2005) 1236-1241. doi:10.1088/0960-1317/15/6/014
- [156] Comco inc., <http://www.comcoinc.com/>
- [157] P. Lerou, G.C.F. Venhorst, C.F. Berends, T.T. Veenstra, M. Blom, J.F. Burger, H.J.M. ter Brake, and H. Rogalla, Fabrication of a micro cryogenic cold stage using MEMS-technology, *Journal of Micromechanics and Microengineering* **16** (2006) 1919-1925. doi:10.1088/0960-1317/16/10/002

- [158] H. Wensink, S. Schlautmann, M.H. Goedbloed, and M.C. Elwenspoek, Fine tuning the roughness of powder blasted surfaces, *Journal of Micromechanics and Microengineering* **12** (2002) 616–620.
- [159] T. Diepold and E. Obermeier, Smoothing of ultrasonically drilled holes in borosilicate glass by wet chemical etching, *Journal of Micromechanics and Microengineering* **6** (1996) 29-32.
- [160] A. Daridon, V. Fascio, J. Lichtenberg, R. Wütrich, H. Langen, E. Verpoorte, and N.F. de Rooij, Multi-layer microfluidic glass chips for microanalytical applications, *Fresenius' Journal of Analytical Chemistry* **371** (2001) 261-269.
- [161] I. Basak and A. Ghosh, Mechanism of spark generation during electrochemical discharge machining: a theoretical model and experimental verification, *Journal of Materials Processing Technology* **62** (1996) 46-53. doi:10.1016/0924-0136(95)02202-3
- [162] X. Zeng, X. Mao, S.B. Wen, R. Greif, and R.E. Russo, Energy deposition and shock wave propagation during pulsed laser ablation in fused silica cavities, *Journal of Physics D: Applied Physics* **37** (2004) 1132–1136. doi:10.1088/0022-3727/37/7/029
- [163] H. Niino, Y. Kawaguchi, T. Sato, A. Narazaki, T. Gumpenberger, and R. Kurosaki, Laser ablation of toluene liquid for surface micro-structuring of silica glass, *Applied Surface Science* **252** (2006) 4387-4391. doi:10.1016/j.apsusc.2005.07.084
- [164] C.K. Chung, Y.C. Sung, G.R. Huang, E.J. Hsiao, W.H. Lin, and S.L. Lin, Crackless linear through-wafer etching of Pyrex glass using liquid-assisted CO2 laser processing, *Applied Physics A* **94** (2008) 927-932. doi:10.1007/s00339-008-4863-x
- [165] S. Nikumb, Q. Chen, C. Li, H. Reshef, H.Y. Zheng, H. Qiu, and D. Low, Precision glass machining, drilling and profile cutting by short pulse lasers, *Thin Solid Films* **477** (2005) 216-221.
- [166] S. Youn, M. Takahashi, H. Goto, and R. Maeda, Fabrication of micro-mold for glass embossing using focused ion beam, femto-second laser, eximer laser and dicing techniques, *Journal of Materials Processing Technology* **187-188** (2007) 326-330. doi:10.1016/j.jmatprotec.2006.11.120
- [167] S. Youn, M. Takahashi, H. Goto, and R. Maeda, Microstructuring of glassy carbon mold for glass embossing - Comparison of focused ion beam, nano/femtosecond-pulsed laser and mechanical machining, *Microelectronic Engineering* **83** (2006) 2482-2492. doi:10.1016/j.mee.2006.05.007
- [168] E. Eklund and A. Shkel, Glass Blowing on a Wafer Level, *Journal of Microelectromechanical Systems* **16** (2007) 232-239.
- [169] S.W. Tsai, M. Loughran, and I. Karube, Development of a microchip for 2-dimensional capillary electrophoresis, *Journal of Micromechanics and Microengineering* **14** (2004) 1693–1699.
- [170] A. Sayah, D. Solignac, T. Cueni, and M.A.M. Gijs, Development of novel low temperature bonding technologies for microchip chemical analysis applications, *Sensors and Actuators A* **84** (2000) 103-108. doi:10.1016/S0924-4247(99)00346-5
- [171] S. Christiansen, R. Singh, and U. Gosele, Wafer Direct Bonding: From Advanced Substrate Engineering to Future Applications in Micro/Nanoelectronics, *Proceedings of the IEEE* **94** (2006) 2060-2106.
- [172] Q.Y. Tong and U.M. Gösele, Wafer Bonding and Layer Splitting for Microsystems, *Advanced Materials* **11** (1999) 17.
- [173] M.A. Schmidt, Wafer-to-wafer bonding for microstructure formation, *Proceedings of the IEEE* **86** (1998) 1575-1585.
- [174] M. Esashi, Wafer level packaging of MEMS, *Journal of Micromechanics and Microengineering* **18** (2008) 073001. doi:10.1088/0960-1317/18/7/073001
- [175] T. Ito, K. Sobue, and S. Ohya, Water glass bonding for micro-total analysis system, *Sensors and Actuators B* **81** (2002) 187-195.
- [176] J. Haisma and G. Spierings, Contact bonding, including direct-bonding in a historical and recent context of materials science and technology, physics and chemistry Historical review in a broader scope and comparative outlook, *Materials Science & Engineering R* **37** (2002) 1-60.
- [177] U. Gösele and Q.Y. Tong, Semiconductor wafer bonding, *Annual Review of Materials Science* **28** (1998) 215-241. doi:10.1146/annurev.matsci.28.1.215
- [178] F. Niklaus, G. Stemme, J.-Q. Lu, and R.J. Gutmann, Adhesive wafer bonding, *Journal of Applied Physics* **99** (2006) 031101-28. doi:10.1063/1.2168512
- [179] Ö. Vallin, K. Jonsson, and U. Lindberg, Adhesion quantification methods for wafer bonding, *Materials Science & Engineering R* **50** (2005) 109-165.
- [180] Q. Tong and U. Gösele, *Semiconductor Wafer Bonding: Science and Technology*, Wiley-Interscience, 1999.
- [181] M. Alexe and U. Gösele, *Wafer Bonding*, Springer, 2004.
- [182] J.A. Dziuban, *Bonding in Microsystem Technology*, Springer, 2006.

- [183] U. Gösele, Q.Y. Tong, A. Schumacher, G. Kräuter, M. Reiche, A. Plößl, P. Kopperschmidt, T.H. Lee, and W.J. Kim, Wafer bonding for microsystems technologies, *Sensors and Actuators A* **74** (1999) 161-168.
- [184] A. Van Wieringen and N. Warmoltz, On the permeation of hydrogen and helium in single crystal silicon and germanium at elevated temperatures, *Physica* **22** (1956) 849-865. doi:10.1016/S0031-8914(56)90039-8
- [185] J. Lichtenberg, E. Verpoorte, and N.F.D. Rooij, Sample preconcentration by field amplification stacking for microchip-based capillary electrophoresis, *Electrophoresis* **22** (2001) 258-271. doi:10.1002/1522-2683(200101)22:2<258::AID-ELPS258>3.0.CO;2-4
- [186] M.M.R. Howlader, S. Suehara, and T. Suga, Room temperature wafer level glass/glass bonding, *Sensors and Actuators A* **127** (2006) 31-36.
- [187] A.D. Brooks, R.P. Donovan, and C.A. Hardesty, Low-Temperature Electrostatic Silicon-to-Silicon Seals Using Sputtered Borosilicate Glass, *Journal of The Electrochemical Society* **119** (1972) 545-546. doi:10.1149/1.2404250
- [188] A. Hanneborg, M. Nese, and P. Ohlckers, Silicon-to-silicon anodic bonding with a borosilicate glass layer, *Journal of Micromechanics and Microengineering* **1** (1991) 139-144. doi:10.1088/0960-1317/1/3/002
- [189] A. Berthold, L. Nicola, P.M. Sarro, and M.J. Vellekoop, Glass-to-glass anodic bonding with standard IC technology thin films as intermediate layers, *Sensors and Actuators A* **82** (2000) 224-228. doi:10.1016/S0924-4247(99)00376-3
- [190] D.J. Lee, B.K. Ju, Y.H. Lee, J. Jang, and M.H. Oh, Glass-to-glass anodic bonding for high vacuum packaging of microelectronics and its stability, *Proceedings of IEEE MEMS 2000* (2000) 253-258.
- [191] Affymetrix, Inc., <http://www.affymetrix.com/>
- [192] Dolomite Centre Ltd, <http://www.dolomite-microfluidics.com/>
- [193] Micronit Microfluidics BV, <http://www.micronit.com/>
- [194] microfluidic ChipShop, <http://www.microfluidic-chipshop.com/>
- [195] The Swagelok Company, <http://www.swagelok.com/>
- [196] Upchurch Scientific, Inc., <http://www.upchurch.com/>
- [197] Valco Instruments Co. Inc., <http://www.vici.com/>
- [198] J.W. Batts, *all about FITTINGS*, Upchurch Scientific, 2003.
- [199] C. Fredrickson and Z. Fan, Macro-to-micro interfaces for microfluidic devices, *Lab on a Chip* **4** (2004) 526-533. doi:10.1039/b410720a
- [200] Z. Yang and R. Maeda, Socket with built-in valves for the interconnection of microfluidic chips to macro constituents, *Journal of Chromatography A* **1013** (2003) 29-33. doi:10.1016/S0021-9673(03)01125-7
- [201] J.H. Tsai and L. Lin, Micro-to-macro fluidic interconnectors with an integrated polymer sealant, *Journal of Micromechanics and Microengineering* **11** (2001) 577-581.
- [202] Y. Tai, S. Wu, and E.F. Meng, *Micromachined fluidic coupler and method of making the same*, Patent #US6672629, January 6, 2004.
- [203] M.T. Blom, E. Chmela, J.G.E. Gardeniers, J.W. Berenschot, M. Elwenspoek, R. Tjissen, and A. van den Berg, Local anodic bonding of Kovar to Pyrex aimed at high-pressure, solvent-resistant microfluidic connections, *Journal of Micromechanics and Microengineering* **11** (2001) 382-385.
- [204] S. Ng, Z. Wang, and N. de Rooij, Microfluidic connectors by ultrasonic welding, *Microelectronic Engineering* **86** (2009) 1354-1357. doi:10.1016/j.mee.2009.01.048
- [205] E.S. Lee, D. Howard, E. Liang, S.D. Collins, and R.L. Smith, Removable tubing interconnects for glass-based micro-fluidic systems made using ECDM, *Journal of Micromechanics and Microengineering* **14** (2004) 535-541.
- [206] A. Puntambekar and C.H. Ahn, Self-aligning microfluidic interconnects for glass-and plastic-based microfluidic systems, *Journal of Micromechanics and Microengineering* **12** (2002) 35-40.
- [207] A.V. Pattekar and M.V. Kothare, Novel microfluidic interconnectors for high temperature and pressure applications, *Journal of Micromechanics and Microengineering* **13** (2003) 337-345.
- [208] C.F. Chen, J. Liu, L.P. Hromada, C.W. Tsao, C.C. Chang, and D.L. DeVoe, High-pressure needle interface for thermoplastic microfluidics, *Lab on a Chip* **9** (2009) 50-55.
- [209] *IDEX Health & Science 2009-2010 Catalog - Products for Chromatography and Fluidic Applications*, IDEX Health & Science LLC, 2009.
- [210] J. Atencia, G.A. Cooksey, A. Jahn, J.M. Zook, W.N. Vreeland, and L.E. Locascio, Magnetic connectors for microfluidic applications, *Lab on a Chip* **10** (2010) 246-249. doi:10.1039/b913331c
- [211] V. Nittis, R. Fortt, C.H. Legge, and A.J.D. Mello, A high-pressure interconnect for chemical microsystem applications, *Lab on a Chip* **1** (2001) 148-152. doi:10.1039/b107836b

- [212] K. Han, R.D. McConnell, C.J. Easley, J.M. Bienvenue, J.P. Ferrance, J.P. Landers, and A.B. Frazier, An active microfluidic system packaging technology, *Sensors and Actuators B* **122** (2007) 337-346. doi:10.1016/j.snb.2006.06.028
- [213] R.M. Tiggelaar, *Silicon-technology based microreactors for high-temperature heterogeneous partial oxidation reactions*, Ph.D. thesis, University of Twente, Enschede, The Netherlands, 2004.
- [214] R.F. Renzi, *Edge compression manifold apparatus*, Patent #US6832787, December 21, 2004.
- [215] D.M. Hartmann, J.T. Nevill, K.I. Pettigrew, G. Votaw, P. Kung, and H.C. Crenshaw, A low-cost, manufacturable method for fabricating capillary and optical fiber interconnects for microfluidic devices, *Lab on a Chip* **8** (2008) 609-616.
- [216] C.H. Chiou and G.B. Lee, Minimal dead-volume connectors for microfluidics using PDMS casting techniques, *Journal of Micromechanics and Microengineering* **14** (2004) 1484-1490.
- [217] A.M. Christensen, D.A. Chang-Yen, and B.K. Gale, Characterization of interconnects used in PDMS microfluidic systems, *Journal of Micromechanics and Microengineering* **15** (2005) 928-934. doi:10.1088/0960-1317/15/5/005
- [218] M. Quaglio, G. Canavese, E. Giuri, S.L. Marasso, D. Perrone, M. Cocuzza, and C.F. Pirri, Evaluation of different PDMS interconnection solutions for silicon, Pyrex and COC microfluidic chips, *Journal of Micromechanics and Microengineering* **18** (2008) 55012-55012.
- [219] T.G. Park, J.J. Kim, S.H. Jung, H.J. Song, J.K. Chang, D.C. Han, and S.S. Yang, Fabrication of Megasonic-Agitated Module for Improving the Characteristics of Wet Etching, *Japanese Journal of Applied Physics* **47** (2008) 5262-5269. doi:10.1143/JJAP.47.5262
- [220] P. Östman, L. Luosujarvi, M. Haapala, K. Grigoras, R.A. Ketola, T. Kotiaho, S. Franssila, and R. Kostianen, Gas Chromatography-Microchip Atmospheric Pressure Chemical Ionization-Mass Spectrometry, *Analytical Chemistry* **78** (2006) 3027-3031. doi:10.1021/ac052260a
- [221] M.J. Kim, L.A. Gruenke, R.J. Saia, and S.S. Cohen, Inhibition of acid etching of Pt by pre-exposure to oxygen plasma, *Applied Physics Letters* **44** (1984) 462-464. doi:10.1063/1.94767
- [222] M. Hara, Y. Shinata, and S. Hashimoto, The galvanic corrosion behavior of coupled nickel-platinum in molten Na₂CO₃, *Corrosion Science* **39** (1997) 627-638.
- [223] P. Rangsten, O. Vallin, K. Hermansson, and Y. Backlund, Quartz-to-Quartz Direct Bonding, *Journal of The Electrochemical Society* **146** (1999) 1104-1105. doi:10.1149/1.1391728
- [224] G. Zhuang, Q. Jin, J. Liu, H. Cong, K. Liu, J. Zhao, M. Yang, and H. Wang, A low temperature bonding of quartz microfluidic chip for serum lipoproteins analysis, *Biomedical Microdevices* **8** (2006) 255-261. doi:10.1007/s10544-006-9142-z
- [225] F.P. Fehlner, N.J. Binkowski, K.R. Salisbury, and L. Button, Alumina barrier layers on LCD glass, *Journal of Non-Crystalline Solids* **195** (1996) 89-94. doi:10.1016/0022-3093(95)00473-4
- [226] E. Aubry, M. Ghazzal, V. Demange, N. Chaoui, D. Robert, and A. Billard, Poisoning prevention of TiO₂ photocatalyst coatings sputtered on soda-lime glass by intercalation of SiN_x diffusion barriers, *Surface and Coatings Technology* **201** (2007) 7706-7712. doi:10.1016/j.surfcoat.2007.03.003
- [227] G. Kychakoff, R.D. Howe, R.K. Hanson, M.C. Drake, R.W. Pitz, M. Lapp, and C.M. Penney, Visualization of turbulent flame fronts with planar laser-induced fluorescence, *Science* **224** (1984) 382-384. doi:10.1126/science.224.4647.382
- [228] M.C. Thurber and R.K. Hanson, Simultaneous imaging of temperature and mole fraction using acetone planar laser-induced fluorescence, *Experiments in Fluids* **30** (2001) 93-101. doi:10.1007/s003480000142
- [229] A.P. London, A.A. Ayón, A.H. Epstein, S.M. Spearing, T. Harrison, Y. Peles, and J.L. Kerrebrock, Microfabrication of a high pressure bipropellant rocket engine, *Sensors and Actuators A* **92** (2001) 351-357. doi:10.1016/S0924-4247(01)00571-4
- [230] J. Lee, K. Naeli, H. Hunter, J. Berg, T. Wright, C. Courcimault, N. Naik, M. Allen, O. Brand, A. Glezer, and W.P. King, Characterization of liquid and gaseous micro- and nanojets using microcantilever sensors, *Sensors and Actuators A* **134** (2007) 128-139. doi:10.1016/j.sna.2006.05.014
- [231] J. Pól, T.J. Kaupilla, S. Franssila, T. Kotiaho, and R. Kostianen, Ionspray microchip, *Rapid Communications in Mass Spectrometry* **24** (2010) 2584-2590. doi:10.1002/rcm.4678
- [232] J. Eijkel, Chip-based HPLC: the quest for the perfect column, *Lab on a Chip* **7** (2007) 815. doi:10.1039/b707464f
- [233] K. Ohno, K. Tachikawa, and A. Manz, Microfluidics: Applications for analytical purposes in chemistry and biochemistry, *Electrophoresis* **29** (2008) 4443-4453. doi:10.1002/elps.200800121
- [234] A. de Mello, On-chip chromatography: the last twenty years, *Lab on a Chip* **2** (2002) 48N-54N. doi:10.1039/b207266c

- [235] A. Benvenuto, V. Guarnieri, L. Lorenzelli, C. Collini, M. Decarli, A. Adami, C. Potrich, L. Lunelli, R. Canteri, and C. Pederzoli, Fabrication of a MEMS-based separation module for liquid chromatography, *Sensors and Actuators B* **130** (2008) 181-186. doi:10.1016/j.snb.2007.07.111
- [236] M. McEnery, A. Tan, J.D. Glennon, J. Alderman, J. Patterson, and S.C. O'Mathuna, Liquid chromatography on-chip: progression towards a μ -total analysis system, *The Analyst* **125** (2000) 25-27.
- [237] W. De Malsche, H. Eghbali, D. Clicq, J. Vangeloooven, H. Gardeniers, and G. Desmet, Pressure-driven reverse-phase liquid chromatography separations in ordered nonporous pillar array columns, *Analytical Chemistry* **79** (2007) 5915-5926.
- [238] W. De Malsche, H. Gardeniers, and G. Desmet, Experimental study of porous silicon shell pillars under retentive conditions, *Analytical Chemistry* **80** (2008) 5391-5400. doi:10.1021/ac800424q
- [239] G. Ocvirk, E. Verpoorte, A. Manz, M. Grasserbauer, and H. Widmer, High-Performance Liquid-Chromatography Partially Integrated Onto a Silicon Chip, *Analytical Methods and Instrumentation* **2** (1995) 74-82.
- [240] A. Ishida, T. Yoshikawa, M. Natsume, and T. Kamidate, Reversed-phase liquid chromatography on a microchip with sample injector and monolithic silica column, *Journal of Chromatography A* **1132** (2006) 90-98. doi:10.1016/j.chroma.2006.07.025
- [241] J. Wen, C. Guillo, J.P. Ferrance, and J.P. Landers, Microfluidic-Based DNA Purification in a Two-Stage, Dual-Phase Microchip Containing a Reversed-Phase and a Photopolymerized Monolith, *Analytical Chemistry* **79** (2007) 6135-6142.
- [242] D.S. Reichmuth, T.J. Shepodd, and B.J. Kirby, Microchip HPLC of peptides and proteins, *Analytical Chemistry* **77** (2005) 527-533.
- [243] B. He, N. Tait, and F. Regnier, Fabrication of Nanocolumns for Liquid Chromatography, *Analytical Chemistry* **70** (1998) 3790-3797.
- [244] A. Bhattacharyya and C.M. Klapperich, Thermoplastic microfluidic device for on-chip purification of nucleic acids for disposable diagnostics, *Analytical Chemistry* **78** (2006) 788-792.
- [245] J. Liu, C. Chen, C. Tsao, C. Chang, C. Chu, and D.L. DeVoe, Polymer Microchips Integrating Solid-Phase Extraction and High-Performance Liquid Chromatography Using Reversed-Phase Polymethacrylate Monoliths, *Analytical Chemistry* **81** (2009) 2545-2554. doi:10.1021/ac802359e
- [246] Y. Yang, C. Li, J. Kameoka, K.H. Lee, and H.G. Craighead, A polymeric microchip with integrated tips and in situ polymerized monolith for electrospray mass spectrometry, *Lab on a Chip* **5** (2005) 869-876.
- [247] D.A. Mair, E. Geiger, A.P. Pisano, J.M.J. Fréchet, and F. Svec, Injection molded microfluidic chips featuring integrated interconnects, *Lab on a Chip* **6** (2006) 1346-1354.
- [248] A. Gaspar, M.E. Piyasena, and F.A. Gomez, Fabrication of Fritless Chromatographic Microchips Packed with Conventional Reversed-Phase Silica Particles, *Analytical Chemistry* **77** (2005) 527-533.
- [249] C.Y. Shih, Y. Chen, W. Li, J. Xie, Q. He, and Y.C. Tai, An integrated system for on-chip temperature gradient interaction chromatography, *Sensors and Actuators A* **127** (2006) 207-215.
- [250] A. Manz, Y. Miyahara, J. Miura, Y. Watanabe, H. Miyagi, and K. Sato, Design of an open-tubular column liquid chromatograph using silicon chip technology, *Sensors and Actuators B* **1** (1990) 249-255. doi:10.1016/0925-4005(90)80210-Q
- [251] L. Ceriotti, N.F. de Rooij, and E. Verpoorte, An Integrated Fritless Column for On-Chip Capillary Electrochromatography with Conventional Stationary Phases, *Analytical Chemistry* **74** (2002) 639-647. doi:10.1021/ac0109467
- [252] S. Le Gac, J. Carlier, J. Camart, C. Cren-Olivé, and C. Rolando, Monoliths for microfluidic devices in proteomics, *Journal of Chromatography B* **808** (2004) 3-14. doi:10.1016/j.jchromb.2004.03.067
- [253] K.W. Ro, J. Liu, and D.R. Knapp, Plastic microchip liquid chromatography-matrix-assisted laser desorption/ionization mass spectrometry using monolithic columns, *Journal of chromatography A* **1111** (2006) 40-47.
- [254] F.E. Regnier, Microfabricated Monolith Columns for Liquid Chromatography. Sculpting Supports for Liquid Chromatography, *Journal of High Resolution Chromatography* **23** (2000) 19-26. doi:10.1002/(SICI)1521-4168(20000101)23:1<19::AID-JHRC19>3.0.CO;2-J
- [255] M. De Pra, W. De Malsche, G. Desmet, P.J. Schoenmakers, and W.T. Kok, Pillar-structured microchannels for on-chip liquid chromatography: Evaluation of the permeability and separation performance, *Journal of Separation Science* **30** (2007) 1453-1460. doi:10.1002/jssc.200600468
- [256] J. Vangeloooven, W.D. Malsche, F. Detobel, H. Gardeniers, and G. Desmet, High-Speed Shear-Driven Flows Through Microstructured 1D-Nanochannels, *Analytical Chemistry* **81** (2009) 943-952. doi:10.1021/ac801691e

- [257] G.A. Lord, D.B. Gordon, P. Myers, and B.W. King, Tapers and restrictors for capillary electrochromatography and capillary electrochromatography-mass spectrometry, *Journal of Chromatography A* **768** (1997) 9-16. doi:10.1016/S0021-9673(96)01081-3
- [258] M. De Pra, W.T. Kok, J.G.E. Gardeniers, G. Desmet, S. Eeltink, J.W. van Nieuwkastele, and P.J. Schoenmakers, Experimental study on band dispersion in channels structured with micropillars, *Analytical Chemistry* **78** (2006) 6519-6525.
- [259] W.D. Malsche, D. Clicq, V. Verdoold, P. Gzil, G. Desmet, and H. Gardeniers, Integration of porous layers in ordered pillar arrays for liquid chromatography, *Lab on a Chip* **7** (2007) 1705-1711.
- [260] V. Spikmans, S.J. Lane, B. Leavens, A. Manz, and N.W. Smith, On-line on-chip post-column derivatisation reactions for pre-ionisation of analytes and cluster analysis in gradient μ -liquid chromatography/electrospray mass spectrometry, *Rapid Communications in Mass Spectrometry* **16** (2002) 1377-1388. doi:10.1002/rcm.727
- [261] J.F. Borowsky, B.C. Giordano, Q. Lu, A. Terray, and G.E. Collins, Electroosmotic Flow-Based Pump for Liquid Chromatography on a Planar Microchip, *Analytical Chemistry* **80** (2008) 8287-8292. doi:10.1021/ac801497r
- [262] E. Meng, P. Li, and Y. Tai, A biocompatible Parylene thermal flow sensing array, *Sensors and Actuators A* **144** (2008) 18-28. doi:10.1016/j.sna.2007.12.010
- [263] C.Y. Shih, Y. Chen, J. Xie, Q. He, and Y.C. Tai, On-chip temperature gradient interaction chromatography, *Journal of Chromatography A* **1111** (2006) 272-278.
- [264] R.M. Tiggelaar, J.W. Berenschot, J.H.D. Boer, R.G.P. Sanders, J.G.E. Gardeniers, R.E. Oosterbroek, A.V.D. Berg, and M.C. Elwenspoek, Fabrication and characterization of high-temperature microreactors with thin film heater and sensor patterns in silicon nitride tubes, *Lab on a Chip* **5** (2005) 326-336.
- [265] S. Tia and A.E. Herr, On-chip technologies for multidimensional separations, *Lab on a Chip* **9** (2009) 2524 - 2536. doi:10.1039/b900683b
- [266] M.M. Robson, M.G. Cikalo, P. Myers, M.R. Euerby, and K.D. Bartle, Capillary electrochromatography: A review, *Journal of Microcolumn Separations* **9** (1997) 357-372. doi:10.1002/(SICI)1520-667X(1997)9:5<357::AID-MCS3>3.0.CO;2-0
- [267] L. DeFrancesco, Product Review: Capillary Electrophoresis: Finding a Niche, *Analytical Chemistry* **73** (2001) 497 A-499 A. doi:10.1021/ac012512h



ISBN 978-952-60-3339-6
ISBN 978-952-60-3340-2 (PDF)
ISSN 1795-2239
ISSN 1795-4584 (PDF)